Technical University of Crete
School of Electronic and Computer Engineering

Hyper Spectral Data Estimation from Power Dimensionality Experimental Imaging

Master thesis by Dimitris Iliou

Supervisor: Professor Costas Balas

Committee: Professor Minos Garofalakis

Professor Vassilis Digalakis

Chania 2014

Acknowledgements

I wish to express my sincere and utmost appreciation to Professor Costas Balas for his invaluable guidance, insight and support during the implementation of this Master thesis.

I am also very grateful to my fellow colleagues and friends in the Optoelectronic Research & Biomedical Imaging Technology Lab, and especially George Epitropou and Vasilis Kavadias, for their guidance, support suggestions for the improvement of the current Master thesis.

I would also like to thank Professors Minos Garofalakis and Vasilis Digalakis for their participation in the presentation and the evaluation of this diploma thesis.

Last but not least, I wish to thank my family and close friends for their advising and support all these years of my studies.

Abstract

We report the first real time modular spectral and color imaging system based on the combination of snapshot spectral imaging, spectral estimation and color reproduction algorithms. A limited number of spectral bands are captured simultaneously, with the aid of specially designed camera, which are subsequently processed with spectral estimation algorithms to obtain a full spectrum per image pixel. We have succeeded to demonstrate complete spectral cube calculation and display of millions of spectra in real-time and to remove trade-off between spectral and spatial resolution. Besides accurate spectral mapping, our approach enables also reliable and device-independent color reproduction based on complete, per-pixel spectra. These achievements hold the promise to provide an indispensable tool in nondestructive analysis and in noninvasive diagnosis.

Table of Contents

Table Figures of

Table of Tables

1 Introduction

Over the last two decades, the field of optical imaging has developed very rapidly providing color imaging (CI) systems with very high resolution that nowadays allow 3D imaging as well as video capture with a very high frame rate. These systems try to emulate human vision in order to reproduce a result (image) that resembles the actual scene as it was perceived by a human eye. Usually these systems produce three-dimensional data (RGB is more commonly used) where each of the three dimensions represents the intensity and chrominance of light.

Although CI systems can provide an accurate representation of the scene at hand, there is a great deal of information that cannot be perceived with these systems or the "naked" eye; information that may dwell within the visible spectrum or beyond it, i.e. UV or Infrared regions of the EM-Spectrum. In order to acquire this "hidden" information, spectral imaging systems are used.

Spectral Imaging (SI) is the application of reflectance spectroscopy to every pixel in a spatial image. Every spatial image captured represents a different wavelength within the electromagnetic spectrum and each pixel represents the spectral power distribution of the scene at that point. The stack of images created from this system is the so called spectral cube (Figure 1-1), and the data is represented in multidimensional, spanning spatial and spectral dimensions (x, y, λ).

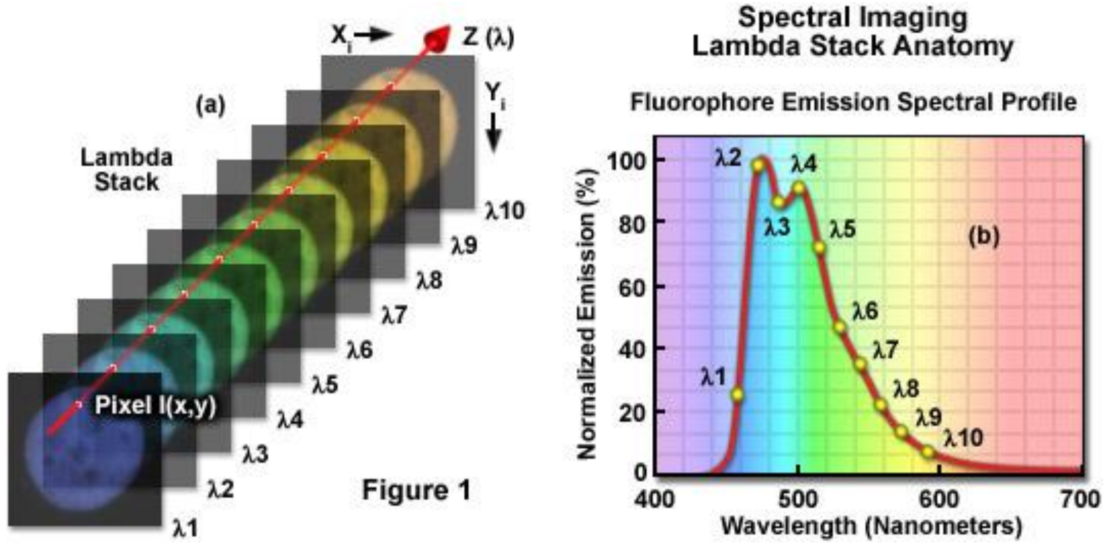

Figure 1-1 Spectral Cube Graphical Representation

Spectroscopy can be used to detect individual absorption features due to specific chemical bonds in a solid, liquid, or gas. Solids can be either crystalline (i.e. minerals) or amorphous (such as glass). Every material is formed by chemical bonds and has the potential for detection with spectroscopy. Actual detection is dependent on the spectral coverage, spectral and spatial resolution, and signal-to-noise of the SI system, the abundance of the material and the strength of absorption features for that material in the wavelength region measured.

SI systems are widely used nowadays in numerous fields such as medicine, astronomy, industry, military etc. and, due to the continuous need to improve the preexisting techniques and methods, many innovations and advances were developed.

The information provided by these systems, which is usually not discernible to the human eye, allows useful facts and phenomena to be revealed. Unfortunately, SI systems are expensive and sizable, which makes them inaccessible for many applications, and the acquisition and computational time needed is very high, which prevents the system from observing any dynamically developing phenomena. Moreover, high fidelity color can be reproduced with post-processing using the spectral cube acquired which effectively does not allow real time color imaging for an SI system.

To address these limitations, real-time snapshot spectral imaging systems need to be developed that allow simultaneous multispectral imaging and have lower cost and size. We have developed and propose a novel real-time multispectral imaging system that can simultaneously acquire six spectral bands and provide spectral information in any desired wavelength within the visible spectrum, as well as reproduce high fidelity color in real-time.

Within this Master Thesis, basic concepts about color and spectral imaging will be discussed as well as the development and validation of the proposed real-time spectral imager.

1.1 Electromagnetic Radiation

Electromagnetic radiation (EM radiation or EMR) is one of the fundamental phenomena of electromagnetism, behaving as waves and also as photon particles propagating through space, carrying radiant energy (Figure 1-2). In a vacuum, it propagates at a characteristic speed, the speed of light, normally in straight lines. EMR is emitted and absorbed by charged particles. As an electromagnetic wave, it has both electric and magnetic field components, which oscillate in a fixed relationship to one another, perpendicular to each other and perpendicular to the direction of energy and wave propagation.

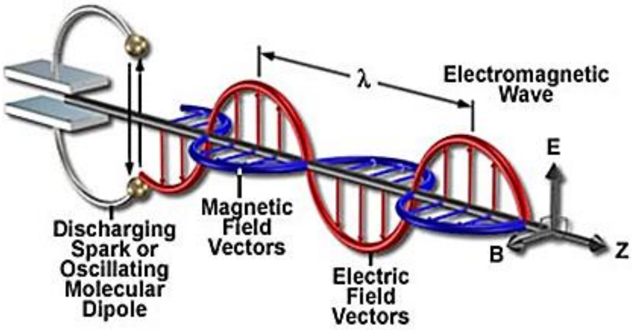

Figure 1-2 The electromagnetic waves that compose electromagnetic radiation can be imagined as a self-propagating transverse oscillating wave of electric and magnetic fields

The modern theory that explains the nature of light includes the notion of wave–particle duality (Figure 1-3). More generally, the theory states that everything has both a particle nature and a wave nature, and various experiments can be done to bring out one or the other. The particle nature is more easily discerned if an object has a large mass, and it was not until a bold proposition by Louis de Broglie in 1924 that the scientific community realized that electrons also exhibited wave–particle duality.

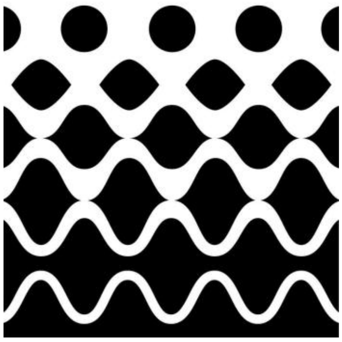

Figure 1-3 Artist's impression, inspired by the work of the artist Maurits Cornelis Escher, of the continuous morphing between particle- and wave-like behaviour of light. Credit: Nicolas Brunner and Jamie Simmonds

EMR is characterized by the frequency or wavelength of its wave. The electromagnetic spectrum, in order of increasing frequency and decreasing wavelength, consists of radio waves, microwaves, infrared radiation, visible light, ultraviolet radiation, X-rays and gamma rays (Figure 1-4). The eyes of various organisms sense a somewhat variable but relatively small range of frequencies of EMR called the visible spectrum or light. Higher frequencies correspond to proportionately more energy carried by each photon; for instance, a single gamma ray photon carries far more energy than a single photon of visible light.

Electromagnetic radiation is associated with EM fields that are free to propagate themselves without the continuing influence of the moving charges that produced them, because they have achieved sufficient distance from those charges. Thus, EMR is sometimes referred to as the far field. In this language, the near field refers to EM fields near the charges and current that directly produced them, as for example with simple magnets and static electricity phenomena. In EMR, the magnetic and electric fields are each induced by changes in the other type of field, thus propagating itself as a wave. This close relationship assures that both types of fields in EMR stand in phase and in a fixed ratio of intensity to each other, with maxima and nodes in each found at the same places in space.

Electric and magnetic fields obey the properties of superposition, so fields due to particular particles or time-varying electric or magnetic fields contribute to the fields due to other causes. (As these fields are vector fields, all magnetic and electric field vectors add together according to vector addition.) These properties cause various phenomena including refraction and diffraction. For instance, a travelling EM wave incident on an atomic structure induces oscillation in the atoms, thereby causing them to emit their own EM waves. These emissions then alter the impinging wave through interference.

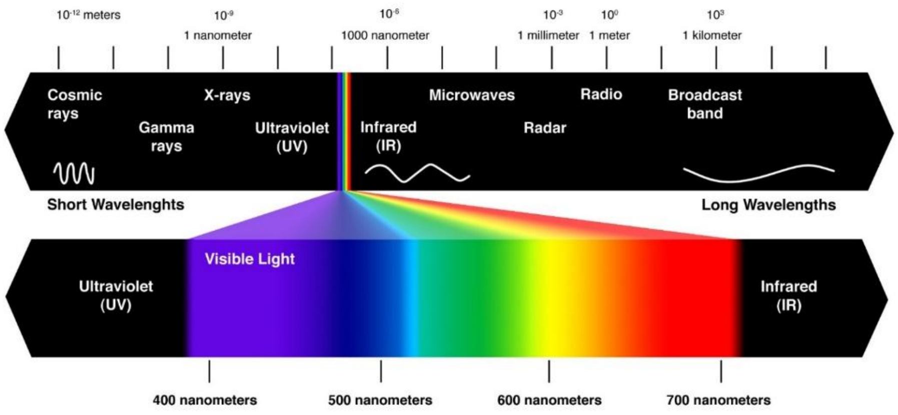

Figure 1-4 Electromagnetic spectrum with visible light highlighted

EMR carries energy—sometimes called radiant energy—through space continuously away from the source (this is not true of the near-field part of the EM field). EMR also carries both momentum and angular momentum. These properties may all be imparted to matter with which it interacts. EMR is produced from other types of energy when created, and it is converted to other types of energy when it is destroyed. The photon is the quantum of the electromagnetic interaction, and is the basic "unit" or constituent of all forms of EMR. The quantum nature of light becomes more apparent at high frequencies (thus high photon energy). Such photons behave more like particles than lower-frequency photons do.

In classical physics, EMR is considered to be produced when charged particles are accelerated by forces acting on them. Electrons are responsible for emission of most EMR because they have low mass, and therefore are easily accelerated by a variety of mechanisms. Rapidly moving electrons are most sharply accelerated when they encounter a region of force, so they are responsible for producing much of the highest frequency electromagnetic radiation observed in nature. Quantum processes can also produce EMR, such as when atomic nuclei undergo gamma decay, and processes such as neutral pion decay.

The effects of EMR upon biological systems (and also to many other chemical systems, under standard conditions) depends both upon the radiation's power and frequency. For lower frequencies of EMR up to those of visible light (i.e., radio, microwave, infrared), the damage done to cells and also to many ordinary materials under such conditions is determined mainly by heating effects, and thus by the radiation power. By contrast, for higher frequency radiations at ultraviolet frequencies and above (i.e., X-rays and gamma rays) the damage to chemical materials and living cells by EMR is far larger than that done by simple heating, due to the ability of single photons in such high frequency EMR to damage individual molecules chemically.

1.2 Color

Color is the characterization of the human visual perception property that can be identified as red, blue, green or other. It derives from the light spectrum in the range of 400nm to 700nm. Eye Light receptors have a certain spectral sensitivity, which combined with incoming light produces the color perception as we know it. In our effort to imprint daily scenes and objects, optical instruments, called (color) cameras, which record images are used. Color cameras are three-band real time devices that emulate human vision. Thus, the three channels used are the primary channels that the human eye can perceive (three types of cone-receptors): Red, Green, and Blue (RGB). By defining a color space, colors can be identified numerically by their coordinates.

1.3 Color Spaces

Most color spaces are defined [1] for practical use in representation and computation and they do not necessarily relate to the way that humans perceive color. Device dependent color spaces can be categorized as: Additive (RGB, HSV, and HLS) and Subtractive (CMY, CMYK or spaces with five or more channels).

1.3.1 Red-Green-Blue (RGB) Color Space

RGB color space is represented by a unity cube (Figure 1-5) and uses additive color mixing, which means that the resulting color is a product of combination of light of two or more channels. So, its color is represented as a triplet (**R**, **G**, and **B**) and all colors are located within the cube.

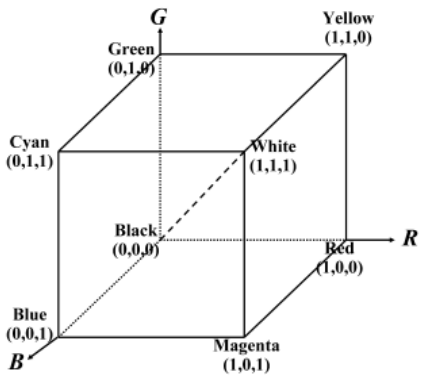

Figure 1-5 RGB Color Space

There are other color spaces based on the RGB [2]. Some are: sRGB, ROMM RGB, Adobe RGB 98, Apple RGB, NTSC RGB, and EBU RGB. They are used as interchange spaces to communicate color or as working spaces in imaging applications. The difference between them can be: on the type (rendered or un-rendered), on the Encoding (8-bit, 10-bit, etc.), on the Gamut and White Point.

1.3.2 Hue-Saturation-Value (HSV) Space

HSV, also known as HSB (**H**ue, **S**aturation, and **B**rightness) has a hexagon shape (Figure 1-6). It is easier to comprehend since color is defined in terms of hue and saturation instead of additive or subtractive color components. Hue represents the angle of the vertical axes. Saturation indicates the strength of the color and it increases by moving from the center to edge of the hexagon. Value indicates the darkness of the color. At the top of the hexagon colors have maximum intensity. Finally, HSV is a transformation of the RGB color space.

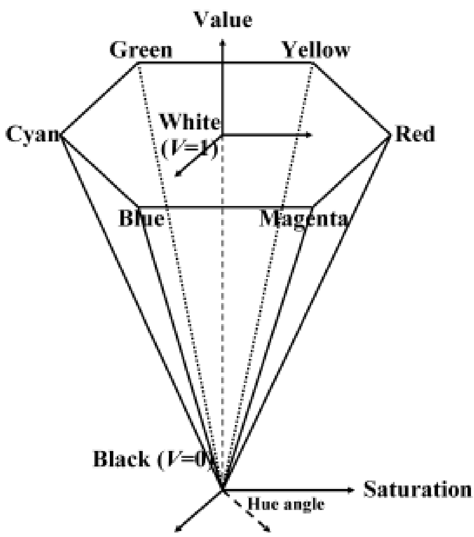

Figure 1-6 HSV Color Space

1.3.3 Hue-Lightness-Saturation (HLS) Space

HLS, also known as HSI (**H**ue, **S**aturation, and **I**ntensity) has a double cone shape (Figure 1-7) and is similar to the HSV color space. Hue and Saturation are defined as with the HSV model while Lightness (vertical axes) indicates the darkness of color.

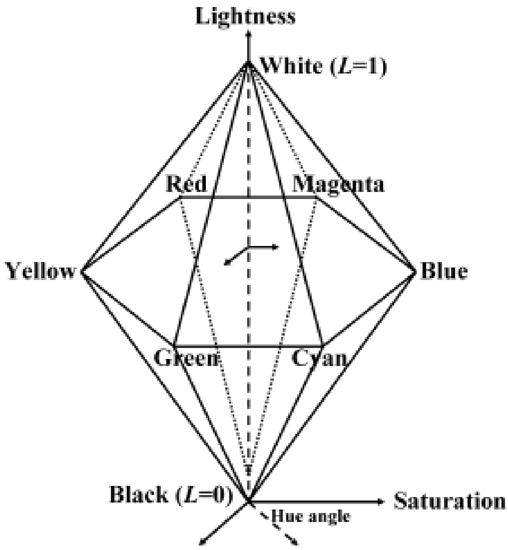

Figure 1-7 HLS Color Space

1.3.4 Cyan-Magenta-Yellow (CMY) Color Space

CMY, as RGB, defines colors within a unity cube (Figure 1-8) by the subtractive color-mixing model. Using the Subtractive color model, the color that a surface displays depends not on the parts that were absorbed but on the parts of the visible spectrum that were not and therefore remained visible. It can be inferred that the CMY system is a complement of the RGB.

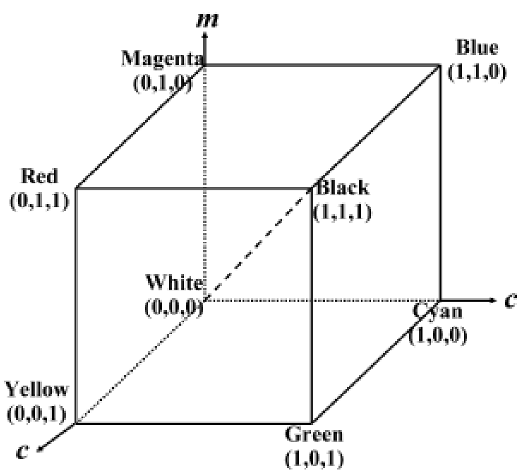

Figure 1-8 CMY Color Space

1.4 CIE Color Spaces

CIE Color Spaces are device-independent and are used to provide a quantitative measure for all colors.

1.4.1.1 CIEXYZ

CIEXYZ color space was one of the first attempts to emulate human color perception. The chromaticity coordinates are derived from the normalization of the tristimulus values XYZ.

1.4.1.2 CIELUV

CIELUV color space is a simple transformation of the CIE XYZ 1931 Color Space that provides perceptual uniformity.

1.4.1.3 CIELAB

CIELAB is a nonlinear transformation of the CIE XYZ 1931 Color Space. It is produced by plotting, along three axes at right angles to one another, the quantities L*, a* and b*. It describes all the colors visible to the human eye and was created to serve as a device-independent model to be used as a reference.

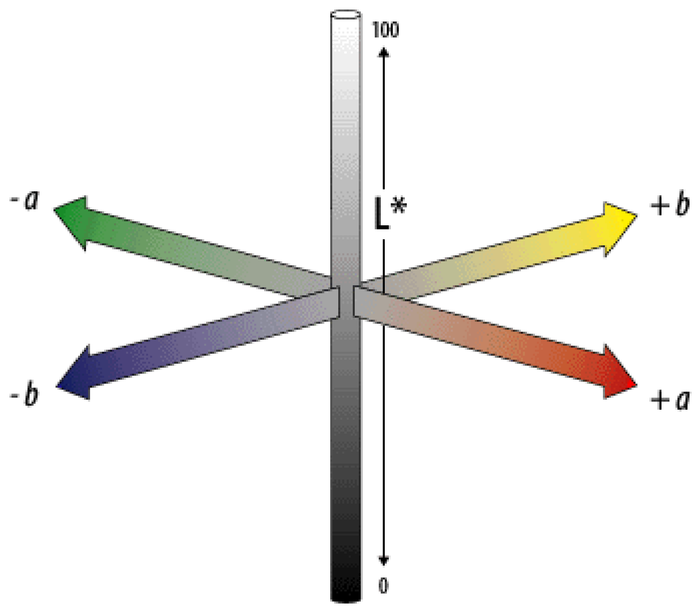

Figure 1-9 CIELAB Space

In Figure 1-9, the central vertical axis represents lightness (signified as L*) whose values run from 0 (black) to 100 (white). This scale is closely related to Munsell's value axis except that the value of each step is much greater. This is the same lightness valuation used in CIELUV.

The color axes are based on the fact that a color cannot be both red and green, or both blue and yellow, as these colors oppose each other. On each axis the values run from positive to negative. On the a-a' axis, positive values indicate amounts of red while negative values indicate amounts of green. On the b-b' axis, yellow is positive and blue is negative. For both axes, zero is neutral gray.

Therefore, values are only needed for two color axes and for the lightness or grayscale axis (L*), which is separate (unlike in RGB, CMY or XYZ where lightness depends on relative amounts of the three color channels).

1.4.1.4 CIE Color Difference Formulas

1.4.1.4.1 CIE 1976(L*a*b*) color difference or CIELAB Color difference

$$\Delta E_{ab}^{*} = \sqrt{(L_2^* - L_1^*)^2 + (a_2^* - a_1^*)^2 + (b_2^* - b_1^*)^2}$$

1.4.1.4.2 CIE94 color difference

$$\Delta E_{94}^{*} = \sqrt{\left(\frac{\Delta L^*}{k_L S_L}\right)^2 + \left(\frac{\Delta C_{ab}^*}{k_C S_C}\right)^2 + \left(\frac{\Delta H_{ab}^*}{k_H S_H}\right)^2}$$

Where:

$$\Delta L^* = L_1^* - L_2^*$$

$$\Delta H_{ab}^* = \sqrt{{\Delta E_{ab}^*}^2 + {\Delta L^*}^2 + {\Delta C_{ab}^*}^2}$$

$$a^* = a_1^* - a_2^*,\ \ \Delta b^* = b_1^* - b_2^*$$

$$C_1^* = \sqrt{{a_1^*}^2 + {b_1^*}^2}$$

$$C_2^* = \sqrt{{a_2^*}^2 + {b_2^*}^2}$$

$$\Delta S_L = 1, S_C = 1 + K_1 C_1^*, S_H = 1 + K_2 C_1^*$$

$$\Delta C_{ab}^* = C_1^* - C_2^*$$

$$k_L = 1, K_1 = 0.045\ , K_2 = 0.015$$

- ΔH_{ab}^* is the Hue difference
- ΔC_{ab}^* is the chromasity difference

When evaluating Color difference using CIELAB, numerically if the result of ΔE_{ab}^* is lower than 5, then high fidelity color reproduction can be performed with no significant perceptual differences from the origin. Two Images with Color Difference ΔE_{ab}^* below 2.3 or less are indistinguishable from one another.

CIE94 is another color difference model that under reference conditions [3] equals ΔE_{94*}. In any other case, ΔE_{94*} becomes smaller than ΔE_{ab*}.

A graphical analysis of the Color Difference [4] is presented in Figure 1-10. “Vector Plots” are used to represent the difference between a*b* and C* L*. The tail represents the measured values and the head the calculated values. The length of each vector represents the magnitude of the chromatic error. Depending on the direction of the vector, Chroma or lightness error is indicated (as seen in the figure). Finally, for all the data measured, a statistical analysis is performed to show the magnitude and the distribution of the color difference in both ΔE_{ab^*} and ΔE_{94^*}.

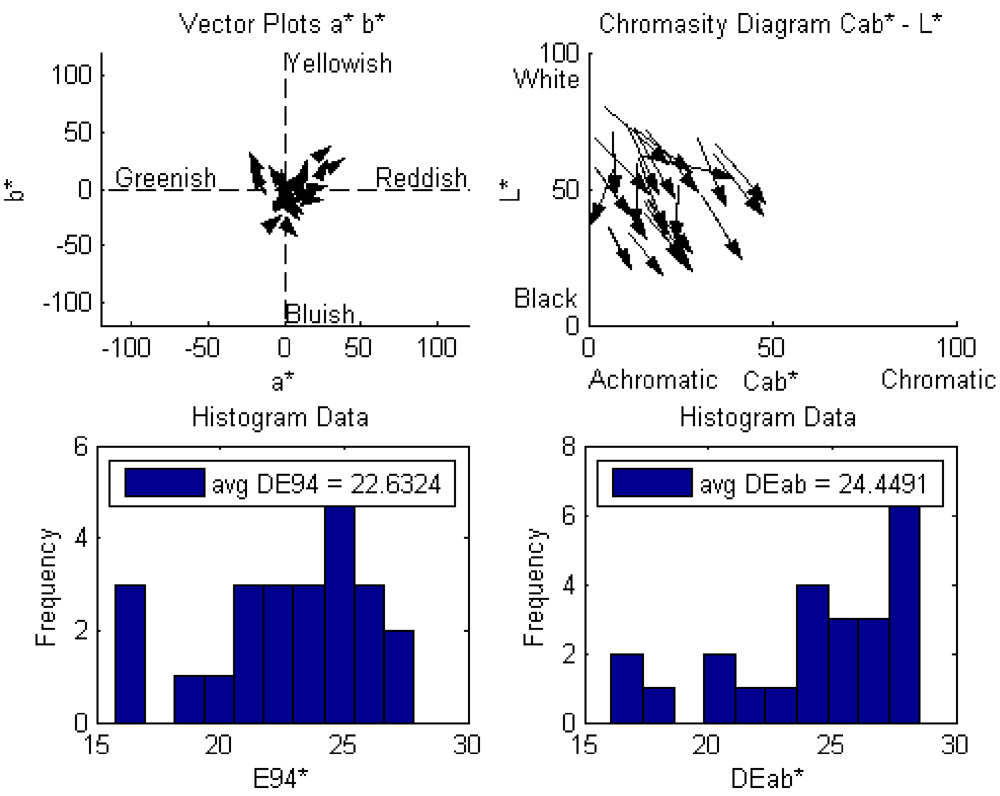

Figure 1-10 DE Graphical and Quantitative Analysis Example

1.5 <u>Metamerism</u>

Human vision, as well as any RGB Imaging system, has some limitations due to phenomena like metamerism. Metamerism [5] is a phenomenon in which two colors match one another, but they have different spectral signature. The amount of difference between the Spectral Signatures of the object determines the degree of metamerism [6]. There are many factors that affect the degree of metamerism such as:

- Illuminant
- Observer
- Geometry
- Device

Illuminant metamerism occurs when the color of two spectrally matched samples - that are viewed under illuminants with different Spectral Power Distribution - is perceived differently by the observer. **Observer metamerism** [6] describes the different perception of color between two individuals (inter-observer metamerism) or one individual himself (intra-observer metamerism). In order to quantify the intra-observer metamerism, a single individual repeated an experiment 20 times. **Geometry metamerism** mostly affects samples that have different surface characteristics e.g. matt or gloss. Samples viewed under different geometry can approximately match if their surface characteristics are the same, whereas with different characteristics the color perceived can be quite different. Lastly, **device or cross-media metamerism** describes the different color perception between visualization systems. For example, the eye has different spectral sensitivity than a camera [8], thus different metameric matches can occur from the same samples. Accordingly, using two instruments (cameras, spectrophotometers etc.) with different spectral sensitivities [9] can result in the same issue.

Metamerism is a phenomenon with great significance since it can affect our ability to capture objects-scenes-samples with high color accuracy that can match the original one. Thus, many methods have been proposed to overcome this phenomenon. Acquiring the Spectral Power Distribution –SPD - of an object (e.g. reflectance spectra) can result in high accuracy color reproduction - independent of metamerism. A well-known method to acquire spectral reflectance is the use of Spectral Imaging Devices.

1.6 Spectral and Color Imaging

Spectral Imaging (SI) devices collect and process information across the electromagnetic spectrum at every location in an image plane. In general, the number of channels in SI exceeds the number of channels of an RGB system.

Humans build sensors and processing systems to provide the same type of capability for application in agriculture, mineralogy, physics, and surveillance and other fields of science. Spectral sensors collect information as a set of 'images'. Each image represents a range of the electromagnetic spectrum and is also known as a spectral band. Spectral sensors look at objects using a vast portion of the electromagnetic spectrum. Certain objects leave unique 'fingerprints' across the electromagnetic spectrum. These 'fingerprints' are known as spectral signatures and enable identification of the materials that make up a scanned object. For example, having the spectral signature for oil helps mineralogists find new oil fields.

The precision of these sensors is typically measured in spectral resolution, which is the width of each band of the spectrum that is captured. If the scanner picks up on a large number of fairly small wavelengths, it is possible to identify objects even if said objects are only captured in a handful of pixels. However, spatial resolution is as important a factor as spectral resolution is. If the pixels are too large, then multiple objects are captured in the same pixel and become difficult to identify. If the pixels are too small, then the energy captured by each sensor-cell is low, and the decreased signal-to-noise ratio reduces the reliability of measured features.

1.6.1 *Color vs. Spectral Imaging*

As aforementioned, color imaging devices are subjectable to the phenomenon of metamerism while spectral imaging devices can help overcome it. In various studies [10]-[11] the two methods are compared in order to specifically answer if spectral imaging ensures higher color accuracy independent of illumination, observer and geometric conditions. Ideally, in order to accurately reproduce color from spectral data [5], spectral data is needed from 380nm to 780nm with 5nm integral along with the spectral sensitivity of the observer and the SPD of the wanted illuminant. In case this data is available in higher integral (e.g. 10 or 20nm) or its range is smaller than indicated (e.g. 420 – 700nm), interpolation or extrapolation of the data is suggested to meet the aforementioned requirements. This means that there is a need of a different narrow band filter for every 5 nm – Hyperspectral Imaging. Other studies indicate that an optimum-minimum number of filters can be selected for accurate color reproduction [12]-[19] –Multispectral Imaging. The filters used can be readily-available filters or Tunable Filters [20] such as Liquid Crystal Tunable Filters (LCTF) and Acousto-Optical Tunable Filter (AOTF). These systems reproduce color of higher quality and accuracy than common RGB Imaging systems and with a lower degree of metamerism.

Moreover, in order to achieve high-fidelity color reproduction, depending on the reproduction medium, the data acquired must be accompanied by information regarding the illumination of the scene, spectral sensitivity of the camera used and imaging conditions.

1.6.2 *Multispectral Imaging and Color*

Most Multispectral Imaging systems usually employ a monochrome camera and interchangeable filters, usually less than 10. Another approach to Multispectral Imaging systems is the use of one [17], two [21][22] or more [19] RGB or CMYK Cameras [23], or a single stereo Camera [24][25], along with readily available Triple or Quadruple band pass filters. The filters modify the spectral sensitivities of the camera and are optimally selected in order to cover the largest possible part of the visible spectrum. The two cameras can be set up perpendicular to one another and with the use of a beam splitter or a dichroic mirror the image is projected to both cameras. Alternatively, a stereoscopic configuration with two cameras or a single 3D can be used, where in both cases 3D depth information is also available whilst stereo matching algorithms are employed to ensure that there is no spatial displacement between the two cameras-images. In the case where more than two RGB cameras are used, a side-by-side configuration is applied and the final image is evaluated by superimposing the images from each camera source. That configuration also allows real-time multispectral color video capture by employing GPU processing.

Usually, the bands acquired are wider and limited in comparison to a Hyperspectral Imaging System. Thus, Spectral Estimation can be performed to reduce the system integral, in which case priori data is needed for an accurate estimation.

1.6.3 Single Exposure or Instantaneous Spectral Imagers

In order to record spectral images, tunable filtered-based Spectral Imaging Systems are used. Those systems record spectral images in a time-sequentially manner and obtain the spectra from post hoc assembly of the time-sequential data. This reveals a major disadvantage of these systems. When we have phenomena that change on a time scale that is shorter than the duration required for recording the spectral cube, the SI systems described cannot perform accurately and give accurate Spectral data. Furthermore, the scene recorded by SI systems must be static otherwise problems will be created in the co-registration of the Spectral Images, which is needed in order to provide accurate spectra.

There are numerous applications (i.e. biomedical or others) that require Spectral Imaging and analysis of transient moving scenes. This is why “Single shot” or “Instantaneous” spectral imagers have been created [26]. SE systems have many advantages over SI systems such as: fast acquisition of accurately registered images, high device robustness and reliability, low cost etc. However, there are many trade-offs in order to achieve all of the above. Due to current technological limitations there is a trade-off between spatial and spectral resolution. That means that SE imagers allow us to capture a small number of spectral images. So, when we have stationary and invariant scenes we use the Spectral Imaging systems described above since the spatial and spectral resolutions are superior to the ones on SE. However, when the acquisition of a small number of predetermined bands is demanded, SE systems are preferred.

1.6.4 Color Reproduction Media

In many cases, the quality of the reproduced color is affected by the reproduction media employed i.e. screen, printers, etc.

For this reason, spectral printing models were created that employ more than just the colors used by a commercial printer, in order to have more degrees of freedom and reproduce color with colorimetric and spectral accuracy. Multi-ink printer models employ various spectral separation algorithms [16][27][28] so as to create the least metameric reproduction relative to the original object.

Another reproduction media that could achieve high colorimetric and spectral accuracy is the screen. As with the printer aspect, more than 3 colors are introduced to achieve that. Six-Color gamut display was introduced [14] which, along with a 16-band multispectral system, could achieve natural color reproduction with high-fidelity.

1.6.5 Spectral Imaging and Applications

Color and Spectral Imaging nowadays is employed in a huge variety of application. As aforementioned, Color Imaging systems have some limitations-constraints that can be surpassed using Spectral Imaging. These applications include medical devices (such as endoscopes, microscopes etc.), telemedicine, image-art archiving, high resolution printing and many more.

In art-preservation and image archiving, the use of Spectral Imaging systems, besides achieving better color accuracy also provide information about the object's physical properties. In general, color imaging systems were used to capture and store art painting and images but those came along with the limitations of those systems regarding the illumination, reproduction medium, viewing conditions, etc. thus making it difficult for an accurate light or hard copy of the object in question. Various methods were proposed, [29][30][31] where spectral imaging systems were designed to achieve high accuracy image archives. In most cases, a monochrome camera along with a Liquid Crystal Tunable Filters (LCTF) or an RGB commercial camera coupled with interference filters was used. Using a LCTF the system can acquire spectral images with a high resolution of 5nm, but that accuracy might be redundant since most of these application are acquired in the visible region of the spectrum, where sharp transitions from high to low reflectance (and vice-versa) are very rare, thus reducing the accuracy of the image acquisition may not result in loss of accuracy. The loss of measurement can be substituted using spectral estimation algorithms or interpolation of the data acquired. That can also resolve in a high-accuracy system with lower cost and hardware complexity. Finally, another approach to image archiving is the fusion of high-resolution lightness image with a low-spatial resolution multi-band image to generate a high-spatial resolution spectral image.

High-accuracy color reproduction is also very important in the field of medicine. For example, electronic endoscopes [32] were developed that used a color CCD camera with RGB broad filters, along with spectral estimation and color reproduction, or Fujinon intelligent chromoendoscopy (FICE) [33] filters. Specifically, Fujinon performs spectral estimation and then assigns spectral images to RGB in order to generate a final F.I.C.E. Processed Image in order to emphasize color differences and detect abnormal parts. The choice of filters varies, depending on the disease that needs to be detected.

Another aspect of medical applications is telemedicine, where the accuracy of the reproduced image at the observation is crucial to be as high as possible for an accurate medical diagnosis. So a Multispectral System is proposed [34], where the multispectral data are acquired along with the illumination spectrum, which afterwards is removed from the acquired so to have independent from illumination spectral reflectance. Finally, in order to have an accurate color reproduction of the object at the observation site, the illumination of that site is needed along with the object's spectra, since human vision changes its spectral sensitivity according to the illumination environment. Also, sometimes Color Imaging might not be sufficient for the diagnosis of certain diseases. For example in dermatology, some skin diseases cannot be detected-rendered accurately by using a color imaging system, while a multispectral imaging system can provide accurate color reproduction along with other useful spectral information [35].

1.7 Spectral Estimation

Spectral Estimation is broadly used in order to project low dimensionality data, such as RGB or a small number of spectral bands, to high dimensionality data, such as a complete spectral cube. Over the years many method have been proposed that result in high accuracy estimation such as Wiener estimation, R matrix, Linear Projection, interpolation etc.

One of the broadly used, linear condition method, is Wiener Estimation [36]-[39] which in most cases requires a priori knowledge of a reference sample (spectral and/or RGB data), such as Gretag Macbeth® Color Checker CC. In the work of Stigell et al [36], spectral estimation was performed using the RGB data of a color camera along with a priori knowledge. After evaluating the estimation matrix using the aforementioned data, the spectral reflectance of the sample in question can be estimated.

Another variation of Wiener Estimation was an edge preserving spatio-spectral estimation derived by Bayesian inference introduced by Shen et al. [37]. In this case, a six-channel camera was used and the noise of the system was also taken into account. That meant that the estimation matrix also contained the noise covariance matrix, which as stated, is updated after Wiener denoising, and propagated to the spectral reconstruction filter achieving the combination of denoising and spectral reconstruction into a single operator. The use of that filter minimized the RMS error of the spectral reconstruction in comparison to standard Wiener estimation methods.

A different approach was introduced by Shen et al [38], where an adaptive Wiener estimation was performed. The training samples were chosen by adaptive selection on how similar these were to the candidate sample. The estimation matrix for this method must be calculated for every pixel which increased the computational time in contrast with the conventional Wiener estimation. It was inferred that if the number of channels used for input was not large (6-7 bands) then the results were better than standard Wiener estimation and in case that more channel were used (11+) the results were slightly better or close to the standard Wiener Estimation.

By dividing a three channel image into several blocks, Murakami et al [39] proposed a method where Spectral Estimation was performed for each block using different estimation matrix for each one. The use of different estimation matrices for each block made the method spatial-adaptive since each estimation matrix was calculated from data derived from multiple points in the scene acquired. The computational time for this process was higher than the traditional Wiener Estimation but no so much. This piecewise approach of Wiener Estimation can provide accurate results with the use of three channels and with reasonable computational cost.

On the basis that no prior knowledge is needed, the work of Shimano [40] proposed a new model to estimate reflectance spectra. In this case a multiband system was used, whose channel responses and channel noise variance were know. Those in conjunction with a Wiener filter allow the estimation of reflectance spectra without any prior knowledge of the spectral information of the object in question.

When non-linearity is introduced the results of the estimation can be degraded. A solution to this is the study of Shen et al [41] where the reflectance spectra are estimated from multichannel camera responses based on high-order polynomials and partial least squares. That solves the non-linearity and compared to other methods, both colorimetric and spectrophotometric, according to the papers, it provides better results than Wiener and polynomial regression solved by ordinary least squares.

Other methods – algorithms can be employed in order to accurate estimate reflectance spectra. Studies, such as [42] by Mansouri et al, introduced linear projection algorithms like PCA, Wavelets and Fourier analysis. These algorithms calculate the basis functions of a linear model of reflectance spectra using the aforementioned a priori data. An improvement of the previous work was adaptive PCA [43] from Mansouri et al. This variation of PCA derives basis functions like PCA but it employed an algorithm that selected the estimated reflectance spectra for each sample, according to their relativity with the training set, just like the aforementioned adaptive Wiener algorithm. In the same premise, Oh-Seol Kwon et al [44] proposed an algorithm that uses aPCA in order to reduce the estimation error of the surface spectral reflectance. In this case the adaptive part is performed by dividing the input training data into populations according to color using Lloyd algorithm. With this method, it is implied that the variance of the estimation error is reduced when using 3-Band RGB cameras as input to estimate reflectance spectra.

Another improvement of classic PCA was presented by Harifi et al [45], where six basis functions – eigenvectors are used, instead of three that are normally used in PCA with RGB input. For six eigenvectors to be produced, a non-linear regression method was employed in order to estimate the color coordinates of the sample under a different light source. The light source estimated was A with 1964 standard observer from its color specification under D65 illuminant with 1964 standard observer. By obtaining two sets of tristimulus values (one with D65 and one with A illuminant) six basis functions could be produced. The performance of the proposed method showed good improvement over the standard PCA approach.

In general, some linear basis projection algorithms produce basis functions that may contain negative values. In order to obtain basis with non-negative values there are non-negative matrix factorization methods. In the work of S. H. Amirshahi [46] an adaptive version of this kind was presented. The non-negative factorization method was applied in order to determine positive bases of spectral reflectances. The number of basis functions can vary from 3 to 5 in this case. The adaptive part is like the aforementioned adaptive PCA and Wiener where the training set of the algorithm was calculated in order to match the sample in question and thus providing a training set closer to it. From the results provided, the proposed method showed better results in both colorimetric and spectrophotometric point of views in comparison to standard approaches.

One more adaptive method was performed from Babei et al [47] where a weighted pseudo-inverse spectral reconstruction method was employed. According to this study the normality of the dataset used as training can affect the outcome of the estimation as well as the generality and similarity of it to the specimen in question. The results provided from this method were approximately the same with other methods like Wiener concerning colorimetrical and spectral performances.

Another interesting study from Zhao and Berns [48]was the use of the matrix R which was based on the Wyszecki hypothesis that any color stimulus can be decomposed into two spectra, a “fundamental stimulus” and a “metameric black” (R-theory). In this study an RGB digital camera was used coupled with two filters. With the use of the camera signals produces from the two filters (6 bands-values), the tristimulus values were calculated and from them the Fundamental stimulus. Also the spectral reflectance factor is calculated using the Metameric Black of the specimen as well. With the combination of metameric black and fundamental stimulus the spectral reflectances of the specimen can be estimated with accuracy. The advantage of this method is that it can estimate color and spectrum with high accuracy.

Linear and least-squares methods are studied in most of the aforementioned studies. However, there are also smoothness methods that try to maximize the smoothness of the resulting estimate by assuming that the results have a minimal squared first or second derivative. In the study of Connah et al [49] a comparison of these three methods was performed in order to calculate which method produced the best results. According to the outcome of this study, smoothness methods are found to provide the best performance. An important fact is that smoothness methods don’t need explicit a priori knowledge in contrast with least-squares and linear methods that depend on the training set provided.

The combination of different techniques for spectral estimation was also studied [50]. In that study, Wiener, Pseudo-inverse and finite-dimensional modeling methods are combined. The final result is the combination of reflectance estimated from each of the aforementioned methods, weighted properly to minimize colorimetric and spectral errors.

Another approach to the spectral estimation procedure is the use of filters. In the work of Imai et al [51] a trichromatic digital camera combined with absorption filters was used. Moreover, a new empirical space was introduced in which PCA is performed to produce eigenvectors (two more spaces are studied in comparison). The eigenvectors produced combined with the trichromatic signals, with or without filtering, produced the final estimation. From the three aforementioned spaces the new empirical space provided the best colorimetric and spectral performance. On the concept of filters, Eva M. Valero et al [52] proposed the use of color filters is proposed (magenta, orange etc.), with the approach of direct-mapping instead of linear transformation etc. It is also noted that there was a difference between rural and urban environments and spectral estimation in each case demands a different training set.

Instead of color filters, a trichromatic digital camera combined with either absorption filters or multi-illumination can be used [53]. In this study the trichromatic camera was preferred rather than the monochrome camera with interference filters due to cost and complexity. Moreover, spectral estimation was performed with PCA, using either simulated camera signals or measured digital counts, in order to check the performance in both cases, which resulted that the estimation depends on the samples used for PCA. Also, the various combinations of absorption filters did not affect the performance of the spectral reconstruction.

A work, towards the goal of measuring the natural illuminant of skylight was performed from Lopez-Alvarez et al [54] where a liquid-crystal tunable filter (LCTF) was used attached to a monochrome CCD camera. Each band on the LCTF was narrow enough (FWHM 7-15nm) to assume that the radiance information provided when a filter mode is tuned corresponds to a central wavelength only. In association with a previous work [55], where a study was made in order to choose the best method, sensors and linear bases so the SPD of the skylight can be acquired accurately. An optimum number of 5 sensors were selected by using seven transmittance modes on the LCTF, and from the data produced, spectral estimation was performed.

An important factor for the accuracy of spectral estimation, regardless of the method used, is the imaging parameters like noise, spectral sensitivity and the number of the channels, illumination etc. Connah et al [56] studied how these parameters affect the results of image acquisition and in turn spectral estimation and created a mathematical model that proved that the increase of color channels was not by itself sufficient for better accuracy. Moreover, another parameter that can contribute to the accuracy of the system is the use of filters and especially their width. Imai et al [57] focused on whether narrow or wide band filters must be employed for spectral estimation. Tunable filters which were either narrow or broad band were used and a comparative result was produced. It was pointed out that the use of multi-channel systems improves the accuracy of spectral estimation and thus the color reproduction since the phenomenon of metamerism is averted. This study also resulted that narrow and wide–band filters perform similarly, despite the fact that theoretically narrow-band filters give better results and it was remarked that this could be an anomaly and will be further studied.

As aforementioned, illumination is also an important factor in color and spectra reproduction as well as in multispectral imaging in general. For instance, in the work of Hardeberg et al [58] an optimum multispectral system was designed by properly selecting the color filters used (sensitivity and number), the spectral properties of the camera as well as the illuminant according to the statistical properties of the object in question. This multispectral imaging system was designed to obtain multispectral images and estimate the spectra of the object in order to reproduce color that was independent of illumination, thus overcoming the problem of metamerism that conventional cameras have.

In some cases though, the direction of the light source and the angle of the sample in association with the illuminant is of interest, especially if the sample is a non-lambertian surface. Plata et al [59] offered a solution to this problem. If the direction of the light changes the RGB values can change from pixel to pixel. That was why in that case albedo values were used instead of RGB. (Albedo or reflection coefficient, derived from Latin albedo “whiteness" (or reflected sunlight), in turn from albus "white", is the reflectivity or reflecting power of a surface. It is defined as the ratio of reflected radiation from the surface to incident radiation upon it). From the RGB values captured by the camera, the albedo values are calculated and then a linear pseudo-inverse method was employed to estimate the spectra of all the pixel of the image using the albedo values as input. With that way, any highlights or shadows that could be created from the direction of light, and provide false results, are avoided.

Multispectral imaging systems can be also created by utilizing illumination. Chi et al [60] presented a simple method for multi-spectra imaging by using active illumination. A large set of theatrical filters are used and with the use of an algorithm, a combination of them was created in order to match the added illumination and the camera spectral characteristics. Moreover, the effect of ambient lighting can be reduced by introducing a combination of filters in front of the light source that work in conjunction with the camera’s RGB filter set. The above are effective in spectral imaging since unknown or additive illumination on the sample can create difficulties on acquiring accurate reflectance spectra. Park et al [61] proposed another work that utilized illumination to create a multispectral imaging system. Multiplexed illumination created by different LEDs and a RGB camera were used. By testing a combination of LEDs, several multiplexed illumination sets were created. So, rather than changing the spectral sensitivity of the camera (time consuming process) the source’s spectral sensitivity is changed rapidly and by having for example N spectrally distinct illuminations and M camera channels the number of effective channels are M*N. Thus, using the aforementioned system spectral information can be calculated by using the multiplexed illumination in synchronization with the RGB camera and acquiring images for each illumination. Moreover, due to the fact that this process is not time-consuming a real time multispectral video imager has been created that acquires multispectral videos at 30fps using a high speed camera of 120fps.

An also interesting study was that of Nieves et al [62] where the SPD of fluorescent lights was recovered with the use of various algorithms like PCA, Direct pseudo-inverse method, independent Component Analysis (ICA) etc. It was found that the SPD of fluorescent illuminant could be accurately, both spectral and colorimetric, recovered and that by increasing the number of sensors, the better computational results are provided whatever the algorithm used and without needing a priori knowledge of the systems camera sensitivities.

Spectral Estimation can be used in many applications that need spectral reflectance estimated fast, with low cost and good accuracy. For example, Lee et al [63] used spectral estimation, by employing Fourier series and Least Square Estimation algorithm, to approximate two spectral radiance factors needed in order to estimate the color appearance of fluorescent materials that can vary under different illuminations.

An area of high interest for spectral estimation is that of recovering reflectance spectra for digital archiving of art paintings. This is very important since by obtaining the spectra of an art painting, the color of it can be accurately reproduced under any illumination conditions since color can be estimated accurately through the spectrum of the object. In the work of Kaneishi et al [31] spectral estimation was performed with the use of Wiener Estimation. The imaging system used in this case consisted of two CCD cameras and an optimum choice of filters (three to six) for multichannel acquisition. On the concept of art, another application was the identification of pigments used on paintings [64]. From the images taken by a Multispectral system, the reflectance spectra of various parts of the paintings were calculated and then compared with a database containing Japanese pigments reflectance spectra.

Spectral Estimation can be also applied in the field of medical imaging. For example, a Spectrum Endoscope System has been created from Chen et al [65]. This system works using a monochrome CCD, one triple band filter (centers: 415,540,610 nm and FWFM: 20nm) and RGB filters. The filters were placed in front the xenon lamp in a rotating disk so that the light source would generate six illumination lights according to each filter. After obtaining the RGB and triple band values spectral estimation was performed using Wiener Estimation Method. Moreover, in order to accelerate the system video processing time FPGA and DSP were used.

2 Material and Methods

In order to quantify and validate the results of this work, many quantitative measures were used along with various test samples, all of which are reported in this chapter.

2.1 Measures of Spectral Similarity

2.1.1 Root Mean Square Error (RMSE)

In statistics, the mean square error or MSE of an estimator is one of many ways to quantify the difference between an estimator and the true value of the quantity being estimated. MSE is a risk function, corresponding to the expected value of the squared error loss or quadratic loss. MSE measures the average of the square of the "error." The error is the amount by which the estimator differs from the quantity to be estimated. The difference occurs because of randomness or because the estimator doesn't account for information that could produce a more accurate estimate.

$$RMSE = \sqrt{\frac{\sum_{i=1}^{n} \Delta x_i^2}{n}}$$

Where in our study n is the number of spectral channels and x the spectral reflectance vector of one pixel. Dx_i^2 is the squared difference of the i-th channel values of 2 spectra.

2.1.2 Goodness of fit (GFC)

GFC is defined as the cosine of the angle between the recovered signal S^ and original signal S, thus

$$GFC = \frac{\sum_{\lambda=400}^{700} \hat{S}(\lambda) S(\lambda)}{\left(\sum_{\lambda=400}^{700} \hat{S}(\lambda)^2\right)^{1/2} \left(\sum_{\lambda=400}^{700} S(\lambda)^2\right)^{1/2}}$$

2.1.3 Spectral Angle Mapper (SAM)

SAM is a non-parametric supervised classifier. The SAM algorithm considers every pixel of the spectral image as a vector, whose length corresponds to the brightness that this pixel has, and the direction of the vector features the spectral characteristics of the pixel. It can be calculated from:

$$\langle x, y \rangle = \|x\| \|y\| \cos(x, y) \rightarrow$$
$$\theta(x, y) = SAM(x, y) = \cos^{-1}\left(\frac{\langle x, y \rangle}{\|x\| \|y\|}\right), \quad 0 \le \theta \le \frac{\pi}{2}$$

SAM is used for the calculation of the angle between the pixel in question and the reference vectors, uses only the direction of the vector and not its length. That's why SAM is independent of lighting. Also, it is independent to the multiplications of a vector with a natural number since it only increases its length and doesn't change the angle. So, SAM is a non-prosthetic distance function.

2.1.4 Euclidean Distance

In mathematics, the Euclidean distance or Euclidean metric is the "ordinary" distance between two points that one would measure with a ruler, and is given by the Pythagorean formula. By using this formula as distance, Euclidean space (or even any inner product space) becomes a metric space. The associated norm is called the Euclidean norm. Older literature refers to the metric as Pythagorean metric. The Euclidean distance between point p and q is the length of the line segment connecting them ($\overline{\mathbf{pq}}$).

In Cartesian coordinates, if p = (p1, p2... pn) and q = (q1, q2... qn) are two points in Euclidean n-space, then the distance from p to q, or from q to p is given by:

$$\mathrm{d}(\mathbf{p},\mathbf{q}) = \mathrm{d}(\mathbf{q},\mathbf{p}) = \sqrt{(q_1-p_1)^2 + (q_2-p_2)^2 + \cdots + (q_n-p_n)^2} = \sqrt{\sum_{i=1}^{n}(q_i-p_i)^2}.$$

2.1.5 Accuracy Validation Thresholds

In order to quantify the spectral match between the measured and estimated spectra, the aforementioned quantitative measures were used in combination to produce three thresholds that indicate the level of accuracy.

- 1^{st} Threshold:
  - GFC >0.9900
  - Spectral Angle < 0.2 rads
- 2^{nd} Threshold:
  - GFC >0.9950
  - Spectral Angle < 0.1 rads
- 3^{rd} Threshold :
  - GFC >0.9990
  - Spectral Angle < 0.1 rads

The level of accuracy was defined by the following:

Estimation Measures < 1st threshold: Satisfactory or poor
≥ 1st threshold: Good estimation
≥ 2nd threshold: Very good estimation
≥ 3rd threshold: Excellent estimation

2.2 Test Samples

2.2.1 *Gretag Macbeth® Color Checker® CC*

Figure 2-1 Gretag Macbeth Color Checker CC

The Macbeth ColorChecker® is a unique test pattern scientifically designed to help determine the true color balance or optical density of any color rendition system. It is an industry standard that provides a non-subjective comparison with a “test pattern” of 24 scientifically prepared colored squares. Each color square represents a natural object—human skin, foliage, blue sky, etc, providing a qualitative reference to quantifiable values. Each color will reflect light in the same way in all parts of the visible spectrum, thus maintaining color consistency over different illumination options. Some applications include spectroscopy, machine vision, photography, graphic arts, electronic publishing, and television. In our study we use Macbeth ColorChecker mostly as a priori samples. From now on when we present plots we know that Pad 1 is the upper left pad and we increase the number by row. So the last pad is the Black on bottom right which is Pad 24.

2.2.2 *Gretag Macbeth® Color Checker® SG*

The ColorChecker® SG consists of 140 squares of paint applied to paper then mounted to a cardboard backing with a black frame around all the patches. There are 14 columns and 10 rows of patches. All the patches have a semi-gloss surface, which is represented by the SG in the name (Semi-Gloss). The outer patches are a pattern of white, gray and black patches.

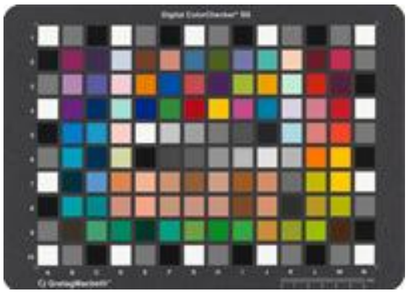

Figure 2-2 Gretag Macbeth Color Checker SG

There is a 6 x 4 pattern of patches which correspond in color to the original ColorChecker®. The spectra and colorimetry of these patches are different from the original ColorChecker® so it cannot be used directly as a profiling substitute for a ColorChecker® without first making a new reference file by measuring this area with a spectrometer.

Just below this 6 x 4 patch area is another row of neutral patches. When combined with three additional gray patches in a nearby column the result is a 15 step neutral scale.

2.2.3 Wooden Pad with pigments with varnish variations

The wooden pad includes a variation of 12 color pigments. For each column these pigments are overlaid with a different type of varnish which alters the spectral and colorimetric values. The values of the pad were measured with Hyper Spectral and Color cameras as well as with a spectrometer.

Finally, is worth noting that the surface of the pigments on the wooden pad are not considered to be a lambertian surface.

2.2.4 Roscolux Films

Roscolux is comprised of two types of plastic. More than 65% of the line is made from co-extruded polycarbonate plastic. The remainder of the line is deep dyed polyester. Sheets: 50 x 61 cm Rolls: 1.2m x 7.62m

How Color Filters Work

Filters create color by subtracting certain wavelengths of color. Thus, a red filter absorbs blue and green, allowing only the red wavelengths to pass. The process is subtractive, not additive, so the light source must emit a full spectrum.

The Rosco swatchbook provides detailed information on the spectral energy curve of each filter. The curve describes the wavelengths of color transmitted through each filter. For example, Roscolux 342 transmits approximately 40% of the violet and blue energy of the spectrum and 75% of the orange and red energy. It absorbs all energy in the yellow and green range.

2.2.5 Variable Frequency Targets

The variable Frequency Targets includes:

- 5 lp/mm to 120 lp/mm or 5 lp/mm to 200 lp/mm
- 1mm Wide Step Size
- 5 lp/mm Step Increments
- Used to Calibrate Video Systems
- Inspect Unknown Resolutions

2.3 Hyper Spectral and Color Cameras

2.3.1 MUSIS Hyper Spectral Camera

MUSIS is a HySI system capable of real time spectral imaging (both reflectance and fluorescence) with high spectral resolution and high throughput ratio, D.Anglos et al [66], C.Balas [67], developed an all-optical imaging monochromator functioning as an electronically tunable narrow band pass optical filter. Displacement of the optical elements of the latter, results in the tuning of the imaging wavelength, which is performed with the aid of electromechanical manipulators controlled from the PC via microcontroller. Mu.SIS HS' Figure 2-3 technical features are:

- Spectral imaging acquisition of 5nm full width half maximum (FWHM), performing in 34 spectral bands of about 20nm each, in the spectral range 360nm (Ultraviolet)–1000nm (Near Infrared).
- Real time capturing & displaying images with an analysis of 1600x1200 pixels.
- Minimum transmittance is 40% across its operational spectral range, which determines the high throughput of the developed monochromator.

- Tuning spectral range of the filtering system is matched with the responsivity spectral range of the charge coupled device (CCD) image sensor, with the capability of extending to longer wavelengths, up to the mid-infrared range (photocathode).
- A megapixel CCD camera, for feeding back the monochromator signal, based on the IEEE-1394 data transferring protocol, capable of acquiring images at a rate of 15 frames/s at full resolution and of more than 30 frames/sat VGA resolution.
- A special calibration procedure [68] is executed before any imaging procedures, compensating for the wavelength dependence of the response of the electro optical parts of the system, such as CCD, illuminators, etc, thus ensuring the full exploitation of the CCD's dynamic range.
- Operating in imaging mode, an image at each wavelength band is acquired while, in spectroscopy mode, a fully resolved diffuse reflectance and/or fluorescence spectrum per image pixel can be recorded (image spectral cube). The combination of spectral and color imaging with calibration enables the system to operate as either Imaging Spectrometer or Imaging Colorimeter.

Figure 2-3 MUSIS HS Camera

2.3.2 xiQ - USB3 Vision Cameras

xiQ is a USB3 Color Vision Camera with low power consumption, high speed, 1600x1200 resolution with 90fps. This CMOS camera will be used for color imaging as well as multispectral imaging by coupling it with Triple Band Pass Filters thus changing the spectral sensitivity of the camera.

In order to acquire correct color and multispectral data, calibration of the camera was performed. Using a white target, the camera was white balanced so all three channels (RGB) would have the same value. Shutter was also adjusted so the images produced would not be saturated.

3 Spectral Prediction from Filtered Color CCD Cameras

In this chapter, the results of the homonymous diploma thesis are described, that constituted the foundation for the results of this work.

Spectral Estimation was studied in depth, and a number of algorithms were chosen to be compared in order to find the more accurate and fast one. To quantify the accuracy of the algorithms, mathematical thresholds were used. Firstly, Gretag Macbeth® Color Checker CC was selected as a priori data and as test set. The goal was to validate the training set so to estimate the accuracy and the speed of the algorithms. Three mathematical measures were used to quantify the similarity of the original and the estimated spectra; the Spectral Angle Mapper (SAM), the Euclidian distance, and the Goodness of Fit (GFC). For an excellent estimation, SAM must be as close to zero as possible and GFC as close to unity.

The RGB data of a color camera, and MUSIS HS, were used to validate the training set. In Table 3-1 the results of this process can be seen. The percentages indicate the number of color patches that surpassed the threshold value indicated. In addition, the time to calculate spectral data for one pixel was measured. The results indicated that Wiener Estimation outperformed the rest of the algorithms in both accuracy and time.

Table 3-1 Spectral Estimation Algorithm Comparison

Algorithm	**Threshold**			**Time**
	One	*Two*	*Three*	
Wiener	75,00%	50,00%	8,33%	0.004710 s
FFT	70,83%	58,33%	8,33%	0.006631 s
PCA	66,67%	50,00%	12,50%	0.016213 s
Wavelets	41,67%	12,50%	0%	0.120807 s
SVD	70,83%	54.17%	4,17%	0.162944 s
Hilbert Trans.	45,83%	37,50%	8,33%	0.012850 s
DCT	65,50%	45,83%	8,33%	0.012850 s

By selecting the best algorithm, the next step was to select the optimum number of bands, within the visible spectrum, that would procure the highest possible accuracy. After testing multiple combinations of RGB and narrow spectral bands data it was concluded that six narrow spectral bands (460-480-540-560-640-680nm) increased the accuracy as it can be seen in Table 3-2.

Table 3-2 Spectral Estimation using Narrow Spectral Bands

	Threshold		
	One	*Two*	*Three*
Wiener with RGB Input	75,00%	50,00%	8,33%
Wiener with Six Narrow Band Input	91,67%	83,33%	50,00%

4 Spectral Estimation of Unknown Samples

After validating the training sample as described above, the need to validate the performance of that work in unknown samples (no a priori knowledge) was at hand. For this purpose four different type of samples will be used:

- Gretag Macbeth® Color Checker SG
- Pigments Wooden Pad with varnish variations
    - Microscopy Data - Roscolux Swatchbook

For all of the above test sets, Gretag Macbeth® Color Checker CC was used as a priori knowledge and training set of the system. Since a six narrow band system was used, the a priori data contain the spectral information of Macbeth as well as the six narrow spectral band data. Under the same premise, the input data for each test set contain six spectral bands and are reproduced and validated within the visible region of the electromagnetic spectrum. Moreover, since every sample used contains a substantial number of color patches, the data are presented in multiple figures (i.e. Macbeth SG needed 7 figures).

4.1.1 Gretag Macbeth® Color Checker SG Spectral Estimation Results

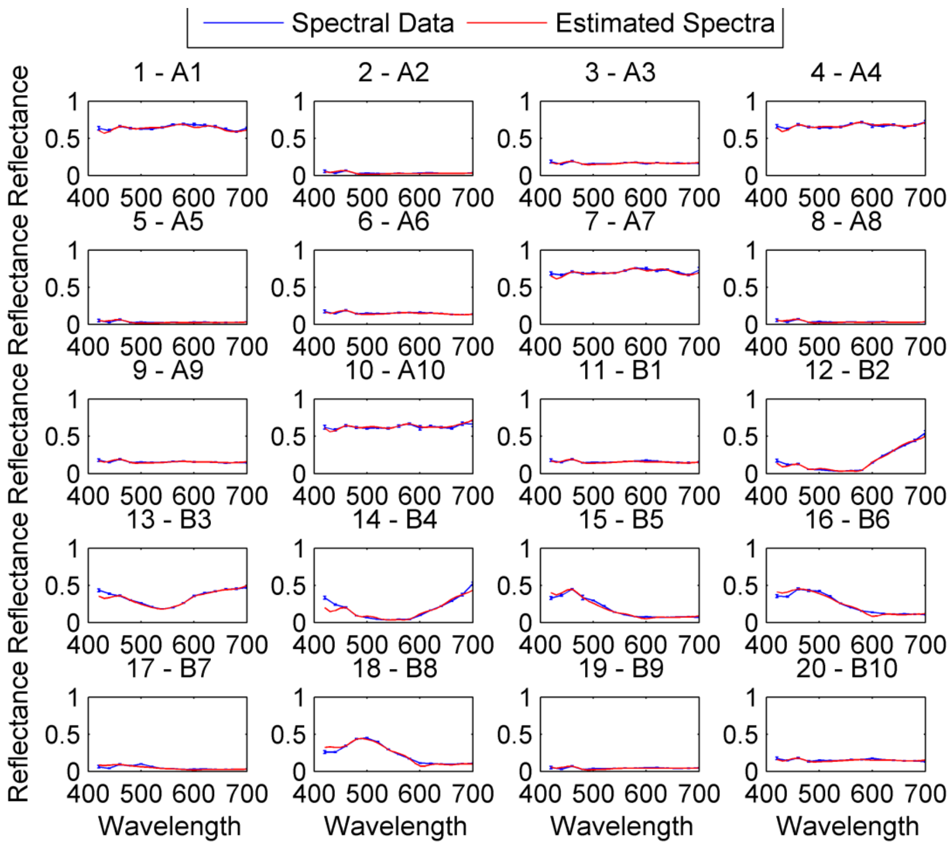

Figure 4-1 Spectral Estimation Macbeth SG (1)

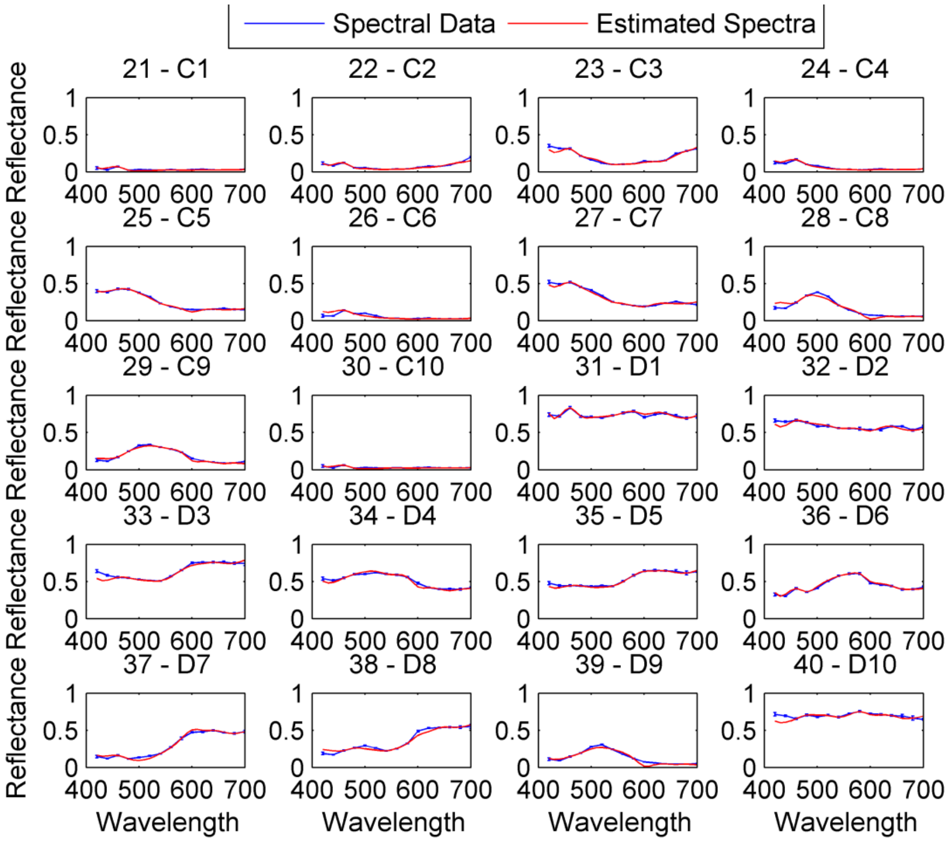

Figure 4-2 Spectral Estimation Macbeth SG (2)

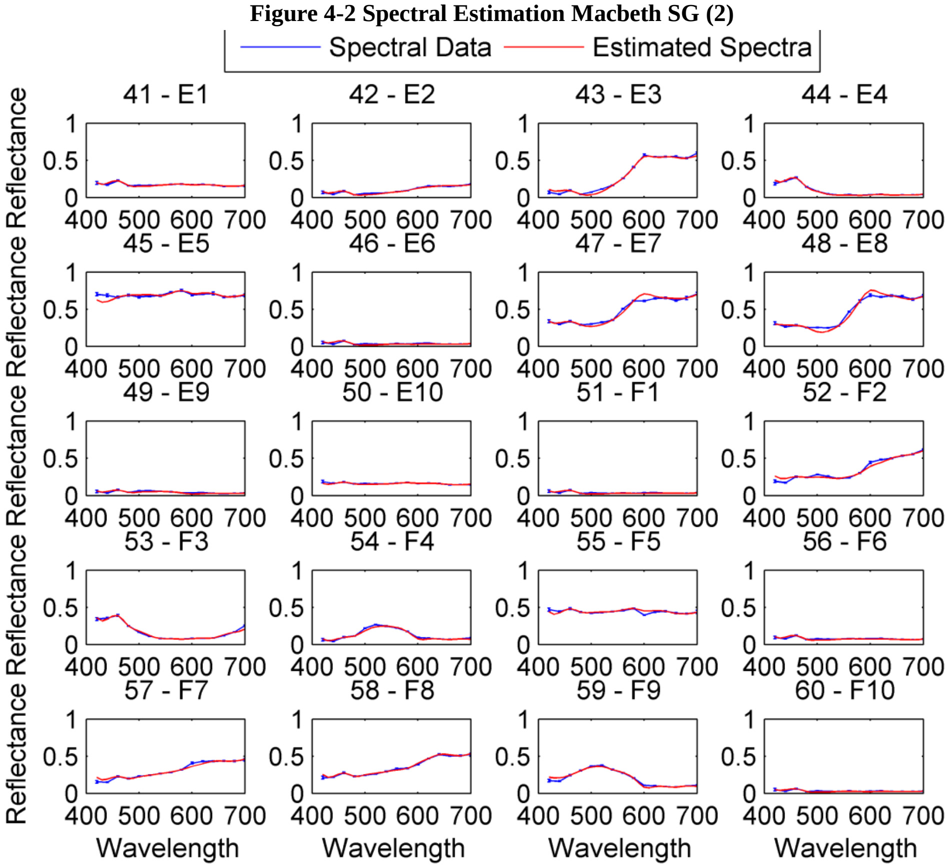

Figure 4-3 Spectral Estimation Macbeth SG (3)

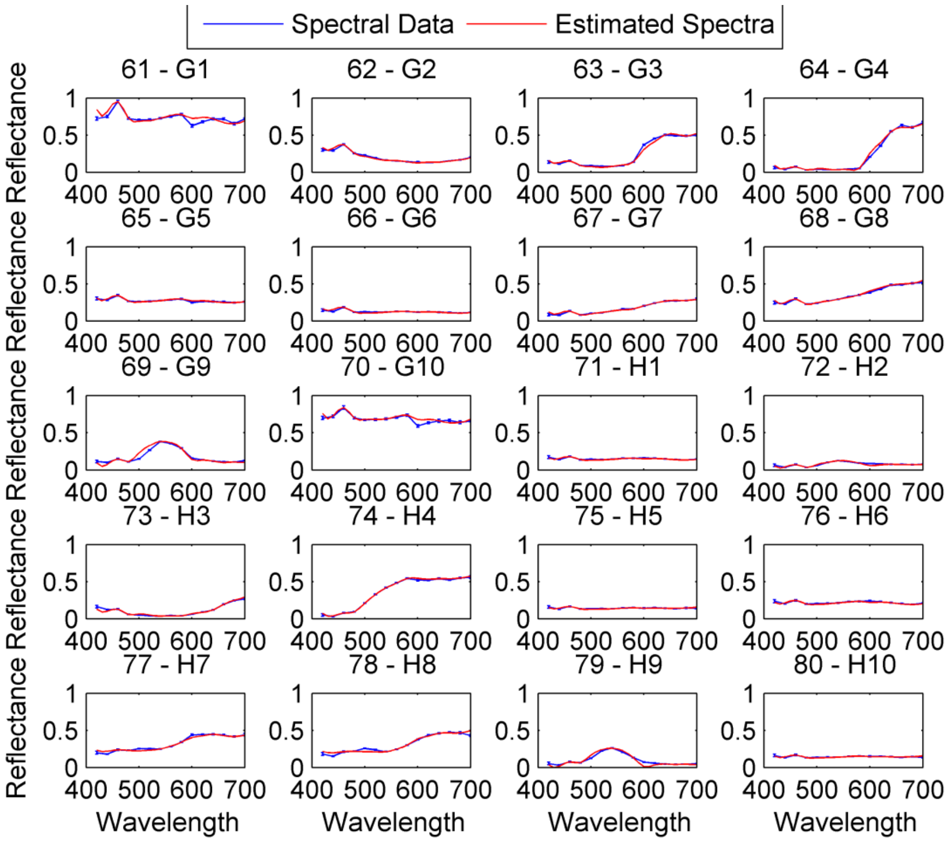

Figure 4-4 Spectral Estimation Macbeth SG (4)

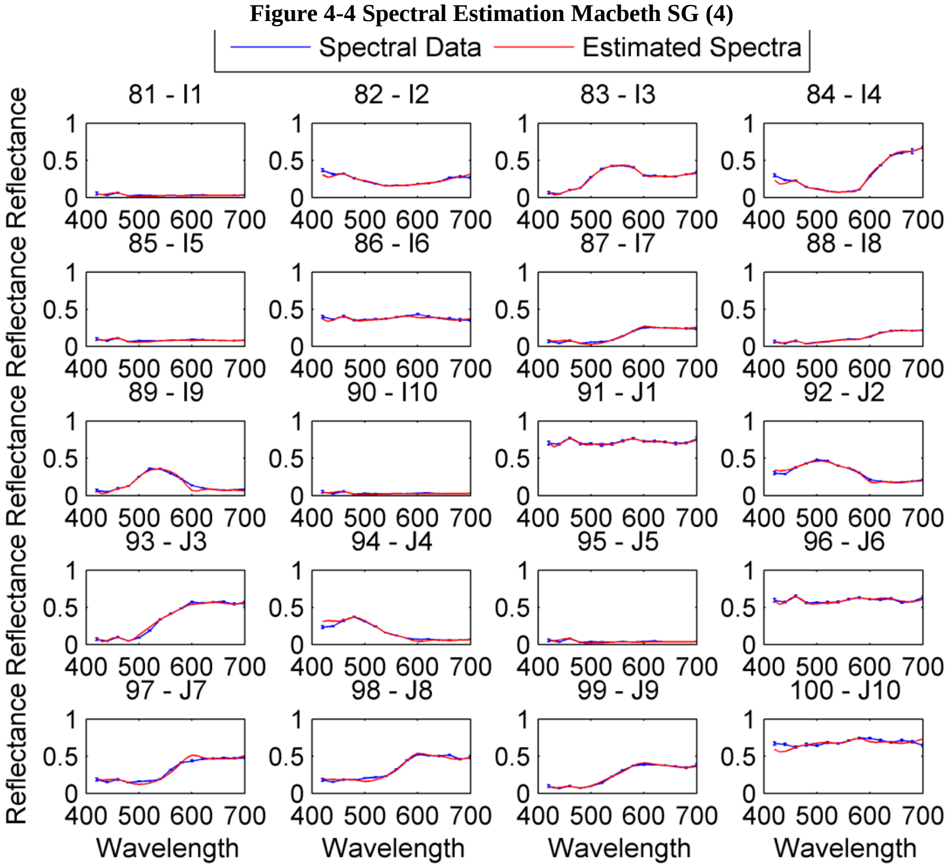

Figure 4-5 Spectral Estimation Macbeth SG (5)

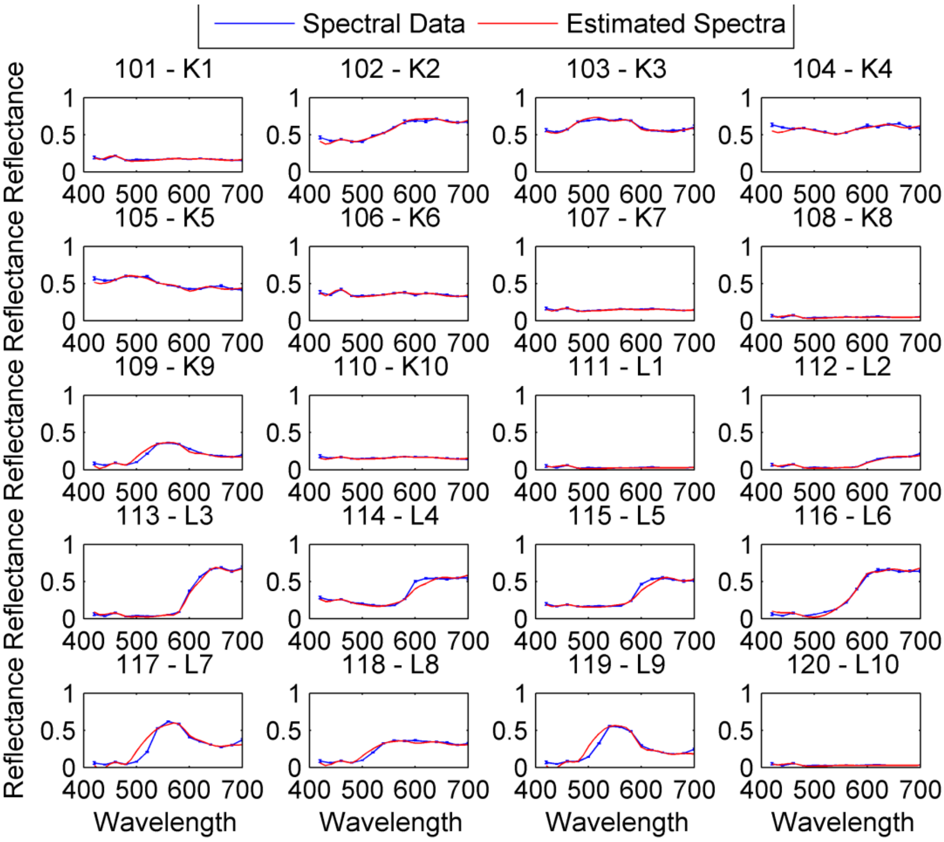

Figure 4-6 Spectral Estimation Macbeth SG (6)

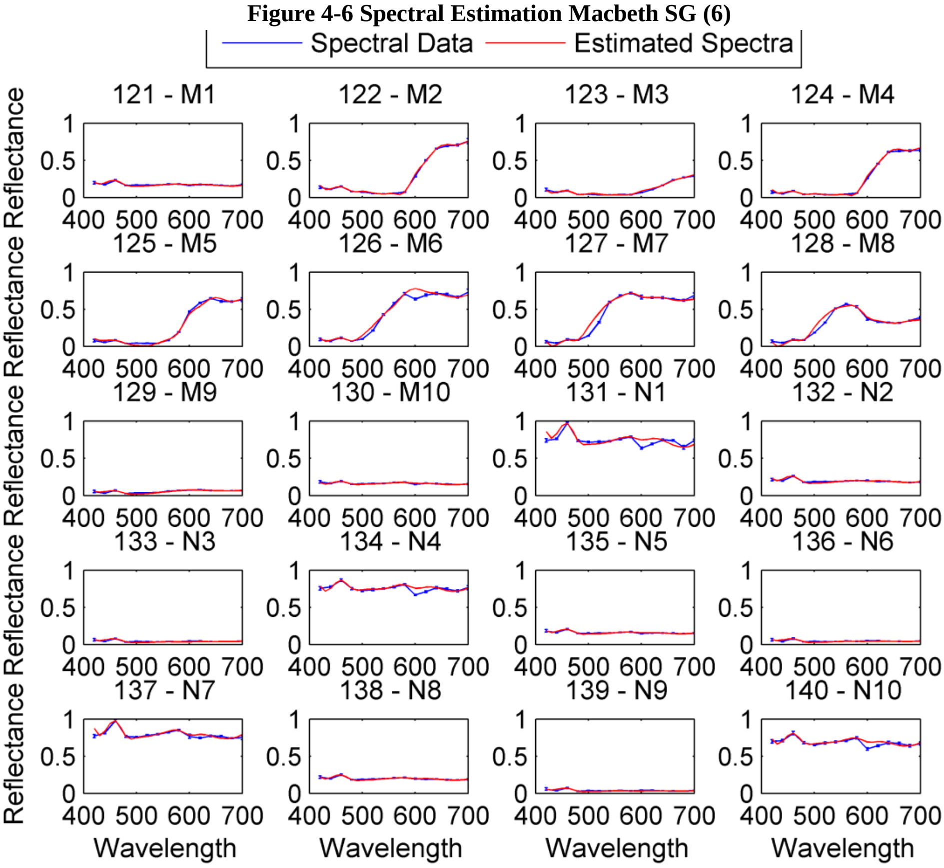

Figure 4-7 Spectral Estimation Macbeth SG (7)

From Figure 4-1 to Figure 4-7 all 140 color patches of Macbeth SG can be seen. The blue line represents the measured spectra, acquired from MUSIS HS camera. The value of each patch is the mean of approximately 2000 pixels and is represented with the mean and standard deviation values using errorbars. From the above, it can be seen that with 24 patches as a priori knowledge, Macbeth SG was estimated with high accuracy, predicting all of the spectral characteristics of each patch, which can also be validated from the quantitative result in Table 4-1.

Table 4-1 Macbeth SG Spectral Estimation Quantitative Results

	Threshold		
	One	*Two*	*Three*
Macbeth Color Checker SG	87,50%	74%	24%

Next up, the spectral image for the complete Macbeth SG was estimated. Macbeth was captured and estimated in four quadrants, each one containing 35 color patches. The difference between the estimated and the predicted spectral images was calculated with the RMSE and their subtraction and can be seen in Figure 4-8 - Figure 4-11. In each figure the measured spectral image can be seen in the left column, the estimated on the middle one and their difference on the right column. As expected, the RMSE of the Bands used as input equals zero. On the other two cases a small RMSE can be noticed and their difference mainly depends on the spectral signature of the color patch as it can be easily seen in Figure 4-11 for the first case.

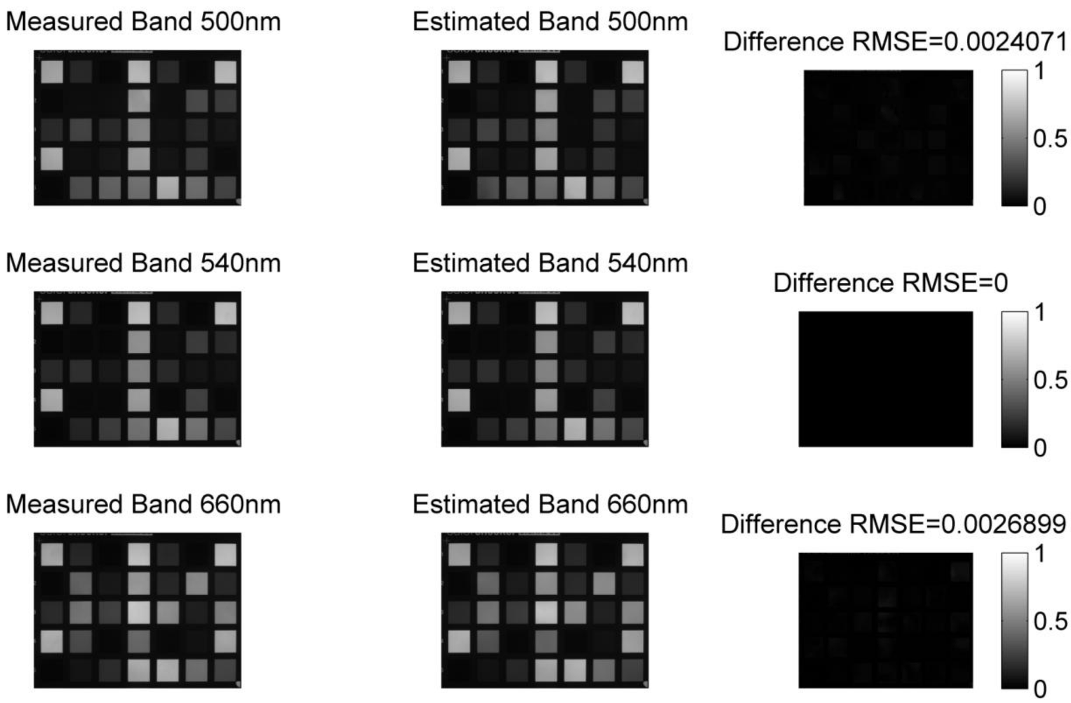

Figure 4-8 Macbeth SG 1st Quadrant Spectral Image Estimation

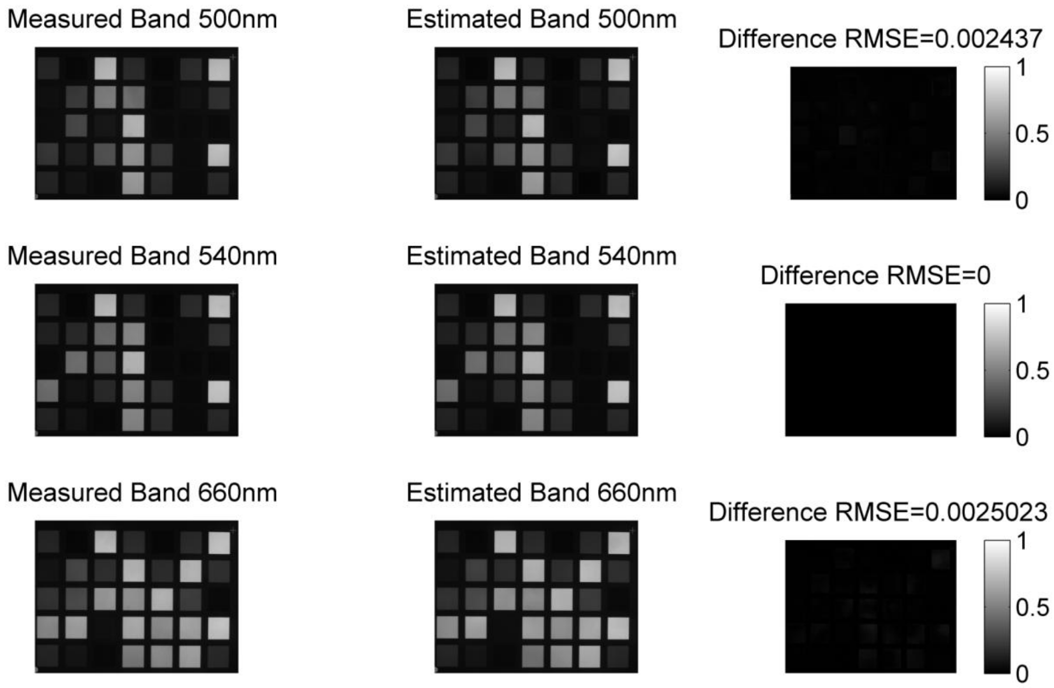

Figure 4-9 Macbeth SG 2nd Quadrant Spectral Image Estimation

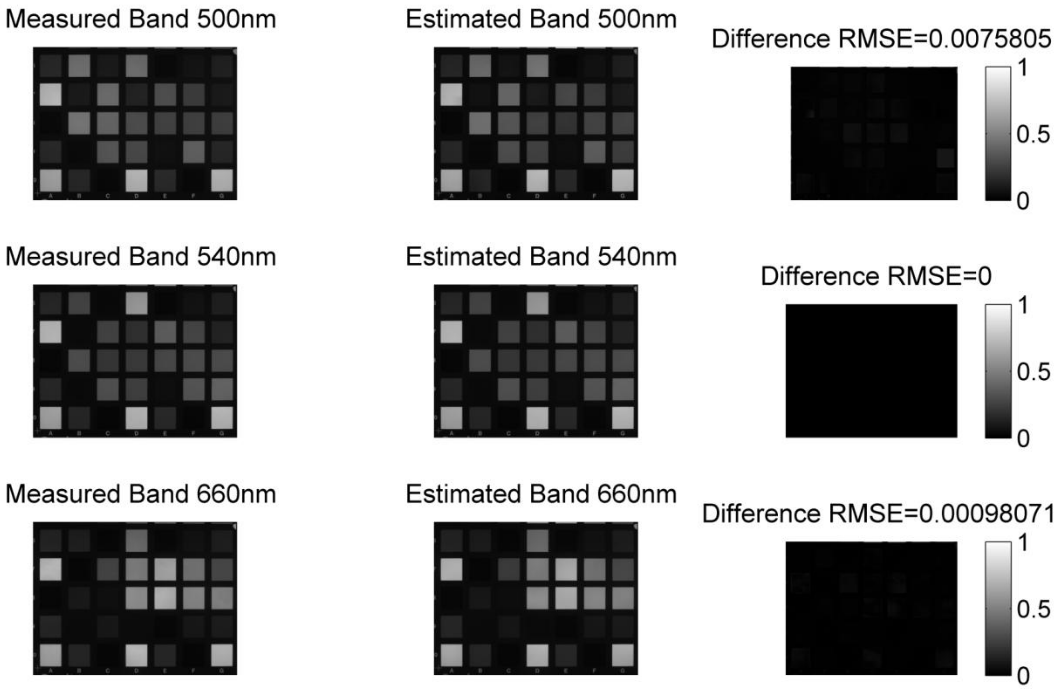

Figure 4-10 Macbeth SG 3rd Quadrant Spectral Image Estimation

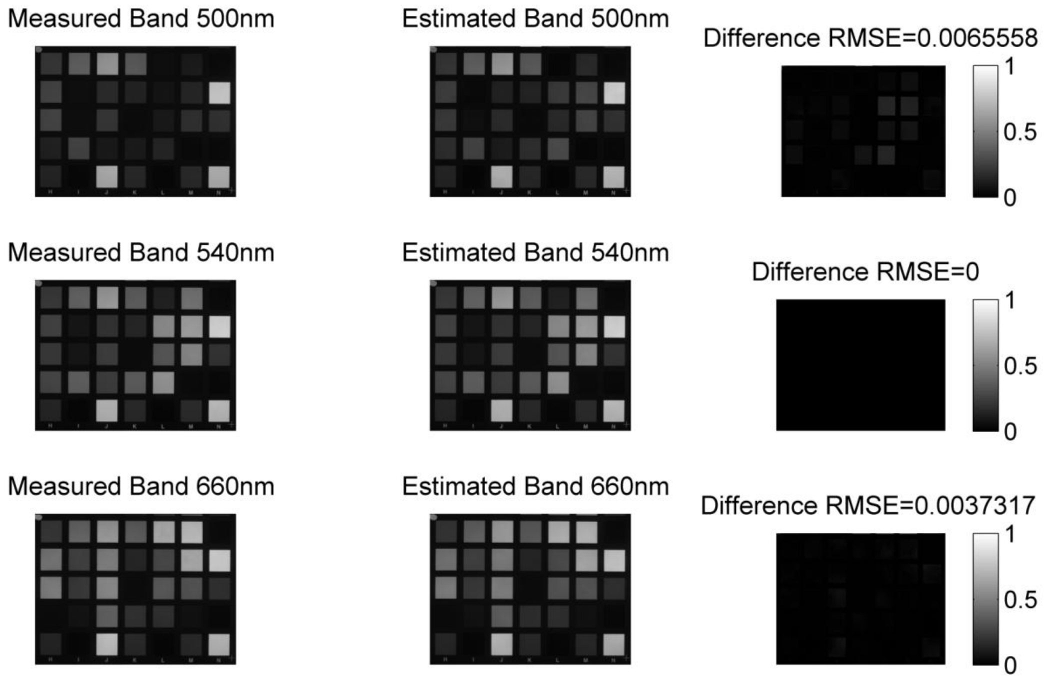

Figure 4-11 Macbeth SG 4th Quadrant Spectral Image Estimation

4.1.2 Pigments Wooden Pad with varnish variations

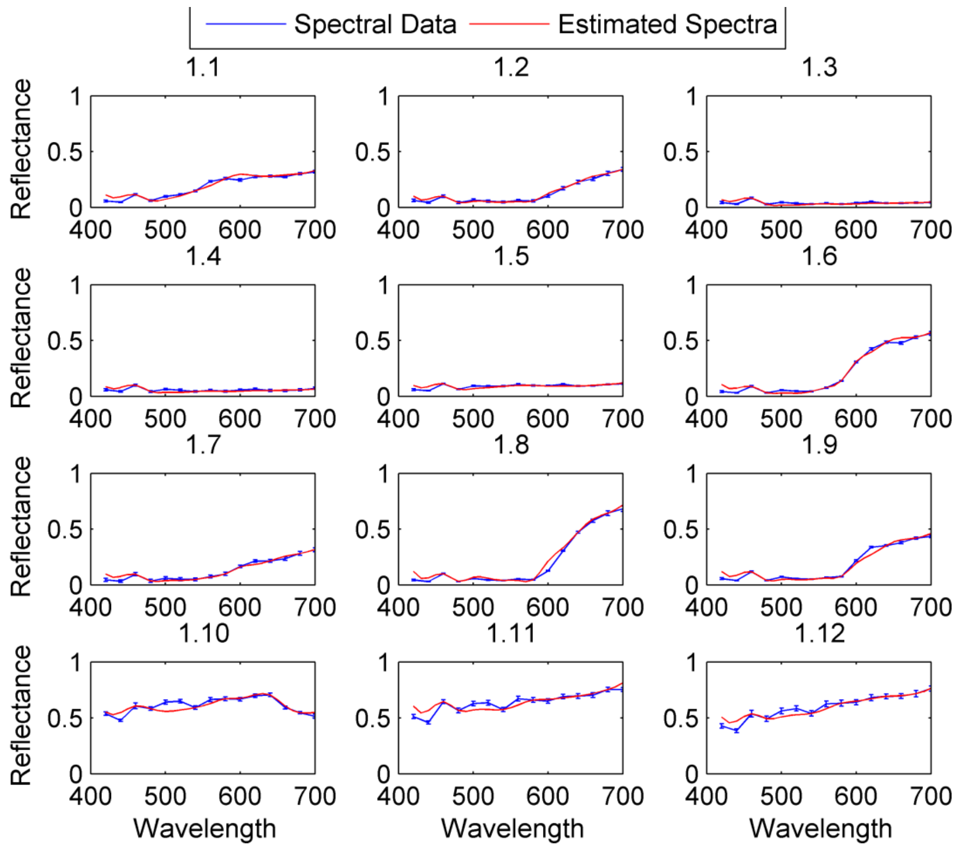

Figure 4-12 Spectral Estimation (Visible) Wooden Pad with Varnish (1)

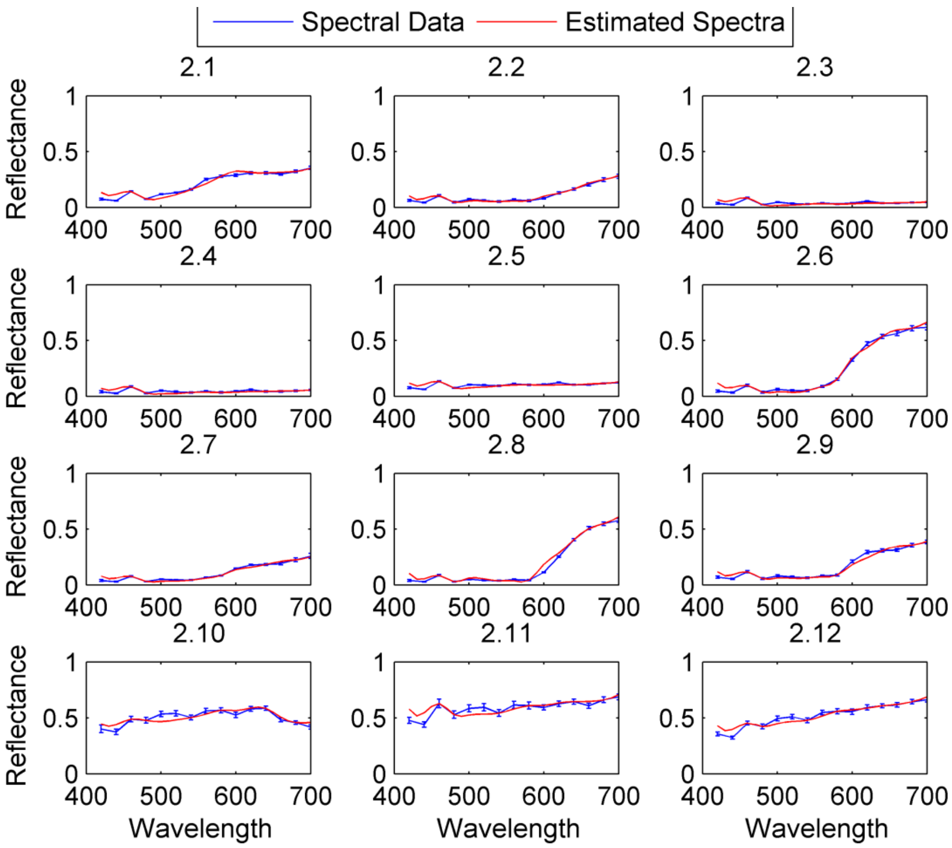

Figure 4-13 Spectral Estimation (Visible) Wooden Pad with Varnish (2)

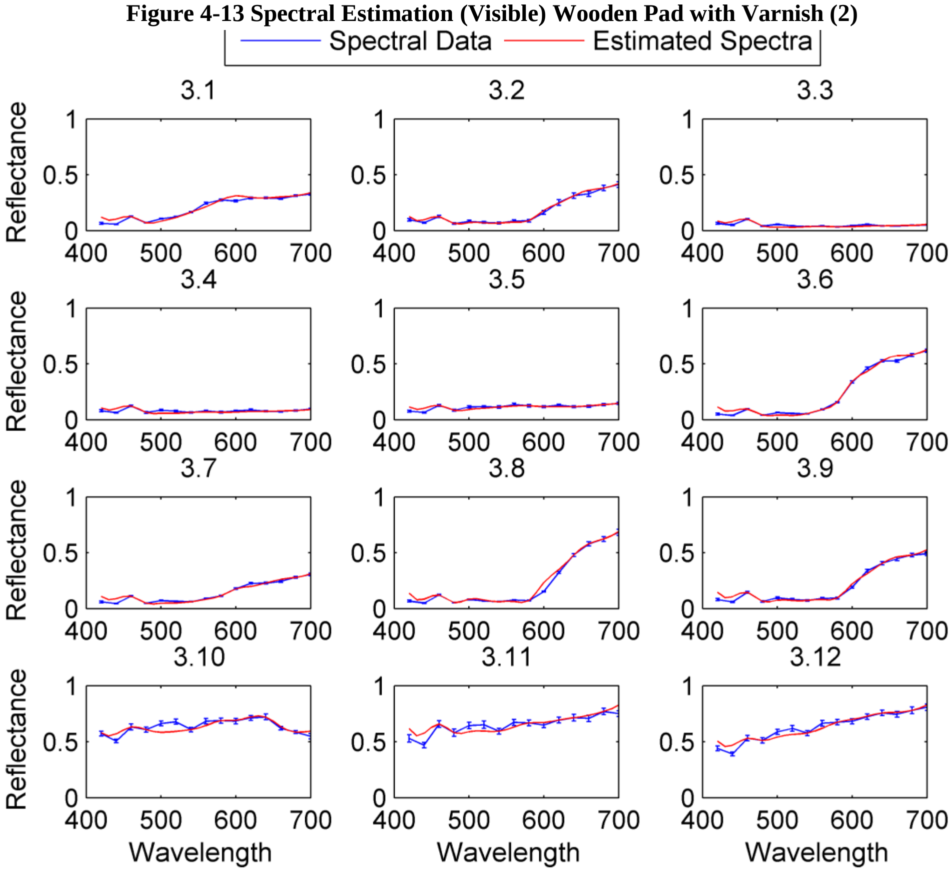

Figure 4-14 Spectral Estimation (Visible) Wooden Pad with Varnish (3)

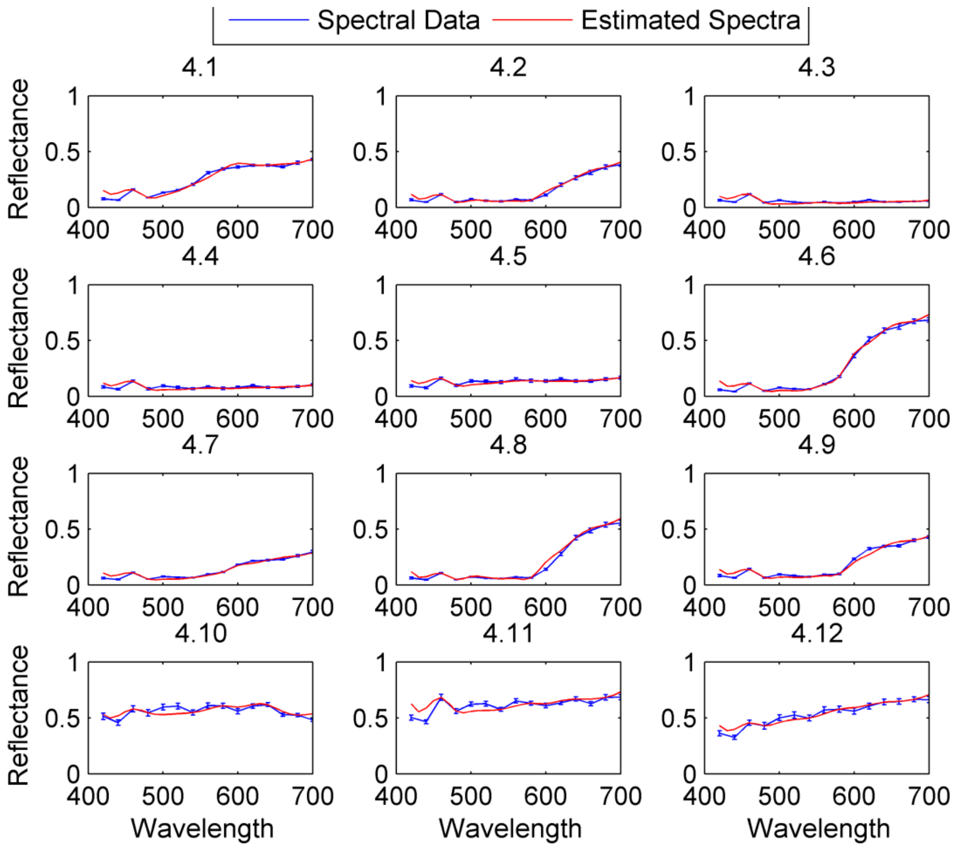

Figure 4-15 Spectral Estimation (Visible) Wooden Pad with Varnish (4)

From Figure 4-12 to Figure 4-15 it can be seen that the spectral estimation procedure managed to predict most of the spectral characteristics of the sample. It is crucial to explain that the color patches of this test set are pigments that are not considered to be lambertian surface and have completely different texture than Gretag Macbeth® Color Checker CC that was used as the training set, which highly increased the error during the estimation process. This can be also seen in Table 4-2 where no color patch qualified to surpass the third threshold while more than half of the color patches qualified for the first two, meaning that most of the spectra were estimated with good accuracy.

Table 4-2 Wooden Pad Spectral Estimation Quantitative Results

	Threshold		
	One	*Two*	*Three*
Pigments Wooden Pad	77%	50%	0%

4.1.3 Roscolux Films

In Figure 4-16 spectral estimation was performed in Roscolux color filters. The first thing to address here is that for the first time Spectral Transmittance was evaluated instead of Spectral Reflectance. It can be seen that the spectral estimation procedure managed to predict most of the spectral characteristics of the samples. Again, Gretag Macbeth® Color Checker® CC was used as the training set, although the data were reflectance spectra.

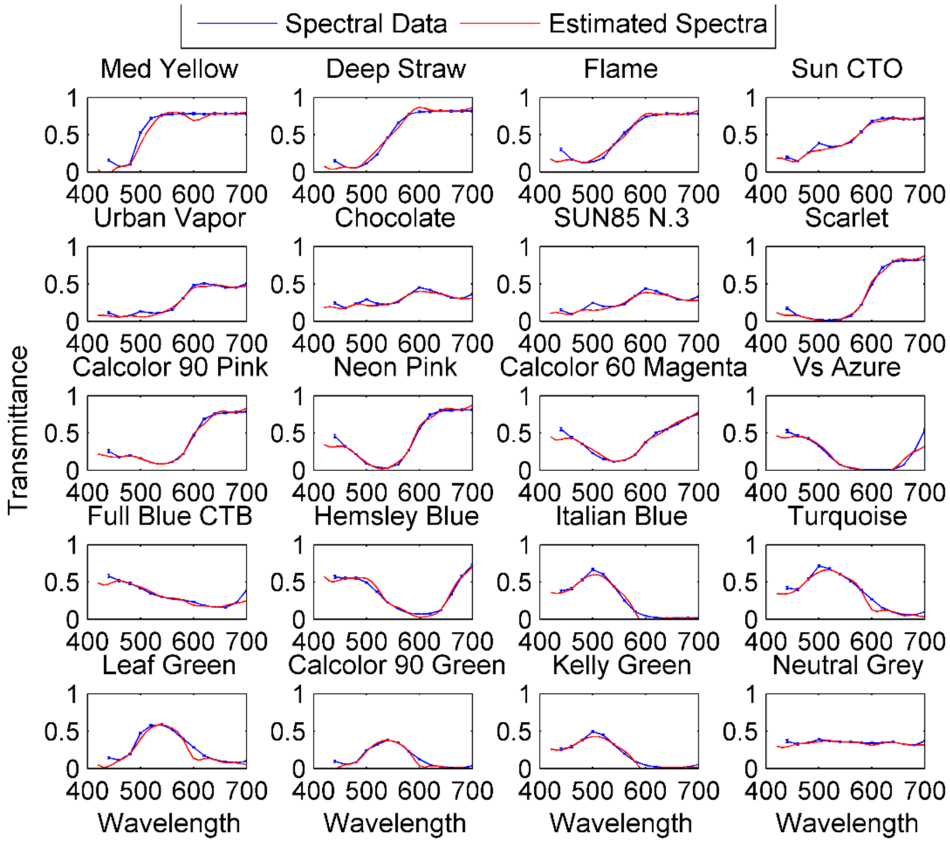

Figure 4-16 Spectral Estimation (Visible) Roscolux films

In Table 4-3 the quantitative results of the estimation process can be seen. The first threshold was met by 75% of the samples and the second was met for more than half of them. The third threshold, indicating the "excellent" estimation, is zero which was expected since the a priori data were from reflectance spectrum whereas the estimated spectra were transmittance.

Table 4-3 Roscolux Films Spectral Estimation Quantitative Results

	Threshold		
	One	*Two*	*Three*
Roscolux Films	75%	55%	0%

5 Spectral Estimation Visible and Near Infrared

Until now, spectral estimation was performed within the visible region of the electromagnetic spectrum. For various applications like astronomy, industry, chemistry and so forth, information within the near infrared part of the spectrum are necessary. As before, it was crucial to determine the number of spectral bands needed that can provide accurate results. In addition, the ability to estimate spectral information in the NIR will be added to the spectral estimation process for the visible region, thus creating a multispectral system that can acquire a fixed number of bands and estimate spectra in both visible and NIR regions.

Again, for testing and validation procedures, Gretag Macbeth® CC was used as training, only this time the information extended to the NIR part of the spectrum. Gretag Macbeth® SG and the Pigments Wooden Pad were used to validate the accuracy of spectral estimation. For each case, four different cases are presented that correspond to the thresholds set for the Quantitative characterization of the results. First graph represents an estimation that doesn't satisfy any threshold, the second one satisfies the first one and so forth.

5.1 Spectral Estimation using 12 Narrow Spectral Bands

For the visible region, from 420nm to 700nm, six narrow spectral bands were used that were complementary to each other covering approximately 300nm. In the same premise, from 700nm to 1000nm, six narrow spectral bands are selected equally distributed within NIR. So, in addition to 460, 480, 540, 580, 640, 680 nm for the visible region, 740, 780, 840, 880, 940, 980 nm were added for the NIR.

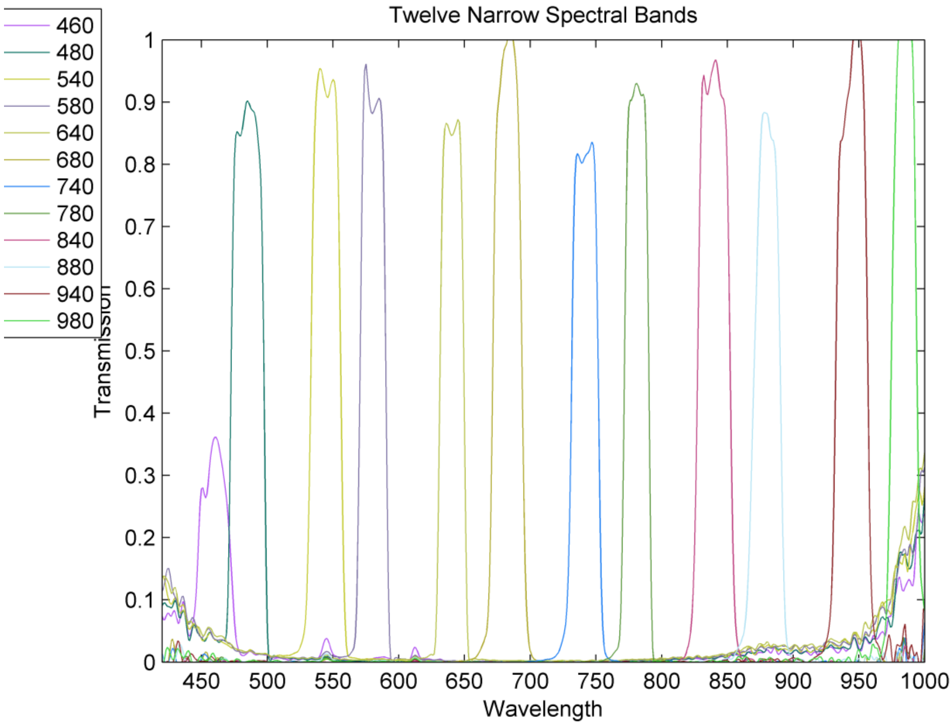

Figure 5-1 Twelve Spectral Bands for Spectral Estimation within the Visible and NIR

5.1.1 Gretag Macbeth® Color Checker SG Spectral Estimation Results

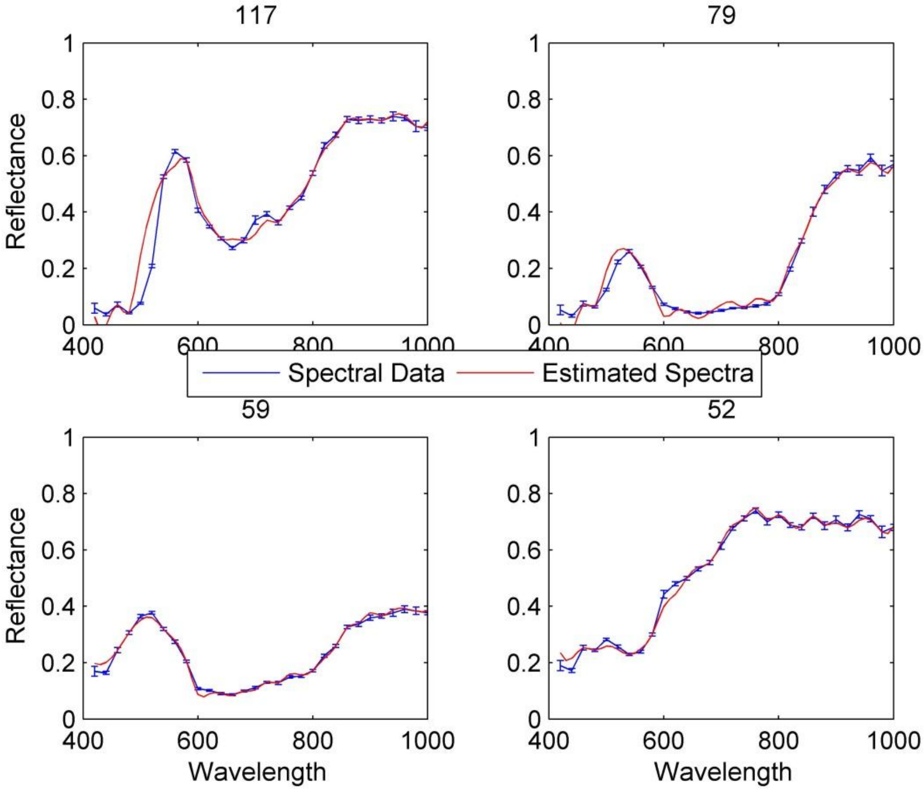

Figure 5-2 Spectral Estimation (12 Bands) Visible and NIR Macbeth SG

In Figure 5-2 it can be seen that the spectrum in both regions of the spectrum can be estimated with very high accuracy. Even in sub-figure one that the result doesn't satisfy any threshold, it can be seen that the estimated spectrum is a good approximation of the measured one. The accuracy of the results can be also verified from the quantitative measures presented in Table 5-1, where the first threshold for the first time reaches 100% and the other two reach their maximum value so far as well.

Table 5-1 Macbeth SG Spectral Estimation (12 Bands) Visible and IR Quantitative Results

	Threshold		
	One	*Two*	*Three*
Macbeth Color Checker SG 12 Bands	100%	95.83%	61.5%

It is crucial to point out that again only 24 patches were used as training set and 140 patches were predicted with excellent accuracy. A next to step is to minimize the number of bands used and check how that affected the results of the spectral estimation.

5.1.2 Pigments Wooden Pad with varnish variations

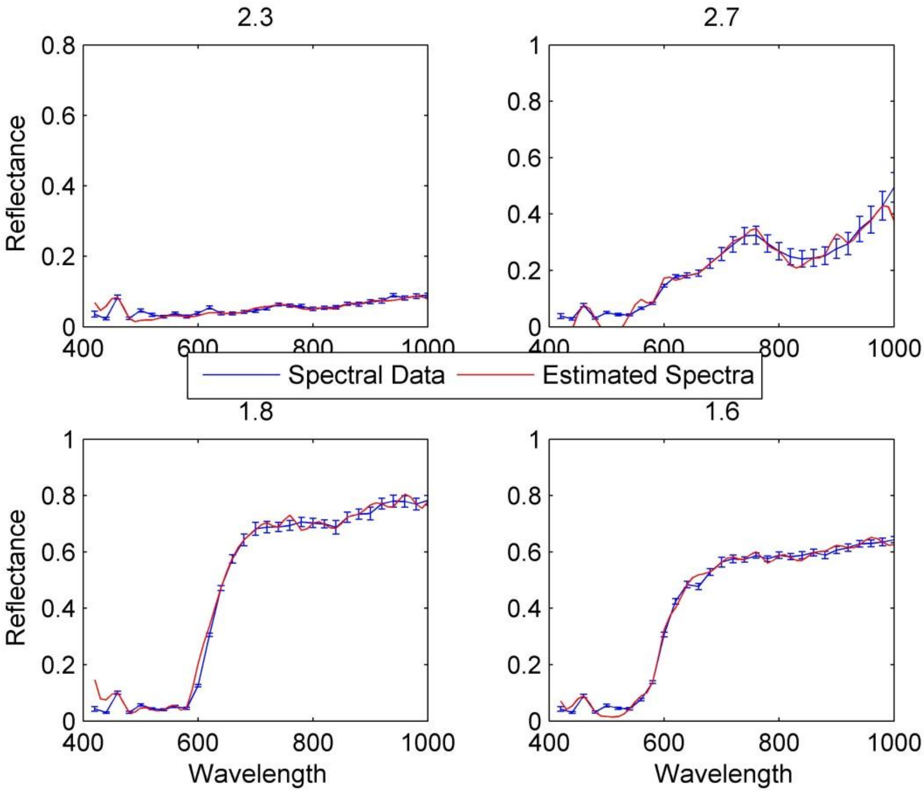

Figure 5-3 Spectral Estimation (Visible and NIR 12 Bands) Wooden Pad with Varnish

In Figure 5-3 it can be seen that the spectrum in both regions of the spectrum can be estimated with very high accuracy. All spectral characteristics of the color patches were predicted with high precision despite the fact, as aforementioned, that the surface of the color patches is not considered lambertian. This can be also seen in Table 5-2 where the percentage of patches satisfying each threshold increased significantly about 20%.

Table 5-2 Wooden Pad Spectral Estimation (12 Bands) Visible and NIR Quantitative Results

	Threshold		
	One	*Two*	*Three*
Pigments Wooden Pad 12 Bands	95.8%	79%	18.7%

All of the above suggest that spectral estimation can be performed accurately in both visible and NIR. One important characteristic to note is that both Gretag Macbeth® SG and the wooden pad contain color patches that have very smoothed spectral reflectance within the NIR. This means that with less spectral bands, high accuracy results can be also achieved. So, in order to validate that assumption, a minimization of the spectral bands used in the NIR will be performed and the result will be compared at the end.

5.2 Spectral Estimation using 11 Narrow Spectral Bands

In this case 11 narrow spectral bands were used. Six for the visible region as before and 5 for the NIR; 740-800-860-920 and 980nm and are presented in Figure 5-4.

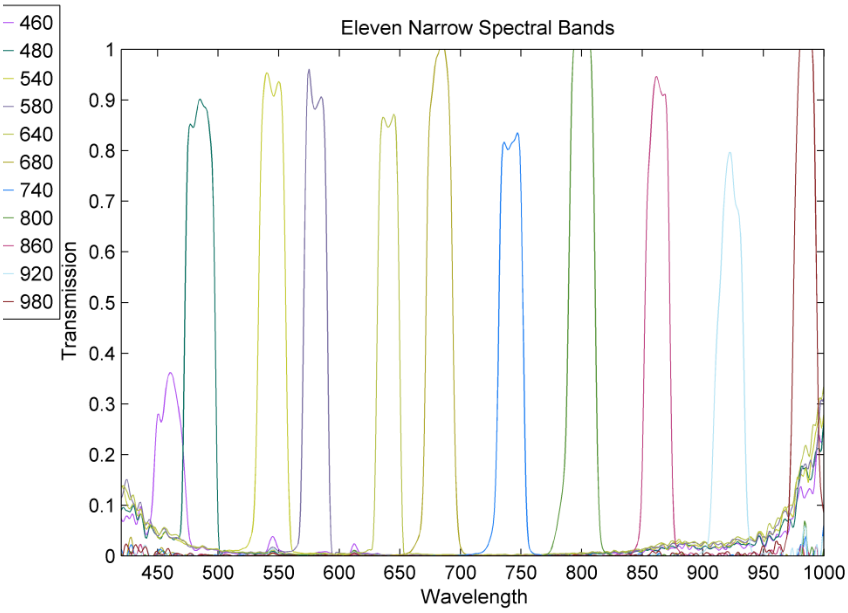

Figure 5-4 Eleven Spectral Bands for Spectral Estimation within the Visible and NIR

5.2.1 Gretag Macbeth® Color Checker SG Spectral Estimation Results

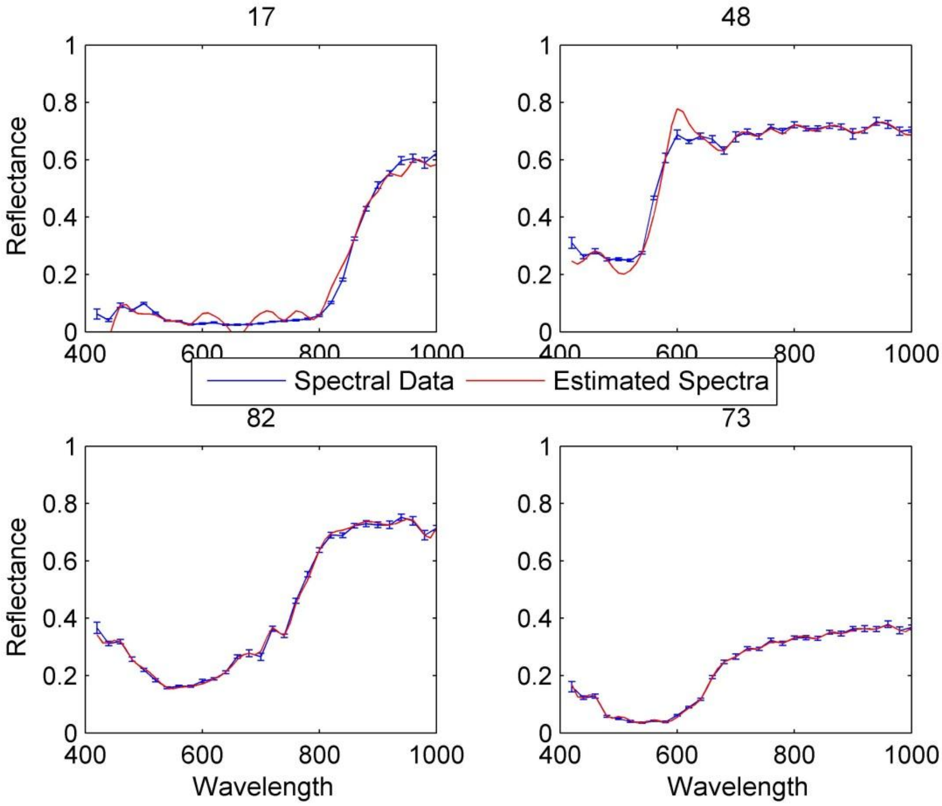

Figure 5-5 Spectral Estimation (11 Bands) Visible and NIR Macbeth SG

In Figure 5-5 Figure 5-2it can be seen that the spectrum in both regions of the spectrum can be estimated with very high accuracy. Even in sub-figure one that the result doesn't satisfy any threshold, it can be seen that the estimated spectrum is a good approximation of the measured one. The accuracy of the results can be also verified from the quantitative measures presented in Table 5-3, where the percentages for the thresholds were approximately of the same, with a small decline of 1-2%.

Table 5-3 Macbeth SG Spectral Estimation (11 Bands) Visible and IR Quantitative Results

	Threshold		
	One	*Two*	*Three*
Macbeth Color Checker SG 11 Bands	97.9%	93.7%	60.4%

5.2.2 Pigments Wooden Pad with varnish variations

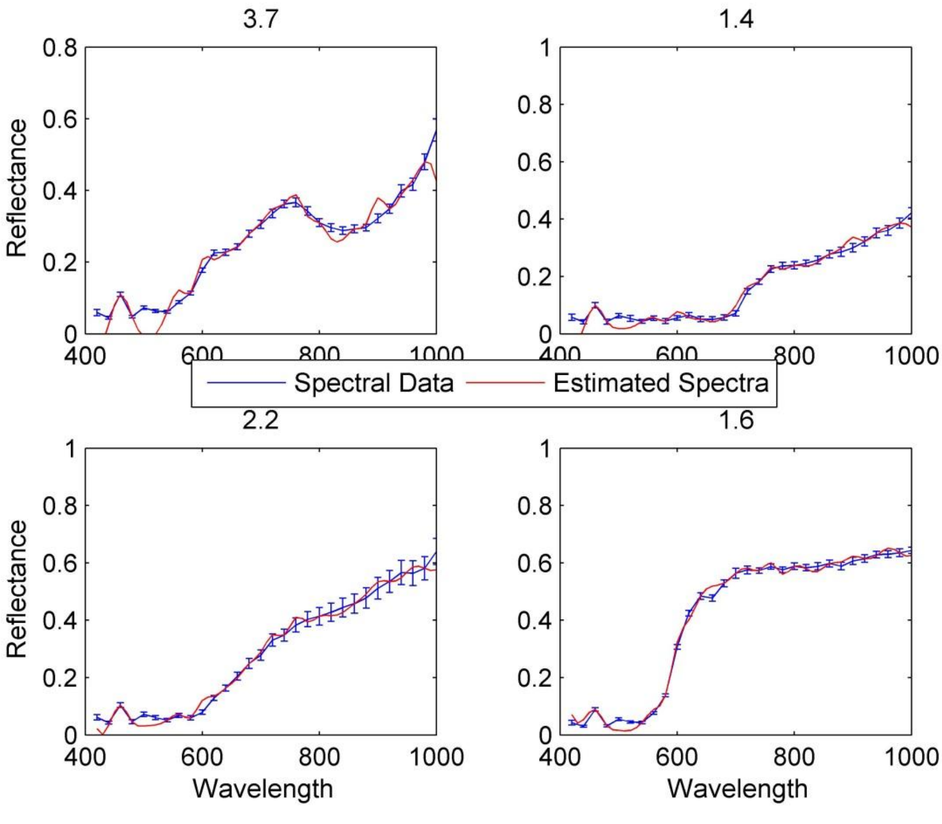

Figure 5-6 Spectral Estimation (Visible and NIR 11 Bands) Wooden Pad with Varnish (1)

In Figure 5-6 it can be noticed that the spectral estimation was performed accurately for both regions of the spectrum as before. All spectral characteristics of the color patches were predicted with high precision. This can be also seen in Table 5-4 where the percentage remained approximately the same as before with a small decline of 2% for the second threshold and about 10% for the first, maintaining however their high value.

Table 5-4 Wooden Pad Spectral Estimation (11 Bands) Visible and NIR Quantitative Results

	Threshold		
	One	*Two*	*Three*
Pigments Wooden Pad 11 Bands	85,41%	75%	18.7%

In this case, where 11 narrow spectral bands were used, the accuracy of the estimation algorithm remained very high, which allowed further investigation by removing one more band to see the affect it would have on the overall performance.

5.3 Spectral Estimation using 10 Narrow Spectral Bands

In this case 10 narrow spectral bands were used; six for the visible region as before and 4 for the NIR; 740-820-900 and 980nm and are presented in Figure 5-7. As the number of bands with the NIR is narrowed down, the bands were selected empirically so they could cover the highest possible range within the NIR region.

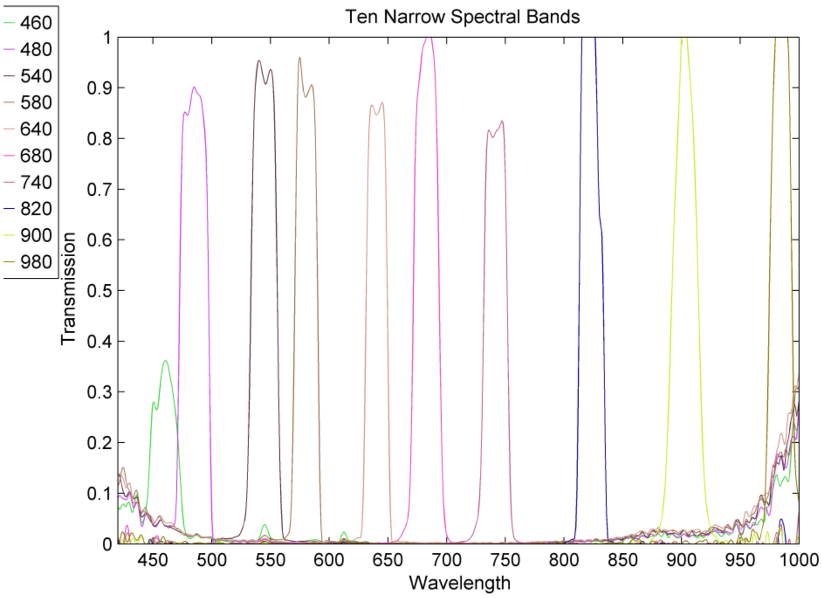

Figure 5-7 Ten Spectral Bands for Spectral Estimation within the Visible and NIR

5.3.1 Gretag Macbeth® Color Checker SG Spectral Estimation Results

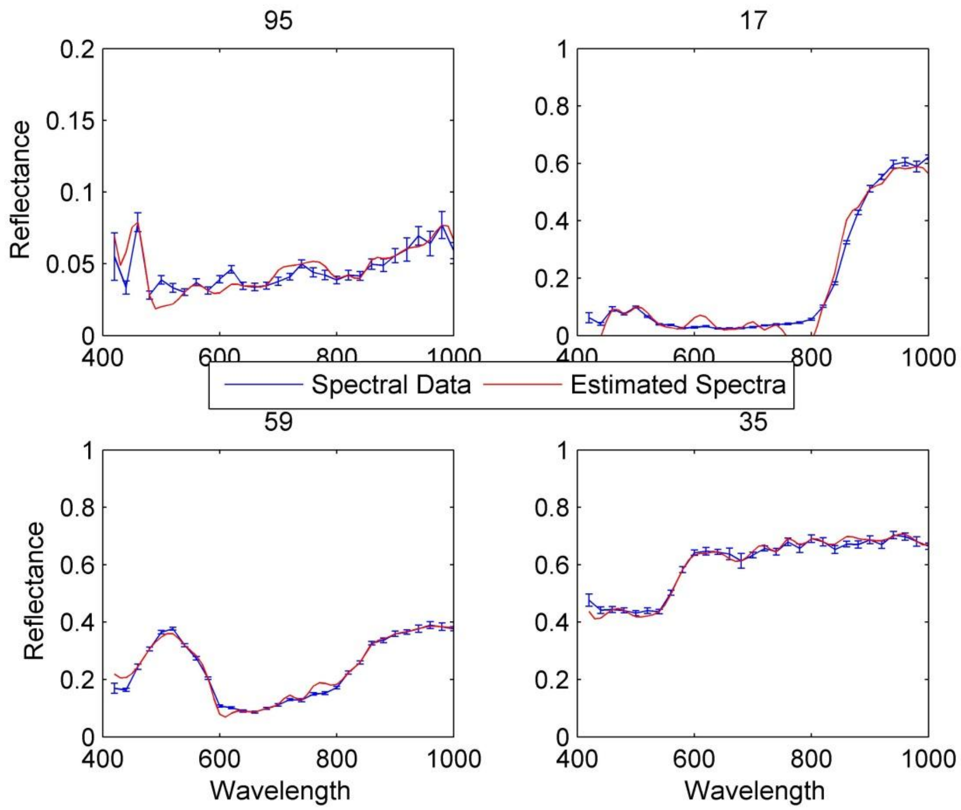

Figure 5-8 Spectral Estimation (10 Bands) Visible and NIR Macbeth SG

In Figure 5-8 it can be seen that the spectrum in both regions of the spectrum is estimated with very high accuracy. Even in sub-figure one that the result doesn't satisfy any threshold, it can be seen that the estimated spectrum is a good approximation of the measured one. For the third time all the spectral characteristics are predicted properly, either smoothed or with sparks, even though only 4 bands are now used in NIR region. That can be also verified from the quantitative measures presented in Table 5-5, where the percentages for the thresholds were approximately of the same with ±1% deviation.

Table 5-5 Macbeth SG Spectral Estimation (10 Bands) Visible and IR Quantitative Results

	Threshold		
	One	*Two*	*Three*
Macbeth Color Checker SG 10 Bands	97.9%	92.7%	61.4%

5.3.2 Pigments Wooden Pad with varnish variations

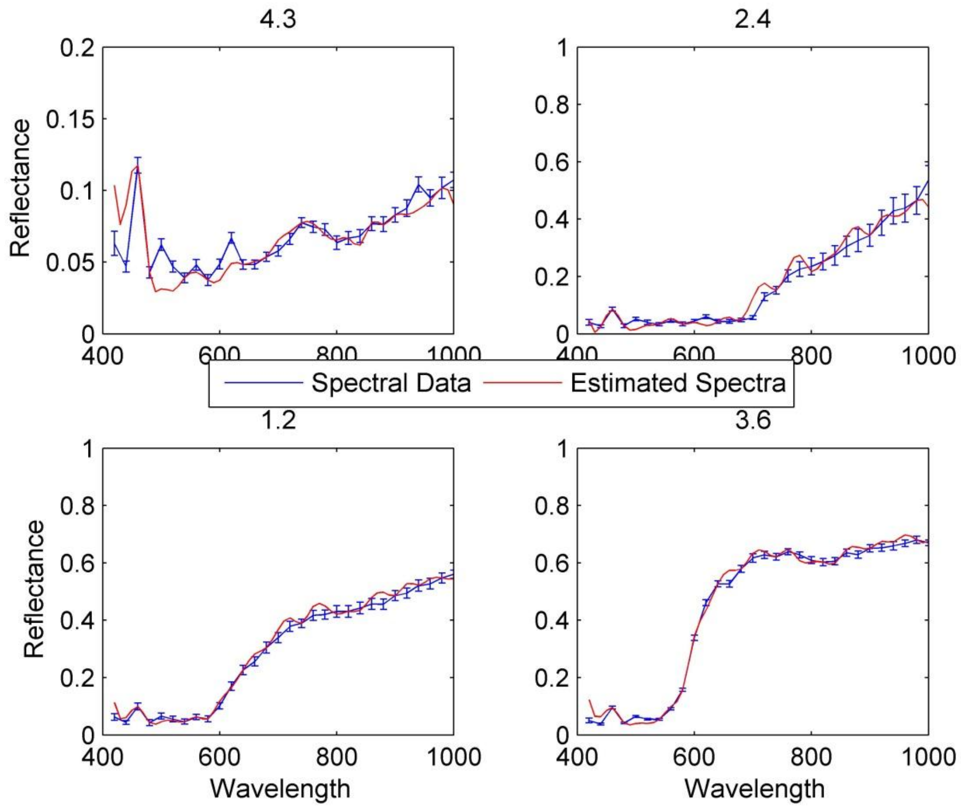

Figure 5-9 Spectral Estimation (Visible and NIR 10 Bands) Wooden Pad with Varnish (1)

In Figure 5-9 can be noticed that the spectral estimation was performed accurately for both regions of the spectrum as before. All spectral characteristics of the color patches were predicted with high precision. This can be also seen in Table 5-6 where the percentage remained high for the first threshold, increased for the second and declined about 10% of the third. The decline of the third threshold can be noticed in the figures from the fact that in some case the estimated spectra might have deviated more than the errorbars' margin.

Table 5-6 Wooden Pad Spectral Estimation (10 Bands) Visible and NIR Quantitative Results

	Threshold		
	One	*Two*	*Three*
Pigments Wooden Pad 10 Bands	85,41%	79,6%	4.16%

In this case, where 10 narrow spectral bands were used, the accuracy of the estimation algorithm remained high, which allowed further investigation by removing one more band to see the affect it would have on the overall performance. Moreover, in this case some of the bands used (i.e. 820nm) were not used before. That could explain the increase of the percentage of the second threshold on Macbeth SG since some information may exist within the width of the specific band and the other set of bands couldn't get adequate information for the estimation.

5.4 Spectral Estimation using 9 Narrow Spectral Bands

In this case 9 narrow spectral bands were used. Six for the visible region as before and 3 for the NIR; 760, 860 and 960nm and are presented in Figure 5-10.

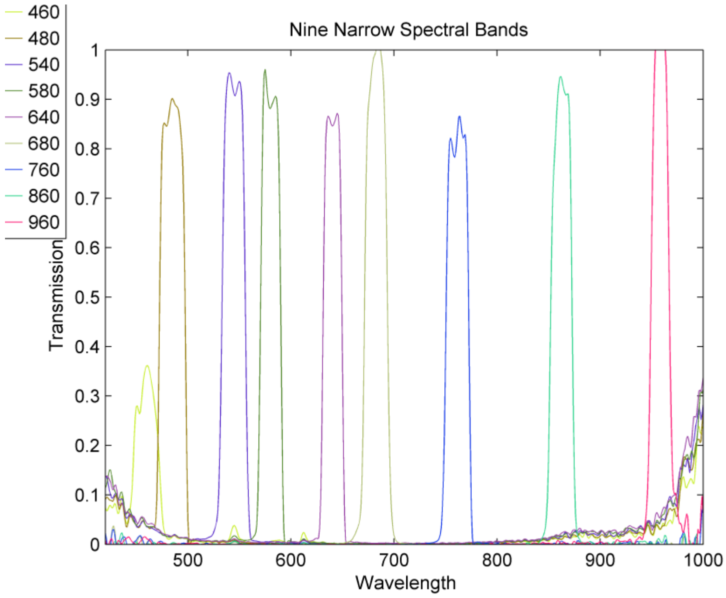

Figure 5-10 Eight Spectral Bands for Spectral Estimation within the Visible and NIR

5.4.1 Gretag Macbeth® Color Checker SG Spectral Estimation Results

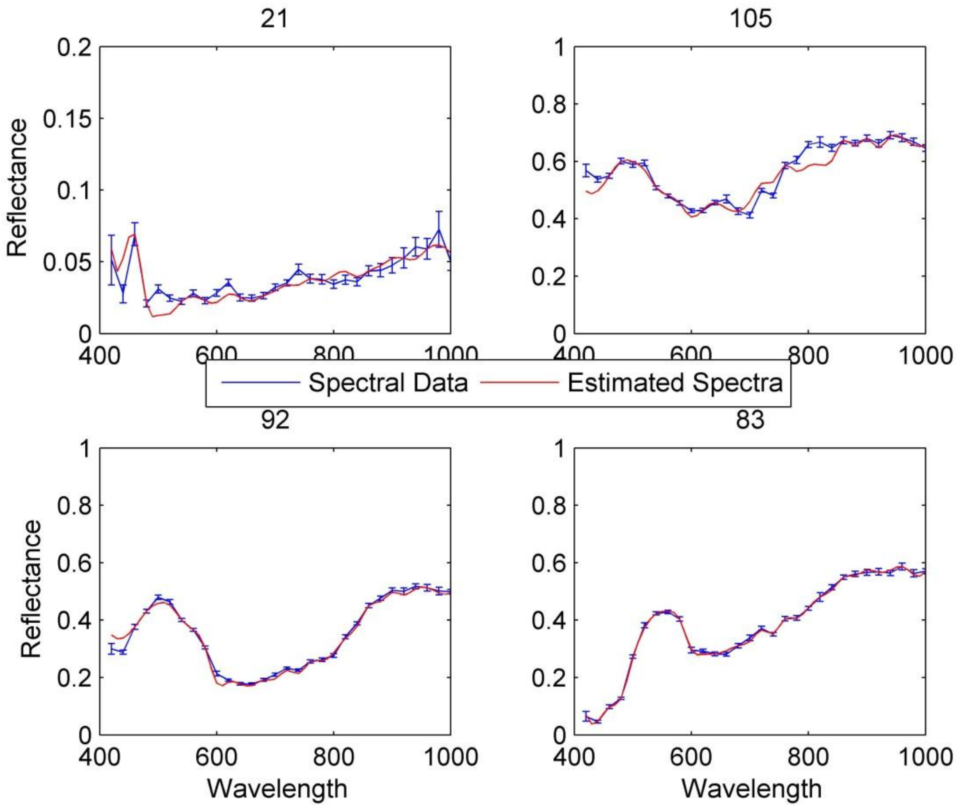

Figure 5-11 Spectral Estimation (9 Bands) Visible and NIR Macbeth SG (1)

In Figure 5-11 it can be seen that the spectrum in both regions of the spectrum is estimated with high accuracy. Although at this point only three bands are used, the results are very satisfactory since even in the case of the first sub-figure, the estimation process approximates all the sparks that are included on the SPD of the sample. That can be also verified from the quantitative measures presented in Table 5-7, where the percentages for the thresholds decline from 2% for the first to 15% for the third.

Table 5-7 Macbeth SG Spectral Estimation (9 Bands) Visible and IR Quantitative Results

	Threshold		
	One	*Two*	*Three*
Macbeth Color Checker SG 9 Bands	97.91%	94.79%	54.16%

5.4.2 Pigments Wooden Pad with varnish variations

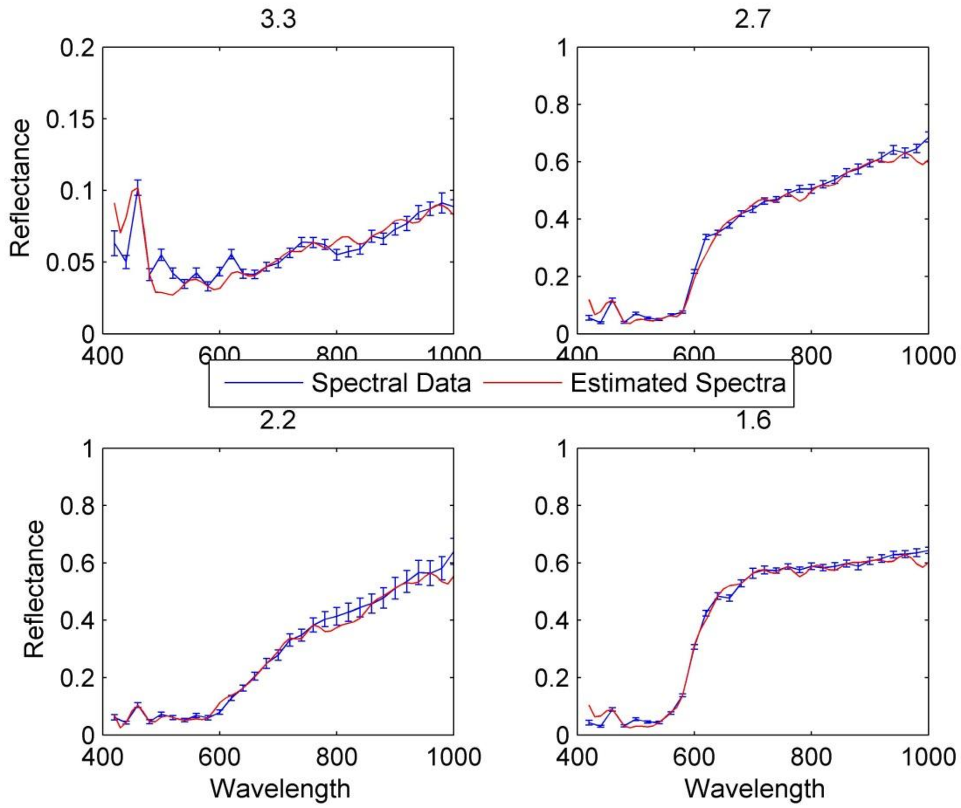

Figure 5-12 Spectral Estimation (Visible and NIR 9 Bands) Wooden Pad with Varnish (1)

In Figure 5-12 can be noticed that the spectral estimation was performed accurately for both regions of the spectrum as before. All spectral characteristics of the color patches were predicted with good precision. This can be also seen in Table 5-8 where the percentage remained adequately high for the first threshold, declined a bit for the second and fell to zero for the third. The decline of the thresholds can be noticed in the figures from the fact that in some case the estimated spectra are deviated more than the error-bars margin.

Table 5-8 Wooden Pad Spectral Estimation (9 Bands) Visible and NIR Quantitative Results

	Threshold		
	One	*Two*	*Three*
Pigments Wooden Pad 9 Bands	91.66%	79.6%	4.16%

In this case, where 9 narrow spectral bands were used, the accuracy of the estimation algorithm remained high, proving that spectral estimation could be performed in both visible and NIR regions of the spectrum even with 9 narrow spectral bands.

In Table 5-9 and Table 5-10 a sum up of the results can be seen for comparison. Overall, the accuracy of the spectral estimation remains high for both cases for most of the thresholds. It is noticeable for the wooden pad (which has "richer" spectral information with the NIR than Macbeth® SG) that a smaller number of bands lead to lower accuracy especially for the third threshold which describes the "excellent" estimation. Moreover, the fluctuation of the percentage for the second threshold states one important fact; spectral bands may need to be selected according to the test sample in question. Many objects or samples have very smooth spectral characteristics in the NIR, which as seen, means that three bands can provide very high accuracy estimates. If the object-sample has an abundance of information within the NIR, 6 bands could be used as well and provide an accurate result.

Table 5-9 Macbeth SG Spectral Estimation Visible and IR Quantitative Results

Macbeth Color Checker SG	Threshold		
	One	*Two*	*Three*
12 Bands	100%	95.83%	61.5%
11 Bands	97.9%	93.7%	60.4%
10 Bands	97.9%	92.7%	61.4%
9 Bands	97.9%	94.79%	54.16%

Table 5-10 Wooden Pad Spectral Estimation Visible and NIR Quantitative Results

Pigments Wooden Pad	Threshold		
	One	*Two*	*Three*
12 Bands	95.8%	79%	18.7%
11 Bands	85.41%	75%	18.7%
10 Bands	85.41%	79.6%	4.16%
9 Bands	91.66%	79.6%	4.16%

5.5 Improving Visible Spectral Estimation through NIR Spectral Estimation

Another important factor to notice was that the spectral estimation process that contains the IR region of the spectrum, could improve the accuracy of the spectra estimated within the visible region. For this reason, for each case of the selected number of bands within the IR, the quantitative results for the visible region are displayed in Table 5-11 and Table 5-12.

Table 5-11 Macbeth SG Spectral Estimation Visible vs. Visible with NIR

Macbeth Color Checker SG	Threshold		
	One	*Two*	*Three*
Visible	87.5%	74%	24%
12 Bands	84.37%	70.83%	34.37%
11 Bands	84.35%	73.95%	34.37%
10 Bands	83.33%	72.91%	31.25%
9 Bands	87.5%	77.1%	31.25%

Table 5-12 Wooden Pad Spectral Visible vs. Visible with NIR

Pigments Wooden Pad	Threshold		
	One	*Two*	*Three*
Visible	77%	50%	0%
12 Bands	70.83%	50%	0%
11 Bands	72.91%	58.33%	0%
10 Bands	68.75%	29.16%	0%
9 Bands	83.33%	54.16%	0%

It is noticeable that the accuracy could improve or not depending on the number of bands used. In both case of Gretag Macbeth SG and the Pigment wooden pad, the case of 9 Bands (6 Visible and 3 NIR), which was the case with the fewer bands, improved the accuracy of the spectral estimation within the visible region of the spectrum. This could be a result due to the nature of the sample since its spectral characteristics may be located on the selected bands.

Although for Macbeth SG the results are approximately the same, for the Pigment wooden pad may differ, as with the case of ten bands, significantly. The main outcome to be kept was that three bands in the IR can provide accurate spectral estimation for the visible and IR region of the spectrum while in the same time improving the estimation accuracy within the visible part.

6 Calculation of Color using Spectral Data

For an accurate color reproduction the following data are required:

- Spectral Data of the sample in question - S(λ)
- The Spectral Power Distribution of the Illuminant - I(λ)
- The Color Matching Function of the observer (by default CIE 1931 Standard Colorimetric Observer) - $\bar{x}(\lambda), \bar{y}(\lambda), \bar{z}(\lambda)$

Given S(λ), I(λ) and $\bar{x}(\lambda), \bar{y}(\lambda), \bar{z}(\lambda)$ the tristimulus XYZ values of the sample can be calculated:

$$X = \frac{1}{N}\int_{\lambda} \bar{x}(\lambda)\, S(\lambda) I(\lambda) d\lambda$$

$$Y = \frac{1}{N}\int_{\lambda} \bar{y}(\lambda)\, S(\lambda) I(\lambda) d\lambda$$

$$Z = \frac{1}{N}\int_{\lambda} \bar{z}(\lambda)\, S(\lambda) I(\lambda) d\lambda$$

Where,

$$N = \int_{\lambda} \bar{y}(\lambda)\, I(\lambda) d\lambda$$

$$\lambda = 380nm\ to\ 780nm\ with\ 5nm\ integral$$

Then XYZ tristimulus values can be transformed to any other color space. RGB data coordinates can be evaluated by multiplying the XYZ values with a transformation matrix M.

$$\begin{bmatrix} R \\ G \\ B \end{bmatrix} = [M]^{-1} \begin{bmatrix} X \\ Y \\ Z \end{bmatrix}$$

Where M is calculated to match the reference white (CIE Illuminants D65, D50 etc.) and RGB working space (sRGB, CIE RGB, etc.)

6.1 Color Reproduction from Spectral Data using MUSIS HS Camera

Reproducing color from spectrum using a Hyperspectral camera can result in color with very high fidelity to the original. So firstly, the MUSIS HS camera was used to acquire the spectral cube of Gretag Macbeth Color Checker SG® within the visible spectrum with 20nm integral. Macbeth contains 140 patches, which makes it too big to fit in one shot. Thus, it is split into 4 Quadrants (referred to as Quads from this on). The spectral cube contained 15 bands for each Quadrant from 420 to 700nm with 20nm integral with 1600x1200 resolution.

6.2 Six Band Color Reproduction using Spectral Estimation

As aforementioned, a smaller number of bands can be selected instead of a complete spectral cube. Then Spectral Estimation can be performed to estimate the missing data. From our former study "Spectral Prediction from Filtered Color CCD Cameras", we established that six bands, equally distributed in the visible spectrum as well as complementary to one another, can be used for high accuracy spectral estimation. These bands are the 460-480-540-580-640-680nm as presented in Figure 6-1.

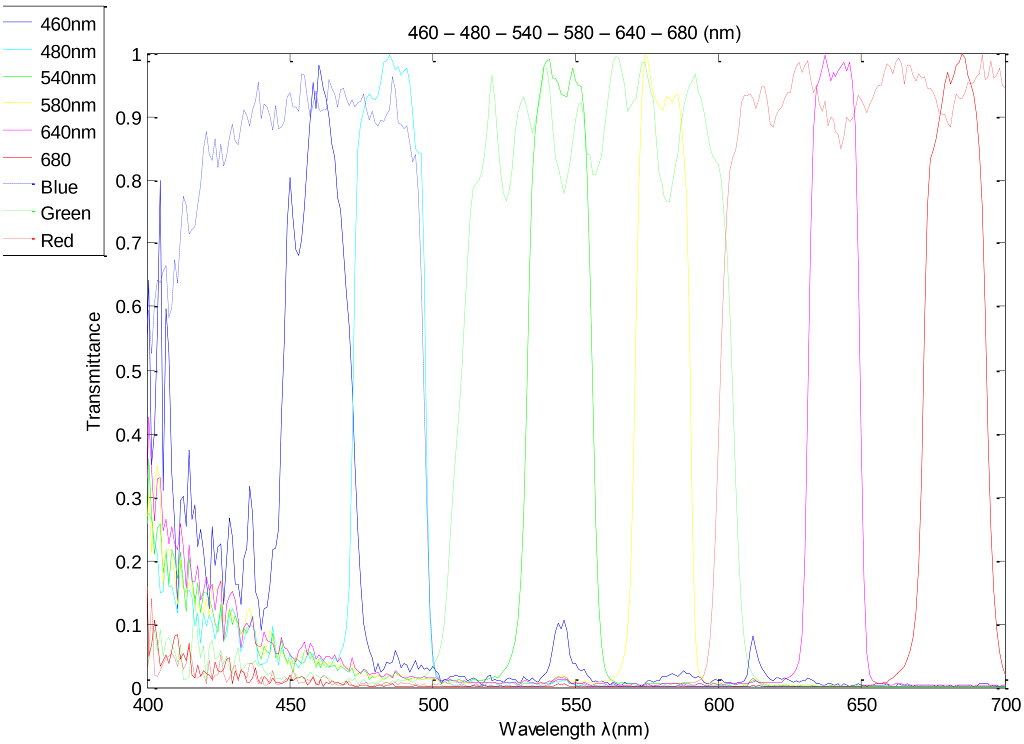

Figure 6-1: Six Spectral Bands and RGB

Figure 6-2 : CR Full and Estimated Spectral Cube (Quad 1,2,3,4 respectively)

In Figure 6-2 the results of the Color Reproduction are presented. In the left column the full cube from MUSIS HS was used for color reproduction while in the right column, Color Reproduction was performed using six bands (Figure 6-1), after using Spectral Estimation. The color reproduced from Hyperspectral Imaging Systems is considered “golden” standard. So, by comparing the color difference between those two results, it can be established if six spectral bands along with spectral estimation can be used for accurate color reproduction. In both cases the illuminant used was the CIE D50 Standard Illuminant.

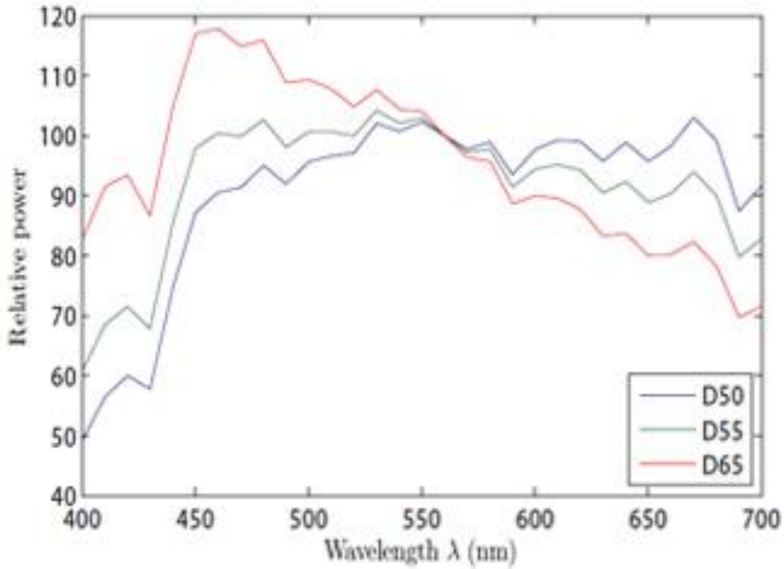

Figure 6-3 : Spectral Power Distributions of the CIE Standard illuminants D50, D55 and D65

To quantify the color difference between the input samples, the following procedure was followed:

1. The SPD of the CIE D50 Illuminant was chosen. (Figure 6-3)
2. The Color Matching Function (CMF) of the CIE Standard Observer was chosen according to the Spectral Cube’s wavelength range and integral.
3. The XYZ tristimulus values were calculated from the Spectral Data, SPD and CMF
4. The XYZ values were transformed to RGB for the output images
5. The XYZ values were transformed to Cielab Colorspace in order to evaluate ΔE_{ab*}. (Table 6-1) and ΔE_{94*} Figure 6-4 - Figure 6-7 for all four Images of MacBeth SG

Table 6-1: Color Difference Results

	Max	**Min**	**Average**
ΔE_{ab*}	*10.01*	*0.33*	*3.67*

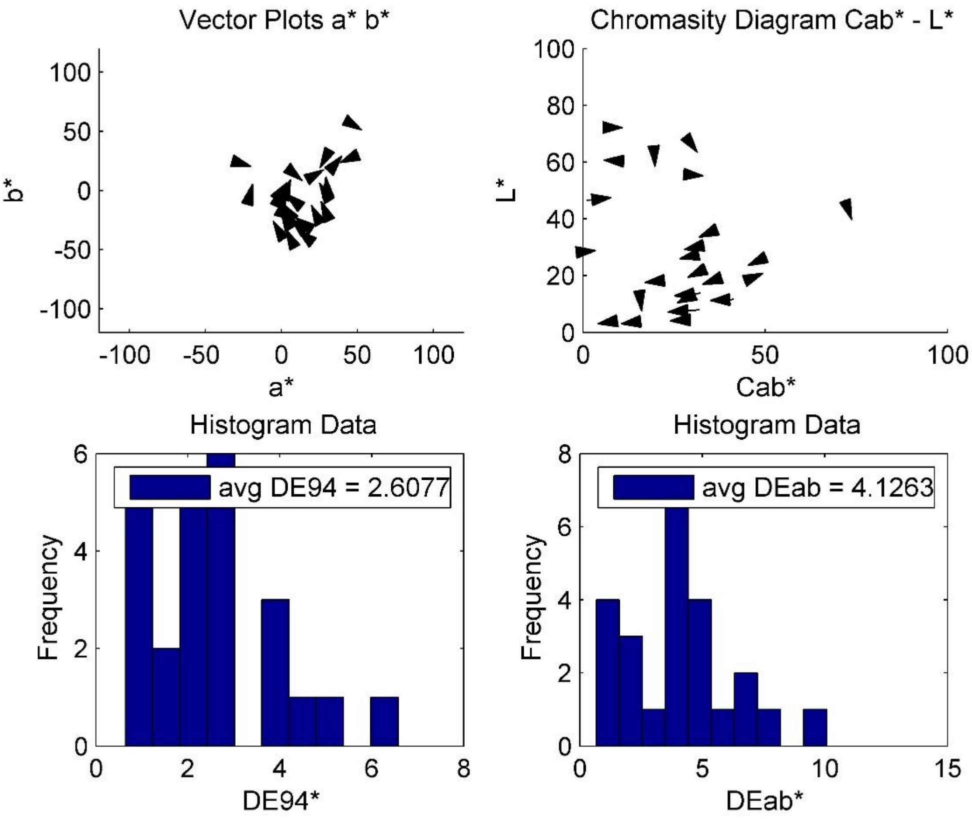

Figure 6-4 CIELAB Metrics Quad 1

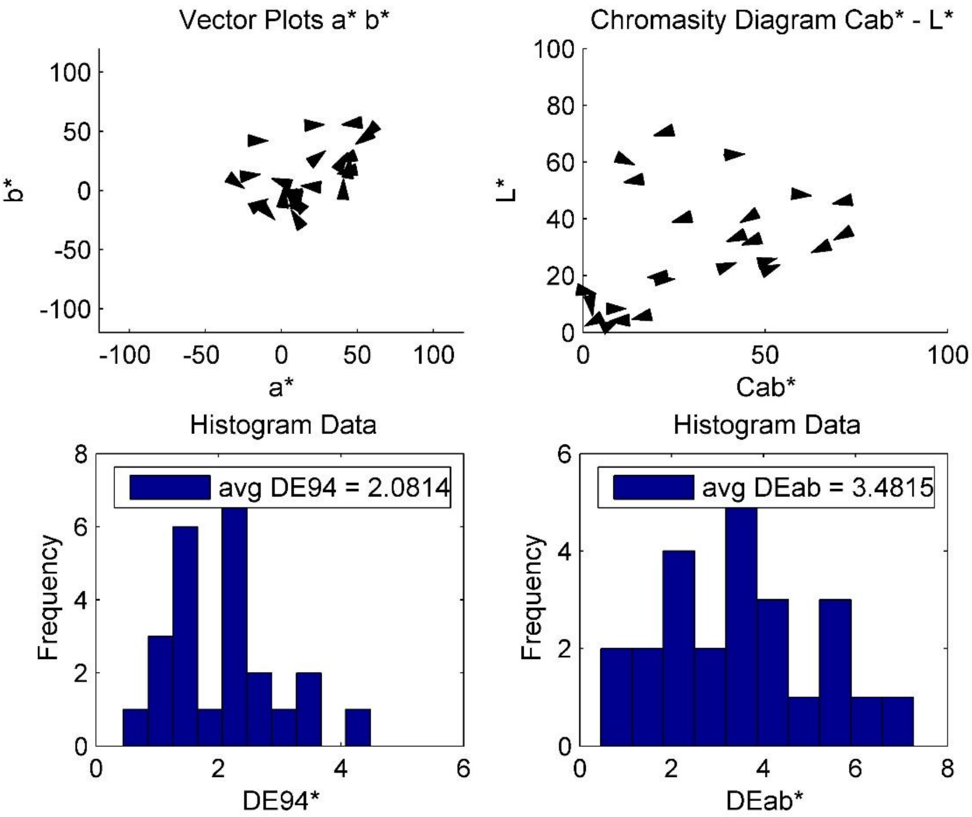

Figure 6-5 CIELAB Metrics Quad 2

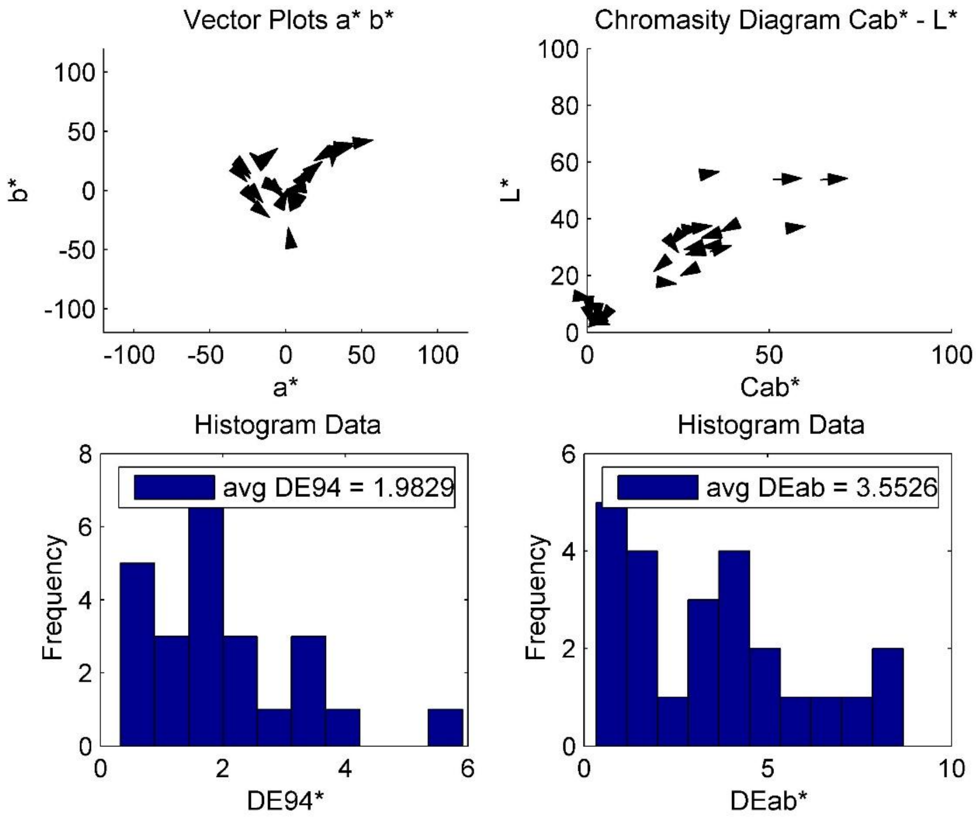

Figure 6-6 CIELAB Metrics Quad 3

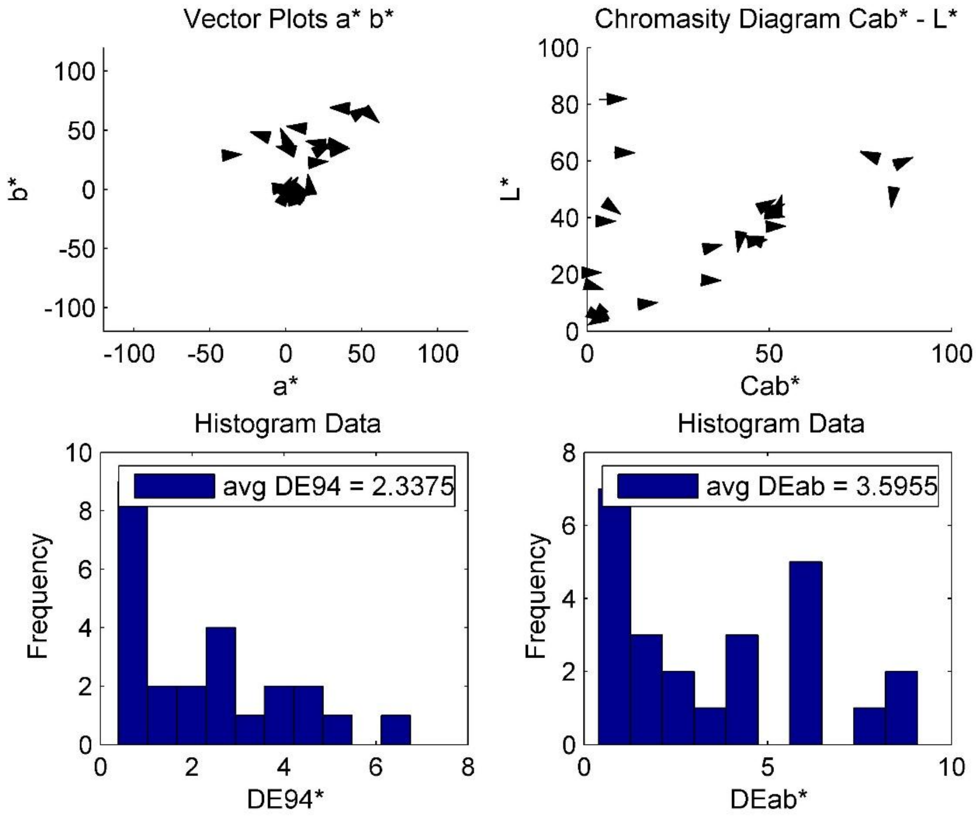

Figure 6-7 CIELAB Metrics Quad 4

The mean value of the color difference ΔE_{ab^*} was 3.67 units, which indicated that high fidelity color reproduction can be performed. This can be also seen in Figure 6-2 where no perceptual difference can be perceived. From Figure 6-4 to Figure 6-7 the graphical color difference can be seen. The length of the vectors is very small indicating very low error and the statistical analysis of the color patches indicates that the vast majority of them was reproduced with ΔE_{ab^*} lower than 3.

The above results indicate that six bands along with spectral estimation can result in high accuracy color reproduction. This procedure thought is a computational and time expensive one. Using a PC with an i7 core processor, around 0.6 seconds are needed to calculate all the data needed (Illuminant, Color Matching Function etc.), perform the computations and display the results. Moreover, the time to calculate a complete spectral cube, especially in high resolution, adds an additional overhead of 0.5 sec to the aforementioned time.

Although this method is validated in the literature and is broadly used, the time needed to complete the process doesn't allow real time applications. So in order to achieve real time reproduction a new method must be implemented which will allow color to be reproduced real time without sacrificing any accuracy.

6.3 Six Band Color Reproduction

Spectral Estimation takes up at least half of the time needed to process the input data, thus in order to minimize the time needed for processing it is removed. By removing spectral estimation only six spectral bands remain as data for the color reproduction. For starters, the color is evaluated as before using the state of the art algorithm containing the illuminant, the Color Matching Function. The main difference in this point is that the size of the spectral cube is smaller (1600x1200x6) instead of the full spectral cube (1600x1200x15) which results in less time for computations. That also will result in less accuracy and probably noticeable perceptual differences between the original image and the reproduced.

Below the images of Gretag Macbeth Color Checker ® are presented for the cases of color reproduction from a complete spectral cube ("golden" standard) and from the six bands without spectral estimation.

Figure 6-8 : CR Full and Six Band Spectral Cube (Quad 1,2,3,4 respectively)

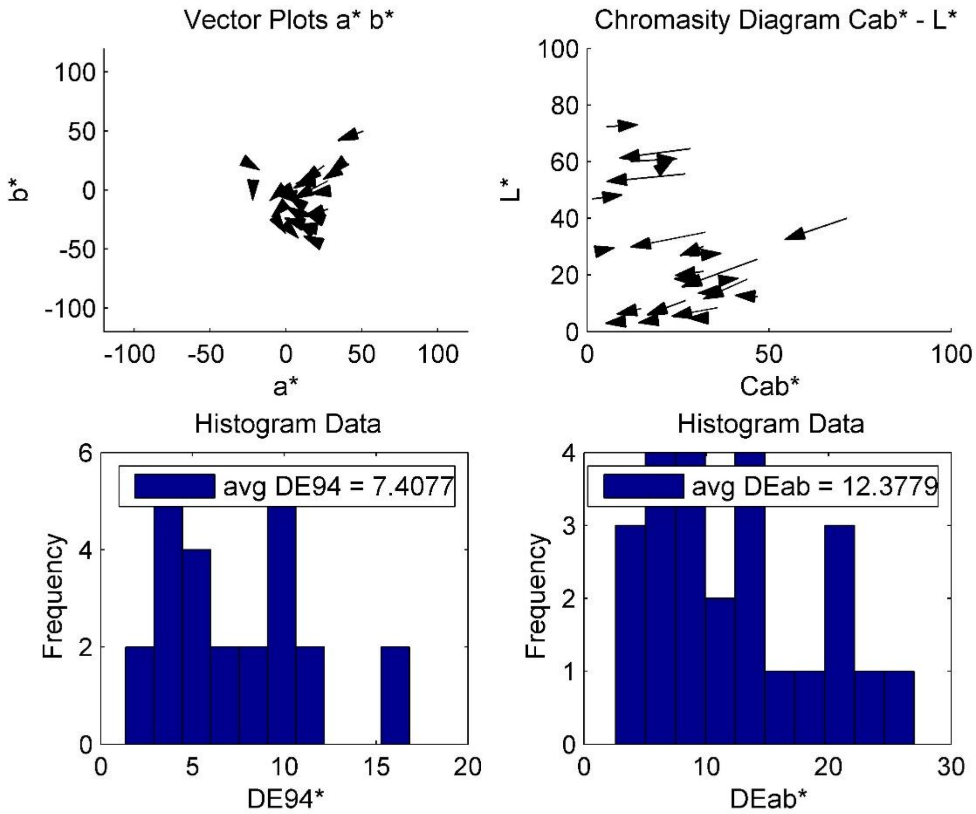

Figure 6-9 CIELAB Metrics Quad1

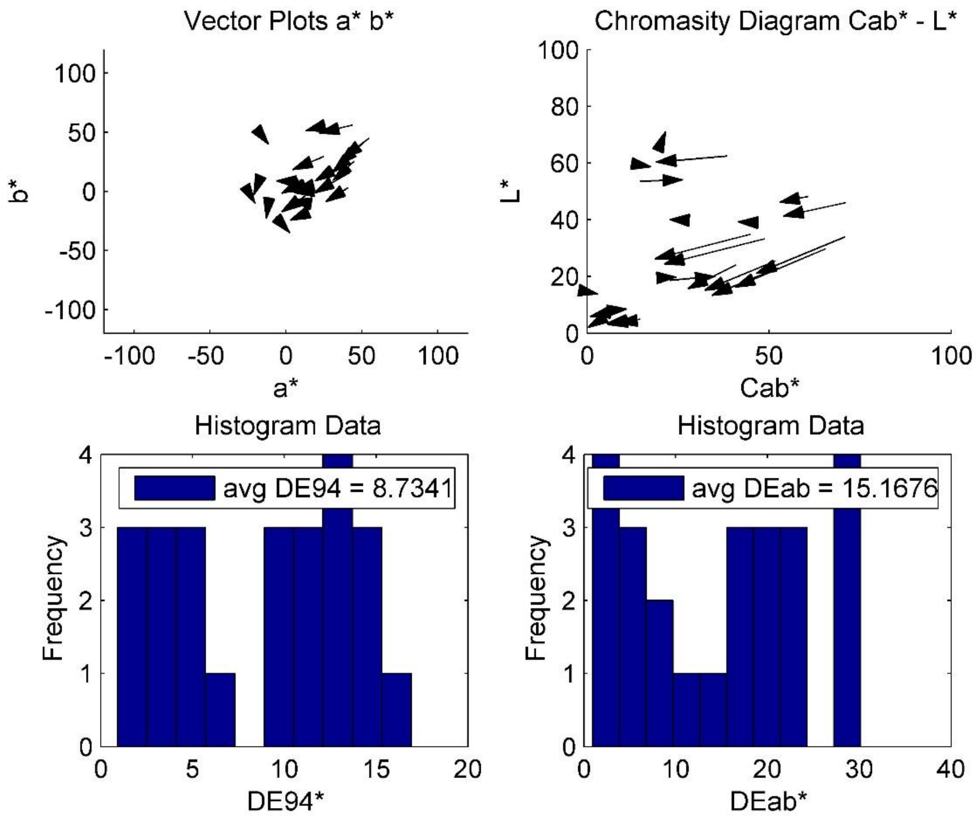

Figure 6-10 CIELAB Metrics Quad2

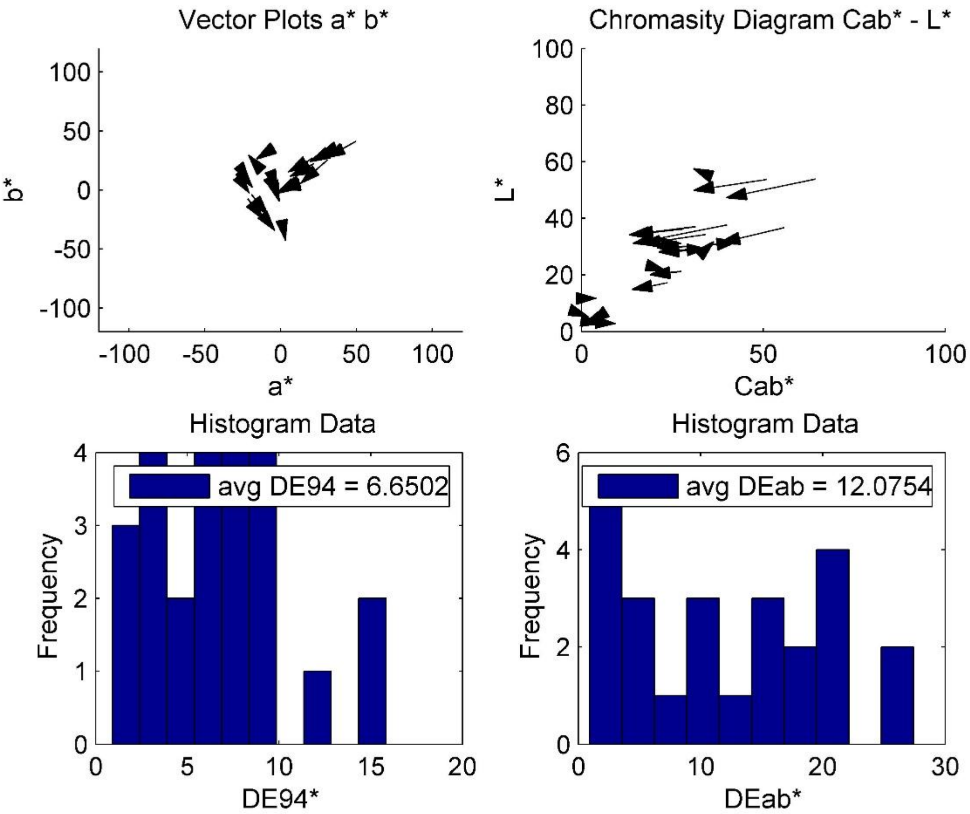

Figure 6-11 CIELAB Metrics Quad3

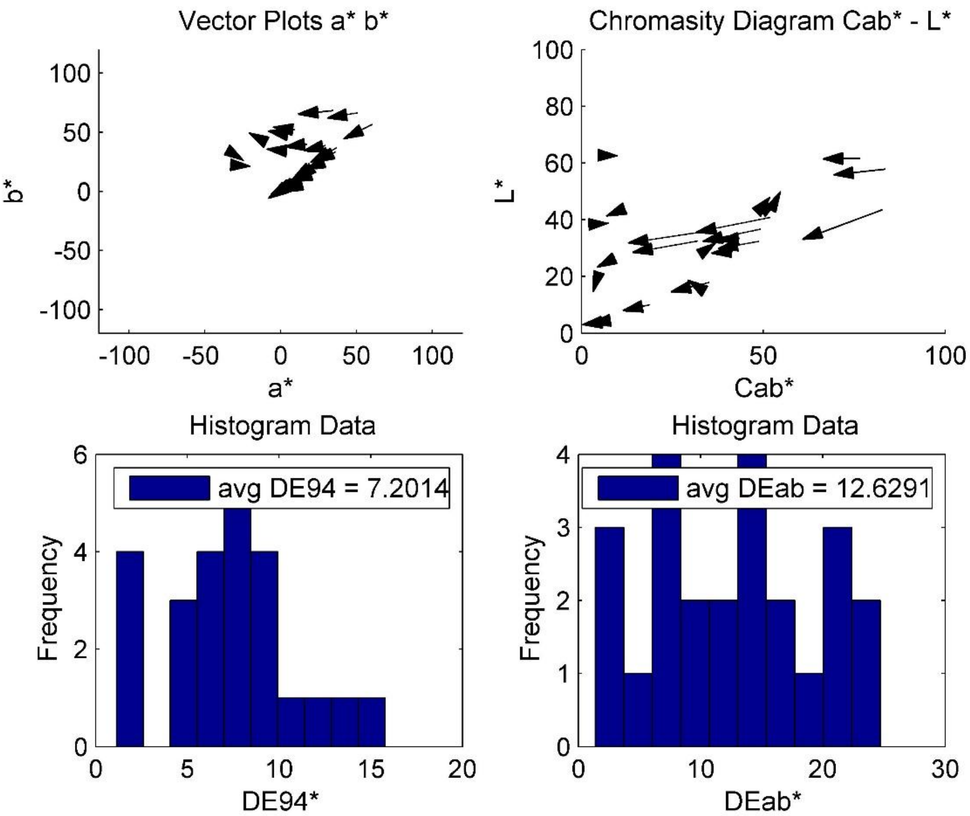

Figure 6-12 CIELAB Metrics Quad4

From the above results the assumption made can be validated. In Figure 6-8 the perceptual differences between the two images are quite high. That is also apparent in Figure 6-9 - Figure 6-12 where the length of the arrows in both vector plots is quite high which effectively means high error thus high color difference. Finally, from the statistic representation of the DE_{ab*} the results of Table 6-2 are evaluated.

Table 6-2: Color Difference Results

	Max	Min	Average
ΔE_{ab*}	*30*	*0.91*	*13.04*

It can be seen that the maximum as well the average color difference are quite high. This infers that using six spectral bands and performing color reproduction with the state of the art process doesn't result in accurate results. For that reason, another method is proposed in order to increase the accuracy of the reproduced color and on the same time try to achieve that in real time.

6.4 Weighted Six Band Color Reproduction

Instead of using Spectral Estimation, a simulation is performed using an a priori sample to create a weight matrix that can allow six spectral bands to be transformed into RGB with high accuracy. The sample used for a priori knowledge is Gretag Macbeth Color Checker® CC which includes 24 color patches. The RGB matrix contains the RGB values that originate from the color reproduced image using a complete spectral cube, and the T matrix contains the values from each spectral band. Thus the following system:

$$\begin{bmatrix} R \\ G \\ B \end{bmatrix} = \begin{bmatrix} W_{1,1} & W_{1,2} & W_{1,3} & W_{1,4} & W_{1,5} & W_{1,6} \\ W_{2,1} & W_{2,2} & W_{2,3} & W_{2,4} & W_{2,5} & W_{2,6} \\ W_{3,1} & W_{3,2} & W_{3,3} & W_{3,4} & W_{3,5} & W_{3,6} \end{bmatrix} \begin{bmatrix} T_{1,R} \\ T_{2,R} \\ T_{1,G} \\ T_{2,G} \\ T_{1.B} \\ T_{2,B} \end{bmatrix}$$

After evaluating the above weight matrix, a validation process is in order, to accurately estimate the performance of this process. As before, a perceptual and quantitative comparison is made between the reproduced image and the "golden" standard using Gretag Macbeth Color Checker® SG to evaluate the performance of this process. It is important to note that the weight matrix was evaluated using only 24 patches out of 140 of Macbeth SG.

Figure 6-13 : CR Full Spectral Cube and Weighted Six Band (Quad 1,2,3,4 respectively)

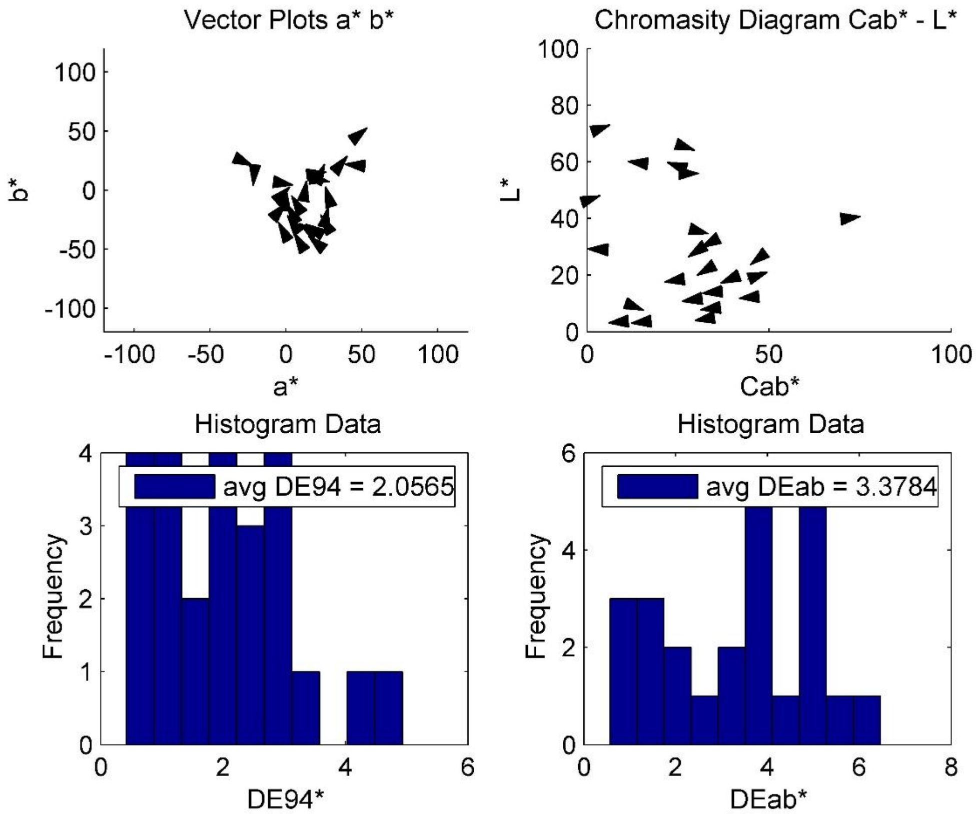

Figure 6-14 CIELAB Metrics Quad1

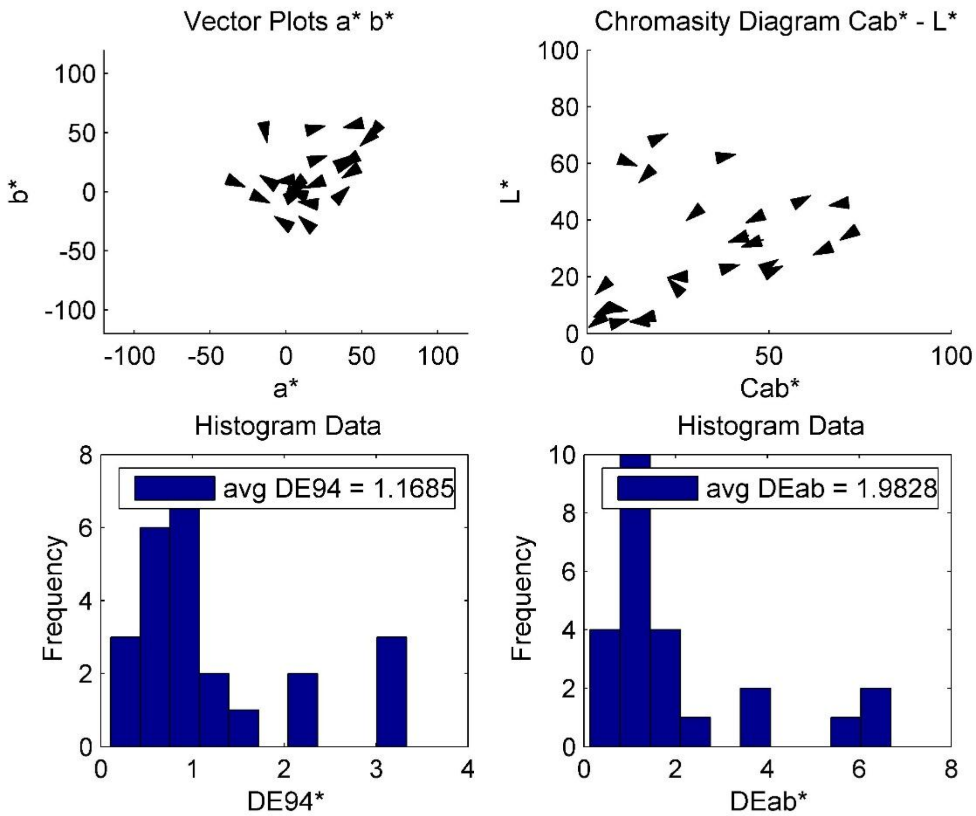

Figure 6-15 CIELAB Metrics Quad2

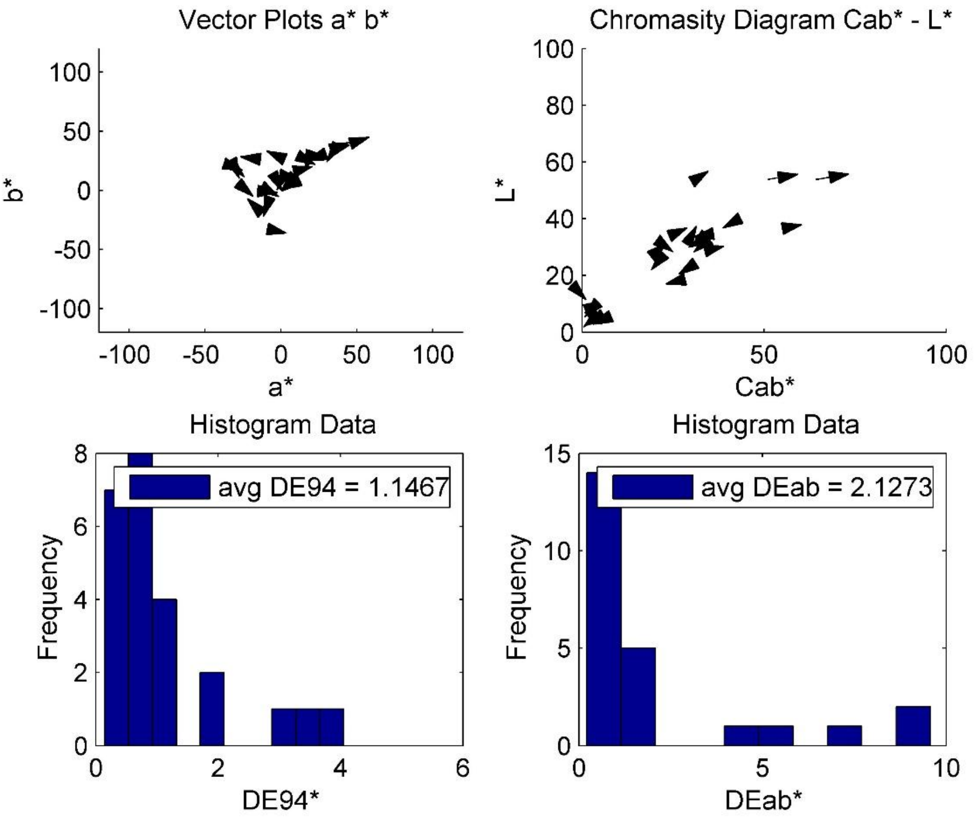

Figure 6-16 CIELAB Metrics Quad3

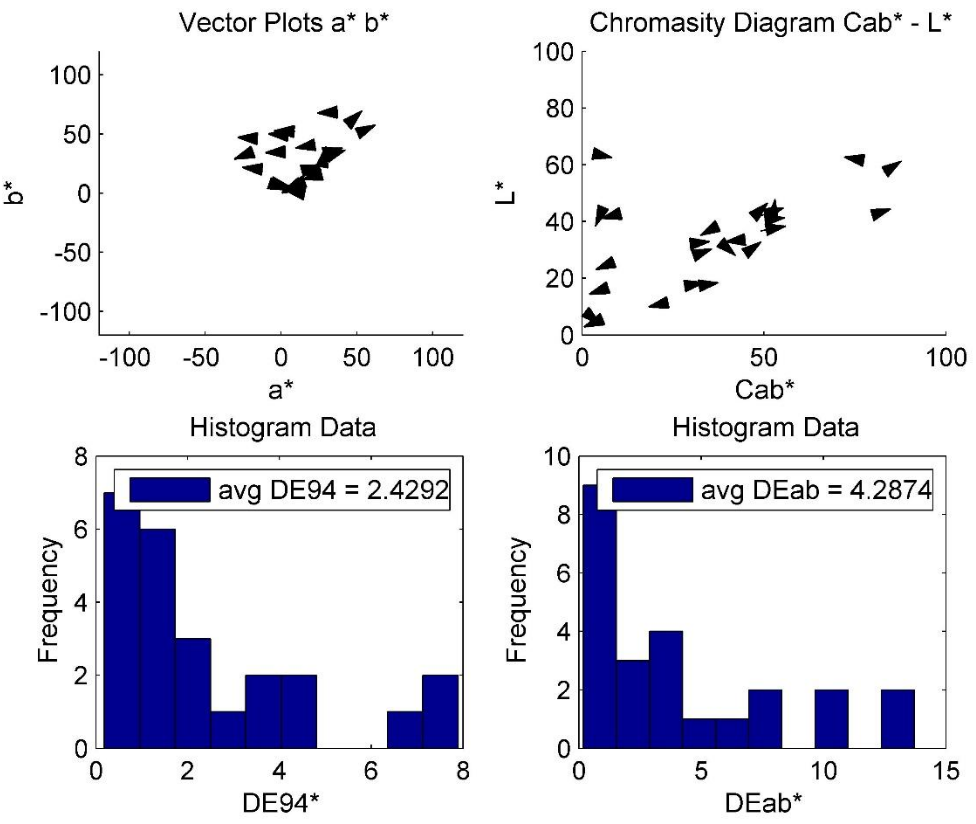

Figure 6-17 CIELAB Metrics Quad4

From the above results it can be clearly seen that the proposed method performs with very high accuracy. By noticing Figure 6-13, no perceptual differences can be found, which can be also validated from the quantitative measures. The arrows in the vector plots appear to have approximately zero length which means very low color difference, and the statistical analysis of the color difference (Table 6-3) indicates that for the majority of the patches, the color difference DE_{ab*} is below 3 which is even lower than the case where color was reproduced using spectral estimation first. It is also important to note the minimum value achiever is approximately reaches zeros meaning perfect color reproduction in every possible aspect.

Table 6-3: Color Difference Results

	Max	Min	Average
ΔE_{ab*}	*13.69*	*0.06*	*2.93*

The last issue to address for this case is the process time needed for the color reproduction. Given that the weight matrix is calculated beforehand and can be used as a priori knowledge the time needed is 0.05 seconds which is significantly less than any other case leading to the solution of the real time problem.

6.5 Color Reproduction from Estimated Spectral Cube vs. Six Weighted Narrows Spectral Bands

It was validated that six weighted spectral bands, as well as color reproduction from the estimated spectral cube, can reproduce high fidelity color. Since both cases managed to do so with low DE, it was a logical step to compare those two results in order to observe the difference between the two color reproduction methods. As before, Gretag Macbeth Color Checker SG was used as test target and both methods were reproduced color under Equal Energy (EE) Illuminant so that it can be compared. In Figure 6-18 the results from the estimated spectral cube can be seen on the left column and the results from the six weighted bands can be seen on the right. Next up, for each of the four quadrants the graphical color difference was presented and finally the average, max and min of DE for all the color patches of Macbeth were calculated.

Figure 6-18 : CR Full and Six Band Spectral Cube (Quad 1,2,3,4 respectively)

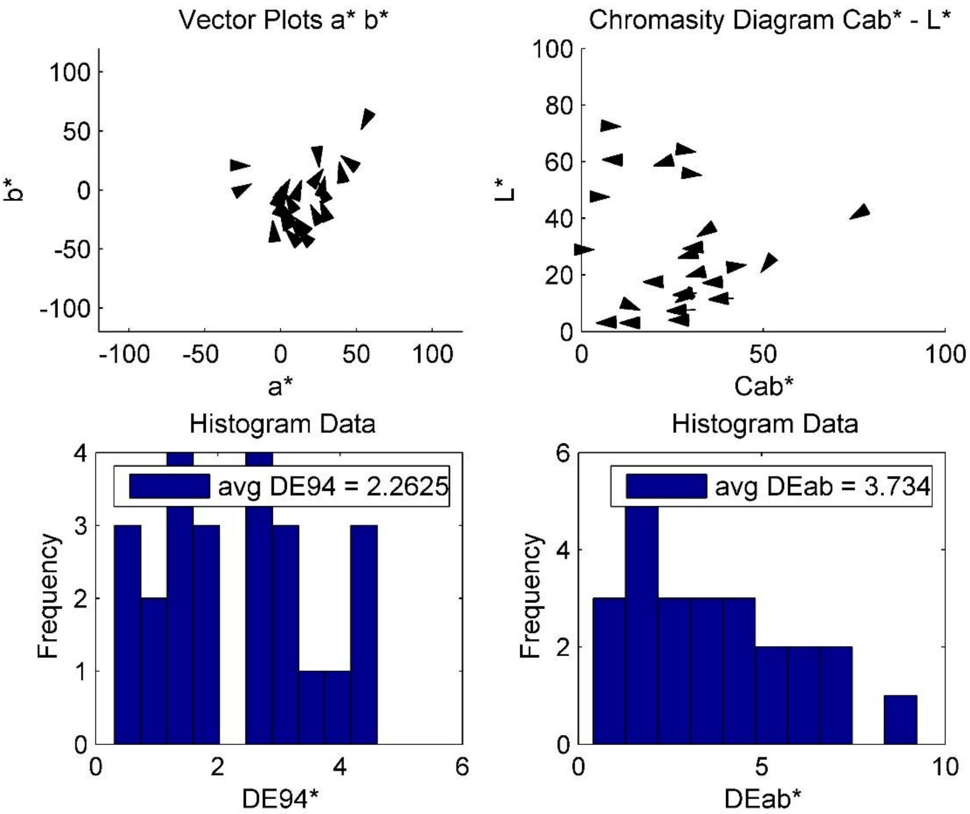

Figure 6-19 CIELAB Metrics Quad1

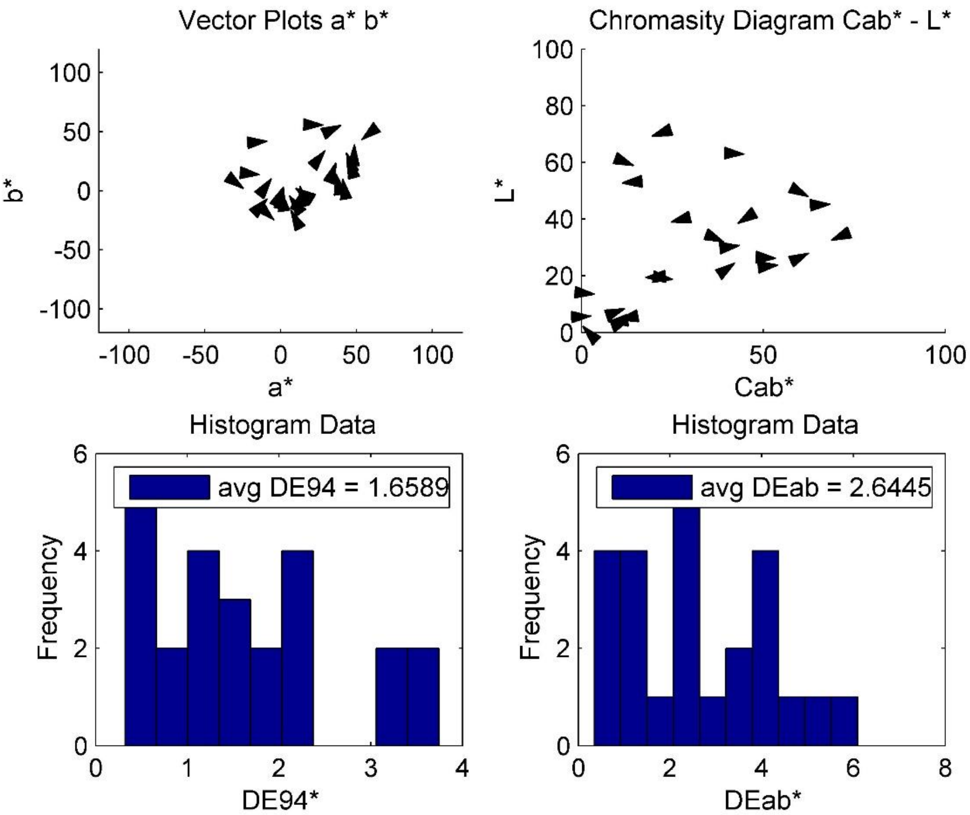

Figure 6-20 CIELAB Metrics Quad2

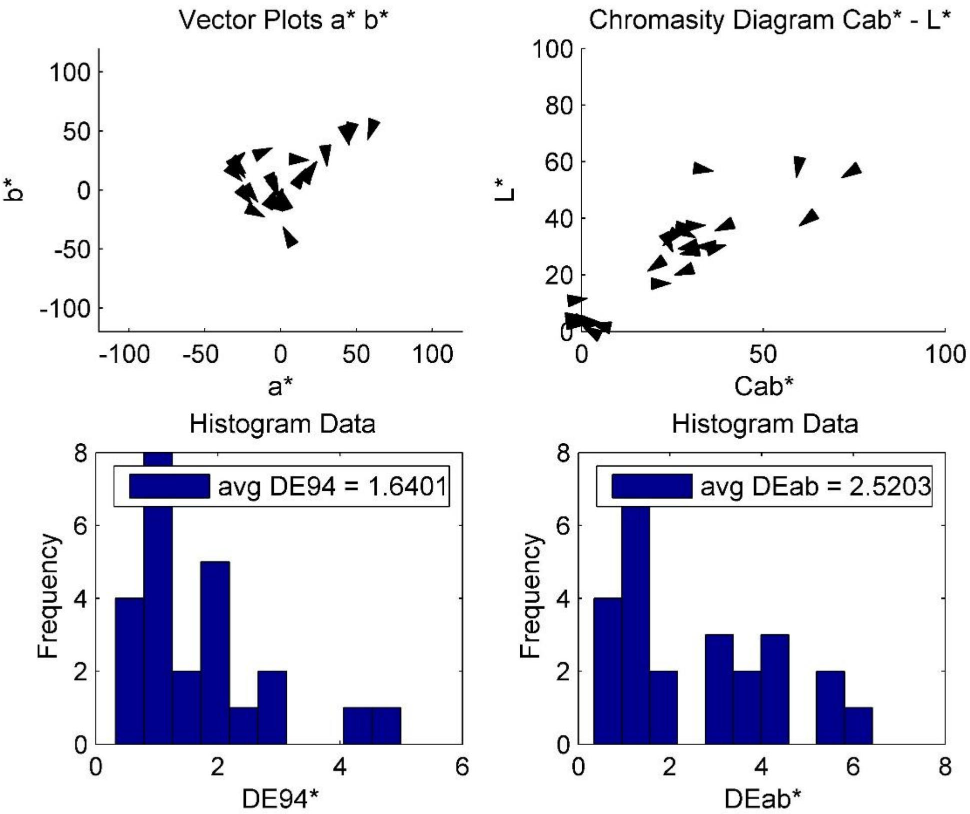

Figure 6-21 CIELAB Metrics Quad3

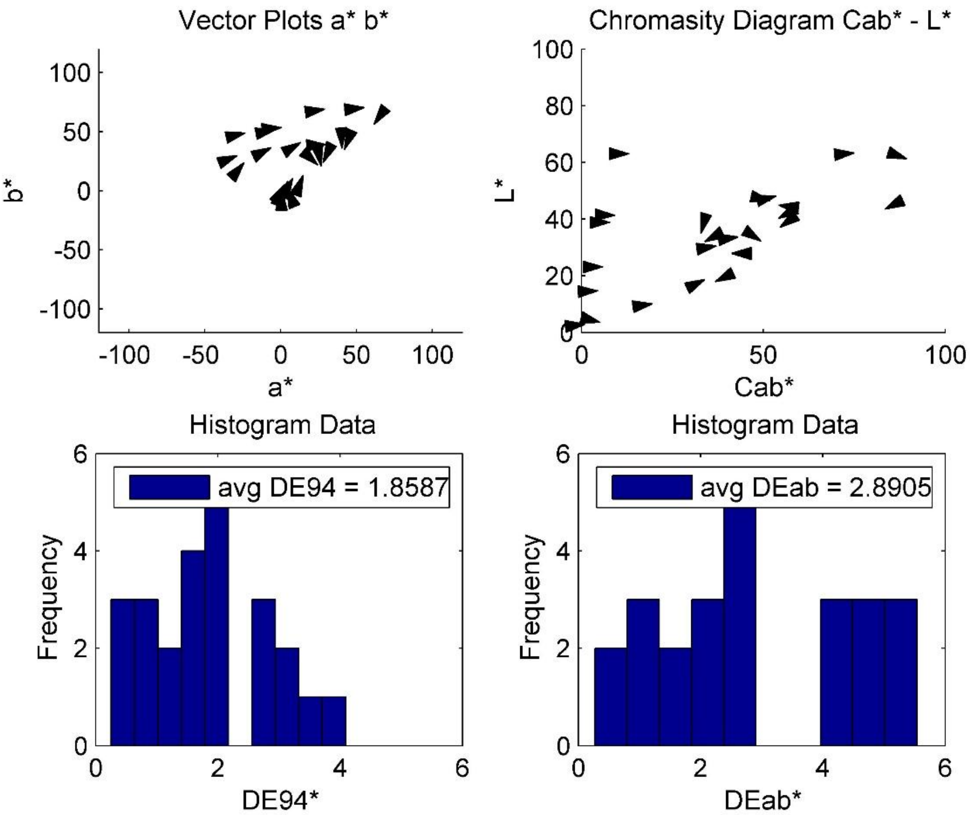

Figure 6-22 CIELAB Metrics Quad4

In Figure 6-18 the perceptual differences between the two images is very low. That is also apparent in Figure 6-19 to Figure 6-22 where the length of the arrows in both vector plots is almost zero which effectively means minimum error thus minimum color difference. Finally, from the statistic representation of the DE_{ab*} the results of Table 6-4 were evaluated.

Table 6-4: Color Difference Results

	Max	Min	Average
ΔE_{ab*}	*9.23*	*0.27*	*2.94*

6.6 Color Reproduction Methods Summary

A final comparison of all the methods and inputs used for color reproduction was made in order to evaluate the best method and their difference between them. In Table 6-5 all these results can be seen. There are three methods that have been used so far; the first was to reproduce color with state of the art techniques using an estimated spectral cube while the second was the same technique but with only six narrow spectral bands as input and the third with the use of six weighted narrow spectral bands. In each case the results were compared with the reproduced color from the measured spectral cube aka golden standard. Six spectral bands performed poorly while the other two methods provided high fidelity color reproduction with the Six Weighted bands having the lowest average and min value of DE. Of course, the main difference between the two methods was that the Color reproduction using a complete spectral cube can be done under any illuminant wanted.

Finally, the two methods were compared in order to evaluate the difference of their result. It can be seen that the average DE* between the Estimated Spectral Cube CR and the Six weighted bands CR was low with the maximum DE being lower than any other case. This means that both methods can be used for high fidelity color reproduction and each one can be selected according to the properties wanted such as real-time CR or color reproduction under various illuminant.

Table 6-5 Color Difference Results Summary

ΔE_{ab*}	Max	Min	Average
Six Band Spectral Estimation CR vs. Measured Cube CR	*10.01*	*0.33*	*3.67*
Six Band Color Reproduction vs. Measured Cube CR	*30*	*0.91*	*13.04*
Six Weighted Bands CR vs. Measured Cube CR	*13.69*	*0.06*	*2.93*
Six Band Spectral Estimation CR vs. Six Weighted Bands CR	*9.23*	*0.27*	*2.94*

7 Six Band Color Reproduction System

After validating that six narrow spectral bands can provide an accurate result, a six band system with two color cameras and two color filters (Figure 7-1) was designed. The filters are optimized to provide high transmission, steep edges and deep blocking for balance in contrast, brightness, and color representation.

Figure 7-1: Transmission spectra for products FF01 422/503/572 (a) and FF01 464/542/639 (b), Semrock, Rochester, NY, www.semrock.com.

7.1 Channel unmixing

When a triple bandpass filter, with central wavelengths λ1, λ2, λ3, is coupled to a Bayer tiled CCD, the sensitivity of each pixel, apart from the spectral characteristics of the Bayer pattern microfilters, is modified again by the transmittance characteristics of the filter. Since RGB microfilters are approximately broad, with each one covering a wide area of the active CCD sensitivity spectrum, when coupling a triple Multiple Band Pass Filter (MBPF), each pixel will unevenly be sensitive to any of the three narrow spectral bands.

This fact implies that a pixel value for the e.g. Red channel will be a summation of captured photons in all three narrow spectral bands of the MBPF. Assuming that the spectral bands of the MBPF are located in the red, green and blue channel sensitivity areas of an optical sensor and that R_{Broad}, is the value of the R channel, then R_{Narrow}, R_{Greem} and R_{Blue}, will be the R channel values recorded at the red, green and blue band of the MBPF. Making the same assumptions for the G and B channels, equation (1) derives:

$$\begin{aligned} R_{Broad} &= R_{Narrow} + R_{Green} + R_{Blue} \\ G_{Broad} &= G_{Red} + G_{Narrow} + G_{Blue} \qquad (1) \\ B_{Broad} &= B_{Red} + B_{Green} + B_{Narrow} \end{aligned}$$

It is therefore essential to disentangle the recorded spectral information for recovering the six spectral images, whose spectral content corresponds to the six transmission/reflection bands of the PM. Due to this fact, an unmixing algorithm that would eliminate the “crosstalking” of the channels in all MBPF’s bands. By advancing mathematically the equation (1), the above hypothesis is possible. Specifically, by noticing that for the e.g. red channel, the R_{Green} value, apart from being a fraction of R_{Broad}, is also a fraction of G_{Narrow}. This may be expressed as a ratio of the areas covered within the region of MBPF’s green spectral band between G_{Narrow} and R_{Broad}. This ratio is furthermore a weighted coefficient between R_{Green} and G_{Narrow}. So, by formulating mathematically the curves of the active spectrum of the RGB channels and by calculating their integrals at the MBPF’s bands, equation (1) leads to eq. (2).

$$\begin{aligned} R_{Broad} &= w_{RR} \cdot R_{Narrow} + w_{RG} \cdot G_{Narrow} + w_{RB} \cdot B_{Narrow} \\ G_{Broad} &= w_{GR} \cdot R_{Narrow} + w_{GG} \cdot G_{Narrow} + w_{GB} \cdot B_{Narrow} \qquad (2) \\ B_{Broad} &= w_{BR} \cdot R_{Narrow} + w_{BG} \cdot G_{Narrow} + w_{BB} \cdot B_{Narrow} \end{aligned}$$

This process enables the concurrent acquisition of any three spectral bands, by using a triple MBPF (TBPF) and an ordinary color camera. This setup may be expanded to the concurrent capturing of four spectral bands, by using CMYG color cameras and quadruple

MBPFs. Also, with the use of optical dispersing elements, more than one camera can be used, to increase the number of the acquired spectral bands.

7.2 Channel unmixing algorithm

To disentangle the spectral information for a TBPF an algorithm was designed that removed any cross-talking between color channels for each corresponding band of the filter. For example, a band with center wavelength at 680nm should contain information from the “red” channel without any interference from the other two (blue and green). That allows each the TBPF to contain “pure” spectral information.

To remove the cross-talking between the TBPF’s bands, a weight matrix was created. This matrix was created by matching the information of the TBPF with spectral information, acquired either with a Hyper-spectral camera or a spectrometer. A test sample was used, in this case Gretag Macbeth® Color Checker CC, to acquire its information with the TBPF and a Spectral Imaging device and then tried to match the values of the TBPF to the specific spectral ones.

The definition of the number of color patches used for this process to minimize the error for the spectral match was of crucial importance. Various combinations of the color patches were tested using 10 to 24 patches. For each number of patches used, all possible combinations were estimated for 100 pixels per patch, and the maximum and minimum errors were calculated. In Figure 7-2 the minimum error results can be seen that ultimately defined the number of patches used for this process to ten. By increasing the number of patches the error increased as well, along with the deviation from the mean value. Nevertheless the error value remained low, below unity, for each number of patches used. By selecting the number of patches with the lowest error it can be ensured that the corresponding TBPF and spectra data have the best match possible during the unmixing procedure. In Figure 7-3, the highest error for each combination can be seen. In this case, while the number of patches increased the error decreased reaching a value of 2.8 from 10^{14}. It is important to note that the scale is logarithmic since the error values are quite high for small number of patches. This process was performed for both TBPF presented in Figure 7-1.

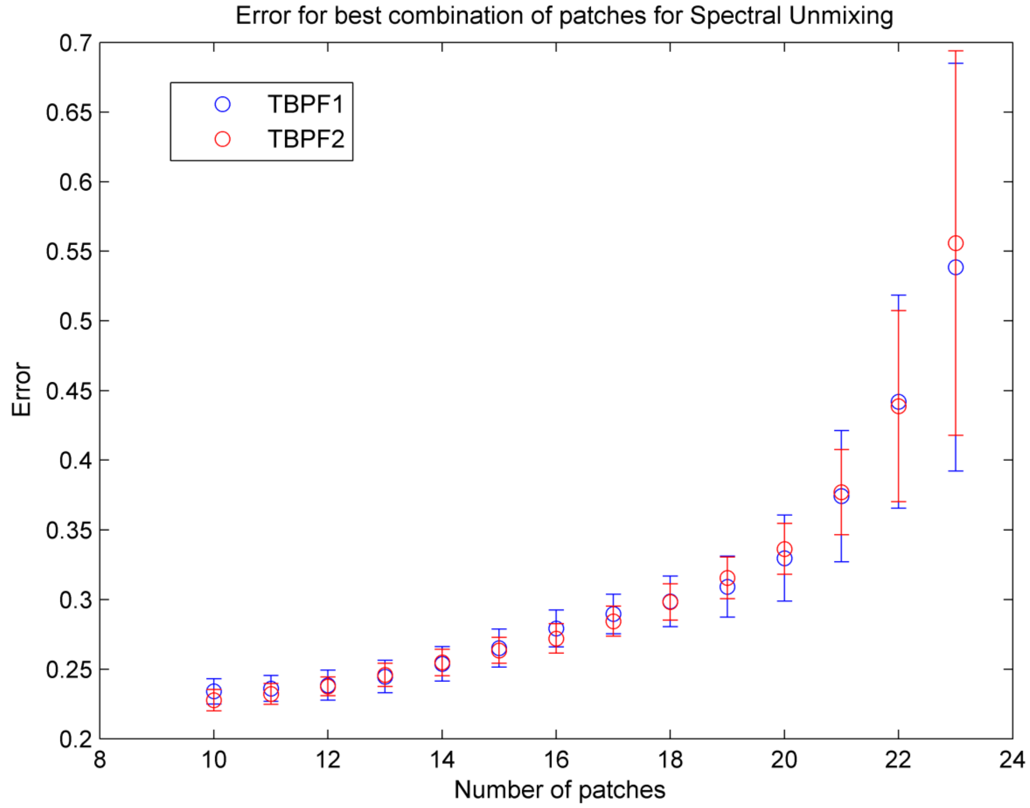

Figure 7-2 Spectral Unmixing - Color Patches Choice with minimum error

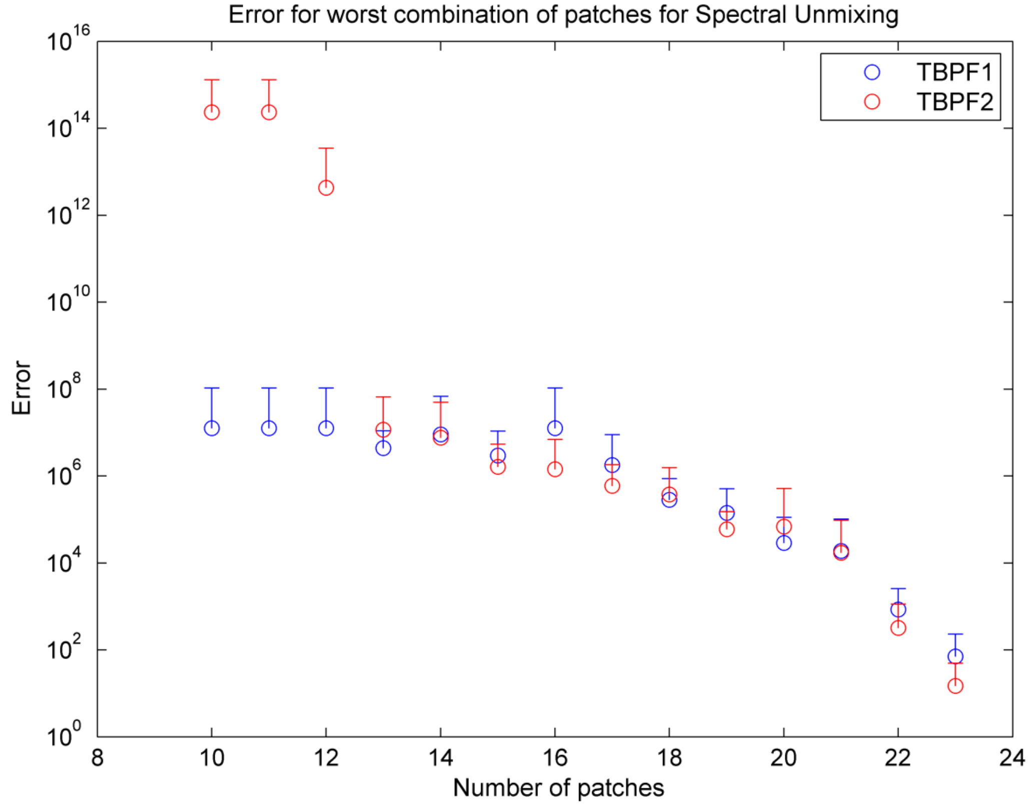

Figure 7-3 Spectral Unmixing - Color Patches Choice with maximum error

7.3 Channel Unmxing based on experimental measurements

Instead of using an algorithm to remove the cross-talking between the six narrow spectral bands, the camera spectral sensitivity can be used. To measure the cameras spectral sensitivity a monochromator, an optical power energy meter, and a light source are employed. Moreover, a beam splitter element was used to split the incoming light between the CCD sensor and the energy meter in order to quantify its energy.

This process was studied and used in the MSc Thesis of Vassilis Kavvadias, Simultaneous Multi-Spectral Imaging System: Application in Real-Time, Unsupervised Spectral Classification in Endometrial Endoscopy.

The monochromator helped stimulate the CCD with a very narrow band illumination, which with the help of an optical power energy meter had the same intensity at every wavelength. A sample of this illumination can be seen in Figure 7-4. With this method the cameras' spectral sensitivity is measured. Moreover, if the camera is coupled with a band pass filter the sensitivity of the two coupled elements can be measured as well the cross-talking between the spectral bands. With this way, the participation of each band can be measured and then be removed physically to decouple the spectral bands.

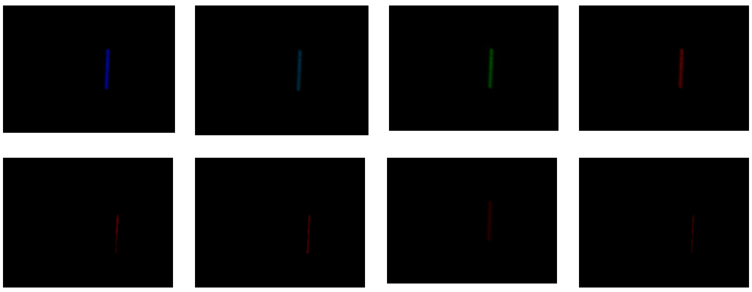

Figure 7-4 Sample output optical signals from a tunable diffraction grating monochromator

The results for the unmixing process can be seen in Figure 7-5 for TBPF 1 and Figure 7-6 for TBPF 2. The color circles represent the RGB values for each triple and the white circle their value after the unmixing process. The spectra data were acquired using a spectrometer under the same illumination conditions as the TBPF. In both cases the unmixed data provided a good spectral match with the measured spectra resulting to successful spectral unmixing process.

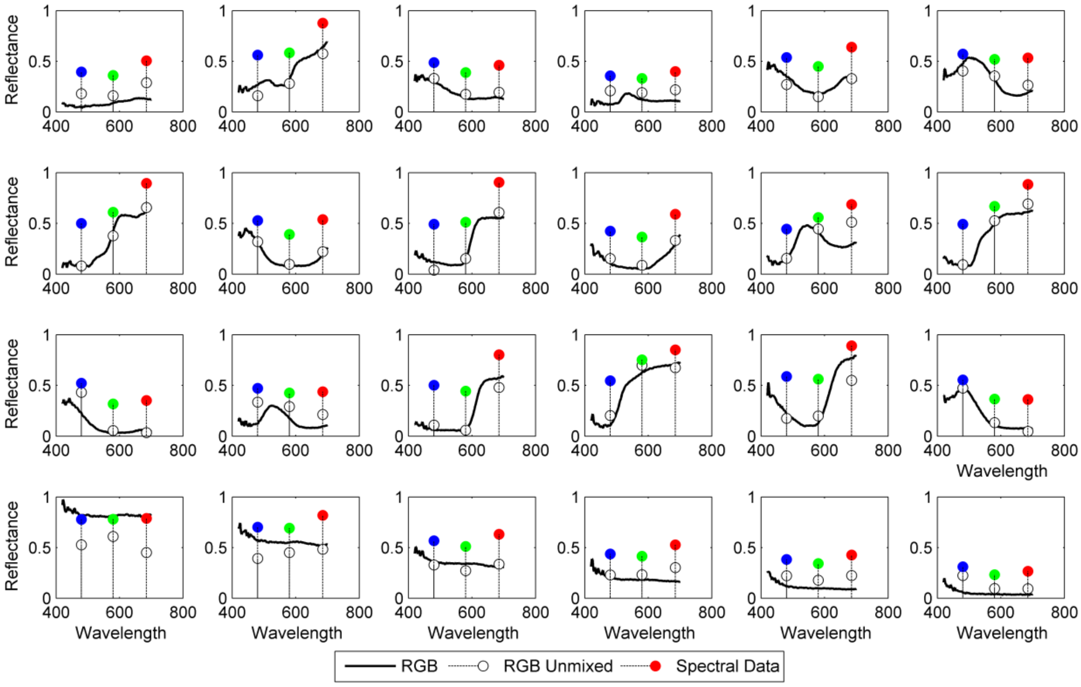

Figure 7-5 Spectral Unmixing Results Macbeth CC TBPF1

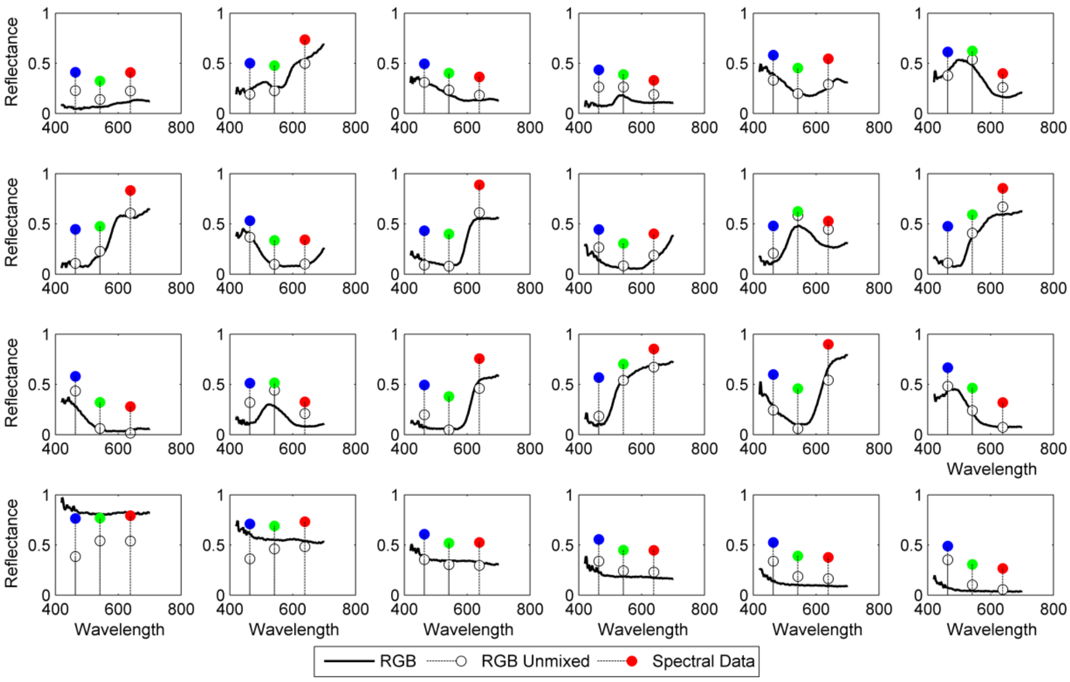

Figure 7-6 Spectral Unmixing Results Macbeth CC TBPF2

8 A novel Real-Time Spectral and Color Imaging System

8.1 System Description

Using the results of all the aforementioned experiments, a novel multispectral imaging system was designed that allows real time spectral and color imaging [69]. Two CCD cameras were used in conjunction with two TBPF, which affected the spectral sensitivities of the CCDs. Channel unmixing was performed on each TBPF to remove any cross-talking between the different bands-channels of the CCD.

The algorithms used on this system for both Spectral and Color Imaging require a priori spectral and colorimetric knowledge. Our system uses by default Gretag Macbeth® Color Checker CC. For the color imaging algorithm, a weight matrix is calculated in advance using the process described in chapter 6.4.

By performing spectral estimation using Wiener estimation, a complete spectral cube could be evaluated using the six narrow bands as input. Moreover, by acquiring data from the cameras in video rate, spectral estimation can be performed real-time and provide a spectral video for the desired spectral band. For the first time, this allows the observation of dynamic phenomena under different spectral bands with the press of a single button in real-time.

Besides spectral imaging, this system was designed to also reproduce color with high fidelity. The six spectral narrow unmixed bands are used and multiplied with the weight matrix. This setup allows real time color imaging with a camera resolution up to 1024x768.

8.2 Optomechanical Engineering

Optomechanical engineering, as a subset of mechanical engineering, specializes in optical systems, which usually have much higher design and manufacturing specifications than most machinery. They often require submicron precision during design and manufacturing. In addition, materials that are used in optical systems, such as glass filters, tend to have unusual physical properties, regarding great sensitivity to heat tolerance and mechanical stress. For the described imaging device, a conceptualization and design of a precision two-CCD camera system should be developed, involving beam splitting elements, relay lens, triple band pass filters and detachable x, y, z stages with micron mobility. The design was modeled using Solidworks 3D CAD design software and manufactured at a specialized in micromachining machinery. A complete model of the snapshot multispectral imaging device is shown in Figure 8-1.

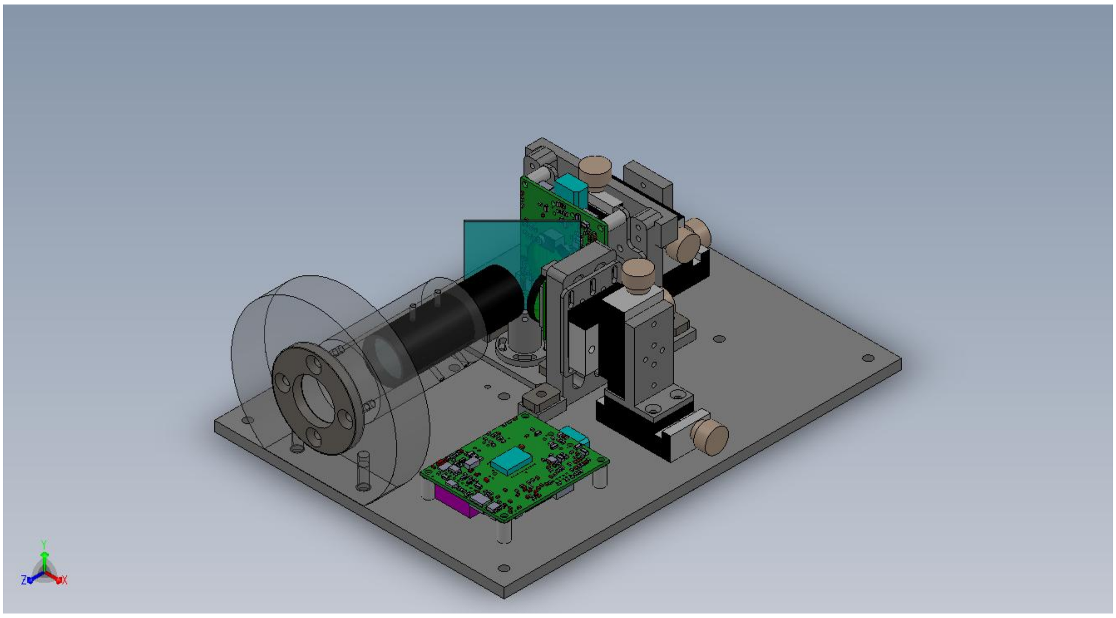

Figure 8-1 Diagonal Experimental Setup

8.3 Real Time Spectral Imaging

As aforementioned, Wiener estimation was used for the spectral estimation process. This method creates an estimation matrix, the so-called Wiener matrix, and multiplies the input data (in our case six spectral bands) to create the Estimated Spectral Cube. For example, given six narrow band images with resolution 1600x1200, the input data would be 1600x1200x6. Given that the a priori knowledge for the visible spectrum would be images from 420nm to 700nm with 10nm integral (29 images), the data required for the calculation of the Wiener matrix would be 1600x1200x29 (Spectral Data - SD) and 1600x1200x6 (Narrow Band Data - SB). To calculate the Wiener matrix the following mathematical procedure is used:

$$R_{vv} = SB * SB^T$$
$$R_{rv} = SD * SB^T$$
$$G = R_{rv} * R_{vv}^{-1}$$

Where R_{vv} and R_{rv} the autocorrelation matrices between the Six Band input (SB) and its transpose and the Spectral Data (SD) and the SB. G is the Wiener estimation matrix.

Now, given the dimensionality described above for the a priori knowledge, G would be 29x6. Since 29 was the number of wavelengths used a priori, each of the rows of the matrix represents the six band value in correlation to a specific wavelength of the spectral cube. Given an input of one pixel (with size 6x1), if the input is multiplied with only one row of the

Wiener estimation matrix, only the value for the specific wavelength would be reproduced as shown in equation (2).

$$r_{est} = \begin{bmatrix} G_{1,1} & \cdots & G_{1,6} \\ \vdots & \ddots & \vdots \\ G_{29,1} & \cdots & G_{29,1} \end{bmatrix} * [SB_1 \quad \cdots \quad SB_6] \ (1)$$

$$r_{est\_wl1} = [G_{1,1} \quad \cdots \quad G_{1,6}] * [SB_1 \quad \cdots \quad SB_6] \ (2)$$

Given that the input was to be 1600x1200, thus 1600x1200x6, the estimation process to calculate a complete spectral cube (1600x1200x29) would be approximately 0.21s whereas to calculate only one band (1600x1200 at a specific wavelength) would be approximately 0.04s. Therefore, if the input data originated from a real-time video feed, each given moment a specific band of the spectrum could be reproduced and shown in full resolution (1600x1200 in that case) in real-time.

It is important to note that the Wiener estimation matrix is calculated beforehand for the given a priori knowledge. To eliminate any errors introduced by different lighting or geometric conditions, look-up-tables were created that corresponded to various conditions to match any desired acquisition setting.

8.3.1 Microscopy Tile

In Figure 8-2 spectral estimation was performed in the Microscopy Tile seen in Figure 8-3. In this case, Spectral Transmittance was evaluated instead of Spectral Reflectance. The two spectral curves represent Hematoxylin and DAB which are also pointed out in the RGB image. It can be seen that the spectral estimation procedure managed to predict most of the spectral characteristics of the samples. Again, Gretag Macbeth® Color Checker® CC was used as the training set, although the data were reflectance spectra.

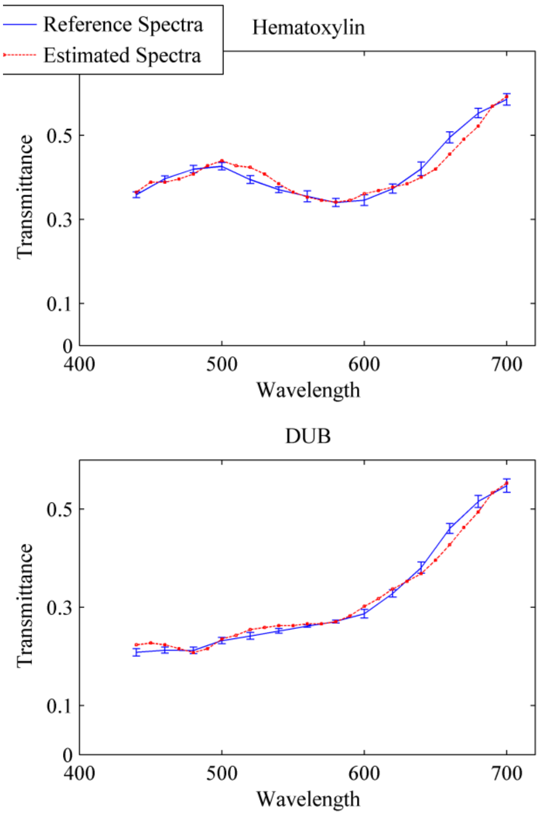

Figure 8-2 Spectral Estimation (Visible) Microscopy Tile - Hematoxylin, DAB

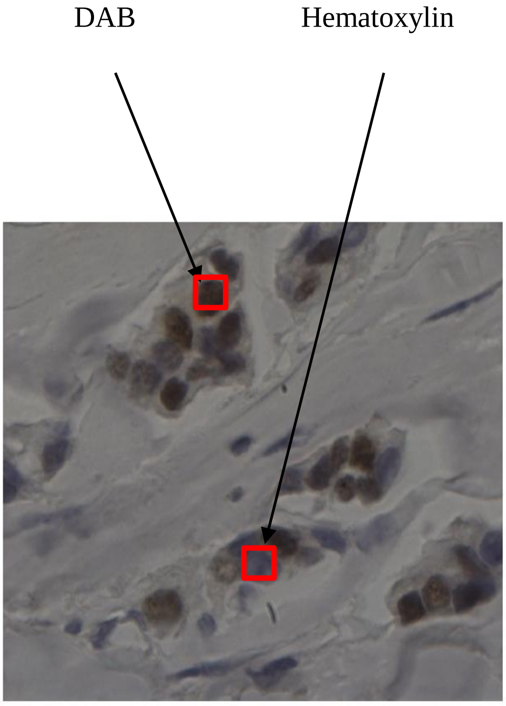

Figure 8-3 Microscopy Tile RGB

In Table 8-1 the quantitative results of the estimation process can be seen. In this scenario no thresholds are employed since there were only two samples to be estimated. Spectral Angle Mapper (SAM) was used to quantify the difference. The mean value of SAM is quite low which the desirable outcome was. That validates that spectral estimation can be performed for transmittance spectra and applied to fields such as microscopy.

Table 8-1 Microscopy Tile Films Spectral Estimation Quantitative Results

	SAM (MeanValue, Standard Deviation)
Microscopy Tile	$0{,}0576 \pm 0{,}0180$

8.4 Real Time Color Imaging

Color can be reproduced with two different methods. The first was by using a complete spectral cube of the object in question and multiplying it with the illuminant desired as well as the Color Matching Function. The second was the newly proposed way of weighted unmixed spectral bands.

The first process is time consuming since for each frame a whole cube as well as all data needed must be calculated as described in the beginning of Chapter 0. To calculate the XYZ values that were derived from the multiplication of the spectral cube, the SPD of the illuminant and the CMF function, 1.34 seconds were needed. Moreover, the output needed to be transformed into RGB, so an extra overhead of 0.04 second was added to calculate the XYZ data with the transformation matrix M. Thus **1.34** for XYZ evaluation, plus **0.04** for RGB Transformation, plus **0.21** for Spectral Cube estimation, summed up to **1.59** seconds which effectively eliminates our ability for real time color imaging.

The second process was less time consuming since the only data needed for the color reproduction was the weight matrices for the unmixing and the weight matrix for the RGB transformation, which were evaluated beforehand. As with spectral estimation, to avoid any introduction of errors, the weight matrices were calculated under different illumination and geometric condition and a look-up-table was created that corresponded to various conditions to match any desired acquisition setting.

Two main processes were at hand; Spectral Unmixing for each of the cameras and the transformation of the six narrow unmixed bands to RGB. The unmixing process took approximately **0.014s** for the TBPF1, **0.012s** for the TBPF2, and the RGB calculation approximately **0.014s**. Those three processes added up to a total of **0.04s** which was significantly less than the **1.59s** needed for the first case. Thus, given a real-time video feed of six narrow spectral bands, spectral unmixing and color reproduction could be performed in real-time.

For both cases, the accuracy of the result was very high as described in Chapters 0 and 0. The speed of the weighted color reproduction outperformed the speed of the traditional one but it came with a tradeoff. The color reproduced could be only under the given illuminant at that given moment (i.e. D50, D65 etc.).

8.5 Color Imaging Using Six Unmixed Spectral Bands

Color reproduction using a Multispectral system like the MUSIS HS camera, can be performed with two ways as described before. One was with Spectral Estimation in order to acquire the whole spectral cube of the specimen within the visible spectrum and the other with a weighted matrix.

A new multispectral system is designed using two RGB cameras coupled with two interference filters, shown in Figure 7-1, along with a beam splitter in order for both cameras to acquire the image properly. This system underwent the unmixing process and can acquire simultaneously six spectral bands that can be used for both Spectral and Color Imaging.

The Color reproduction results will be called RGB_Unmixed to indicate the use of unmixed spectral bands. In order to evaluate the quality of the reproduced color, a comparison was made between the RGB_Unmixed, as well as each triple band both mixed and unmixed, with the actual RGB image under the same illumination and geometric conditions. The weights used for both triple band unmixing and RGB transformation were created using the Gretag Macbeth Color Checker® CC.

The specimen used for testing was the Gretag Macbeth Color Checker® SG, which contains 140 color patches. The external surrounding patches are black, grey and white with the same Spectral and Color characteristics so they are not used in this comparison. Since the Color Checker is quite sizable, it is split into four quadrants (Quads) each containing 24 color patches. For each Quad from first to fourth, the black-white-gray patches excluded from the quantitative comparison are located in the corners of each color image. Top left for the first quad, top right for the second, bottom left for the third and bottom right for the fourth. In order to equally distribute the number of patches within the four images a white spot was placed that marked the center of the Macbeth® SG. That exclusion process left 96 color patches for the quantitative testing.

Thus for each of the four quadrants, 4 figures will be presented for each comparison case. Firstly the RGB values were compared with the RGB_Unmixed ones. Afterwards the RGB values were compared with both TBPFs for mixed and unmixed data.

The results provided can help evaluate the quality of the color reproduction both numerically and perceptually. The reproduced image, side by side with the measured RGB one for each case, is the first result available in order to identify the perceptual difference. Afterwards the quantitative measures of CIELAB color difference were evaluated. For each case, the statistical analysis for both ΔE_{94^*} and ΔE_{ab^*} can be seen, as well as the two vector plots that provide the magnitude of the error for chromasity and lightness.

When all five cases were presented (RGB_Unmixed, TBPF1, TBPF1_Unmixed, TBPF2 and TBPF2_Unmixed) an overall assessment was made and the best case scenario was chosen. In advance, it was expected that the RGB_Unmixed would have the best performance, followed by TBPF2 and TBPF1 and lastly by the Unmixed TBPFs.

Images captured with the Cameras coupled TBPFs provided a result that resembled the RGB images but still had high perceptual differences. Depending on the peak transmission of each TBPF according to the RGB spectral sensitivity, the color may appear more, or less, saturated. For example, if the peak transmission of a TBPF matched the peak transmission of the RGB channels, the colors of the image would be more saturated, “warm”, whereas in an opposite case the color would seem “cold”. The overlapping of the Spectral Sensitivity curves of the RGB with each TBPF can be seen in Figure 8-4 and Figure 8-5 for TBPF1 and TBPF2 correspondingly.

Since the Unmixed TBPFs contained “pure” spectral information, the color reproduced by using each of the three bands as the corresponding color (i.e. 464nm as Blue, 542 as Green and 639 as Red) wouldn’t be close to a normal RGB image. That was because by coupling the CCD with the TBPFs the spectral sensitivity of the Camera sensor was changed and along with the spectral unmixing, the information of the bands became “pure” spectral. The RGB image produced by using those three bands creates a “pseudo color” RGB image that illustrates the color produced by three spectral bands.

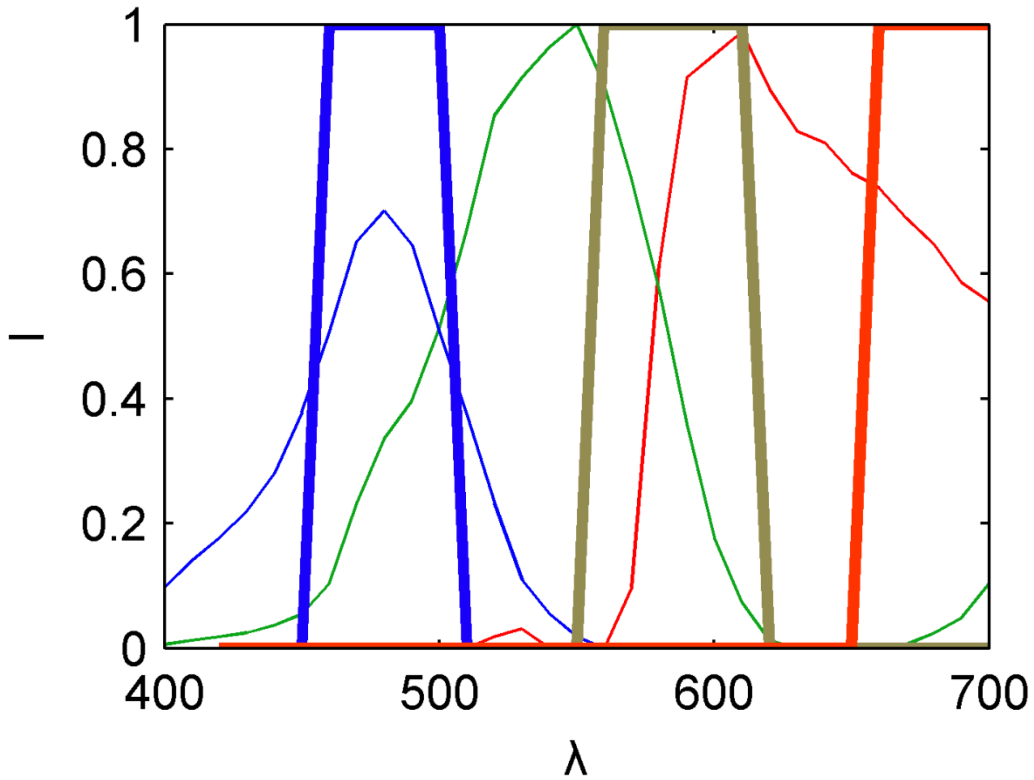

Figure 8-4 RGB Spectral Sensitivity Coupled with TBPF1

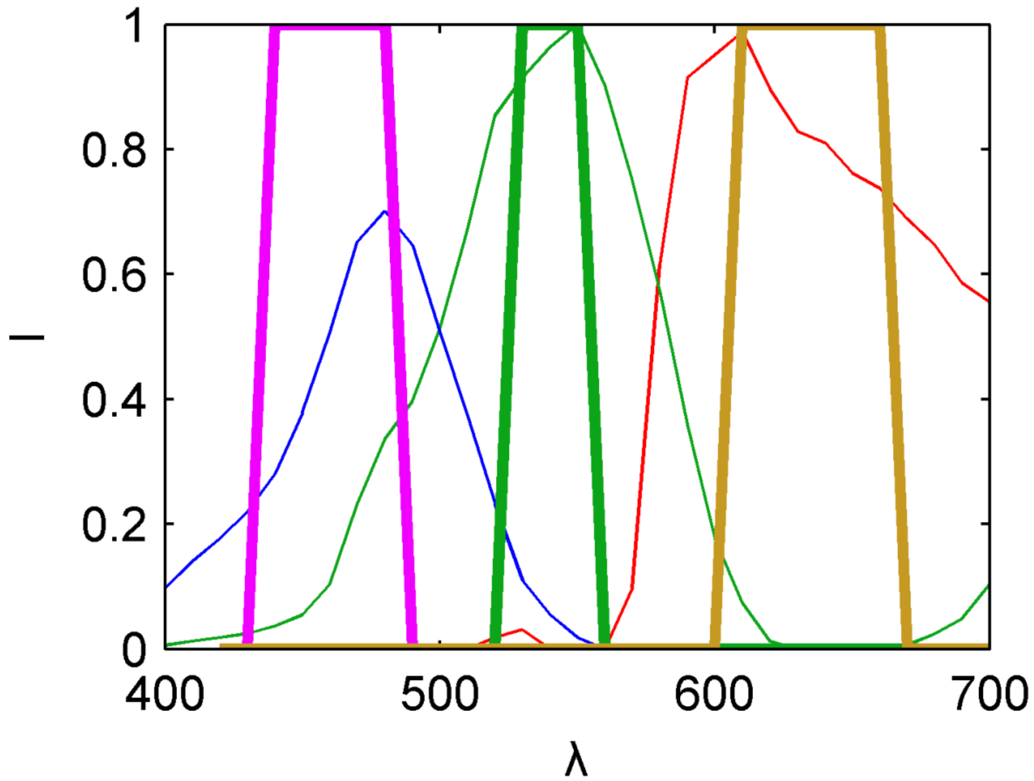

Figure 8-5 RGB Spectral Sensitivity Coupled with TBPF2

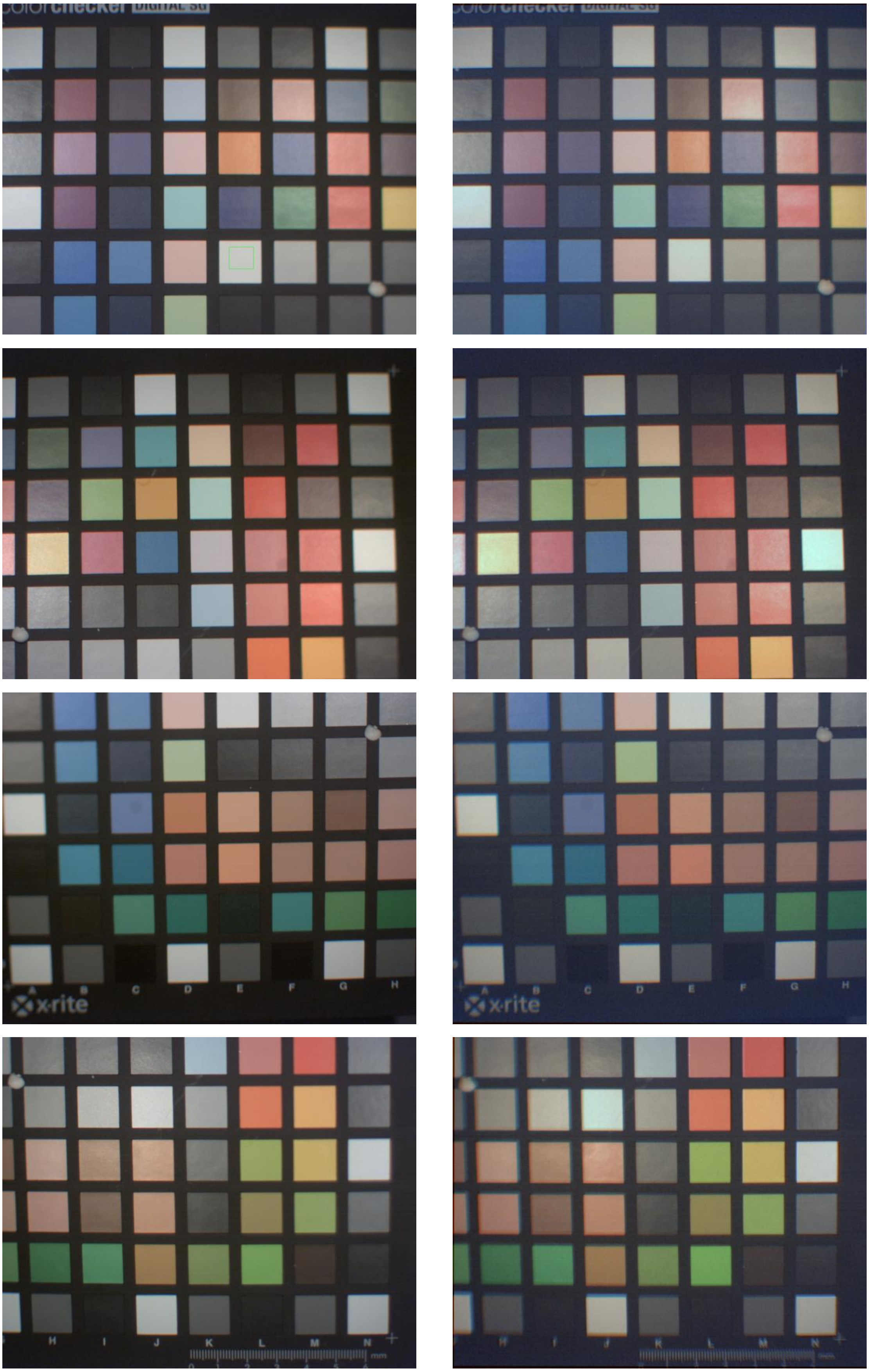

Figure 8-6 RGB (Left Column) and RGB_Unmixed (Right Column) Images Macbeth SG Quad1-4 Respectively

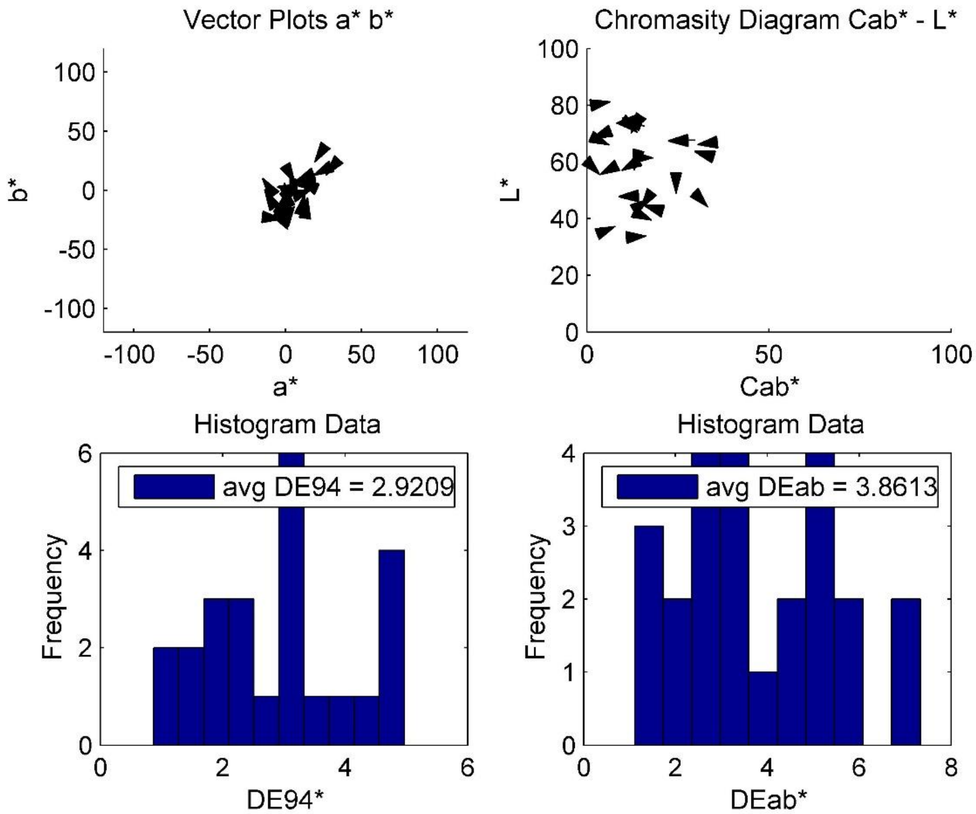

Figure 8-7 CIELAB Metrics Quad 1 RGB vs. Unmixed RGB

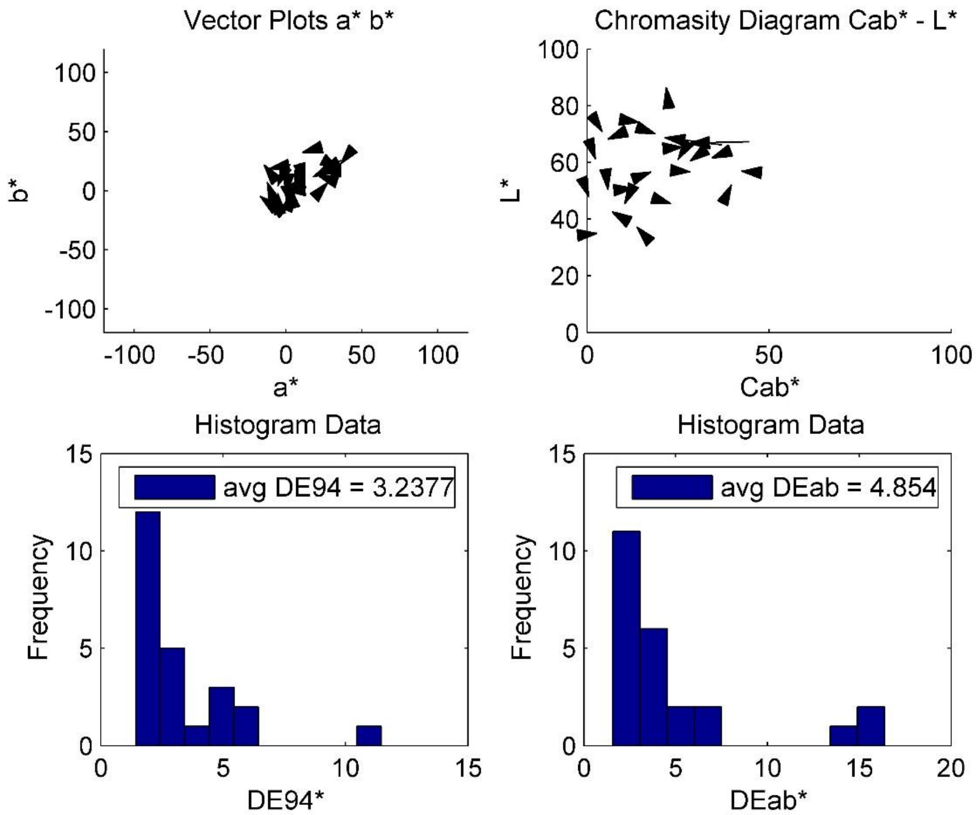

Figure 8-8 CIELAB Metrics Quad 2 RGB vs. Unmixed RGB

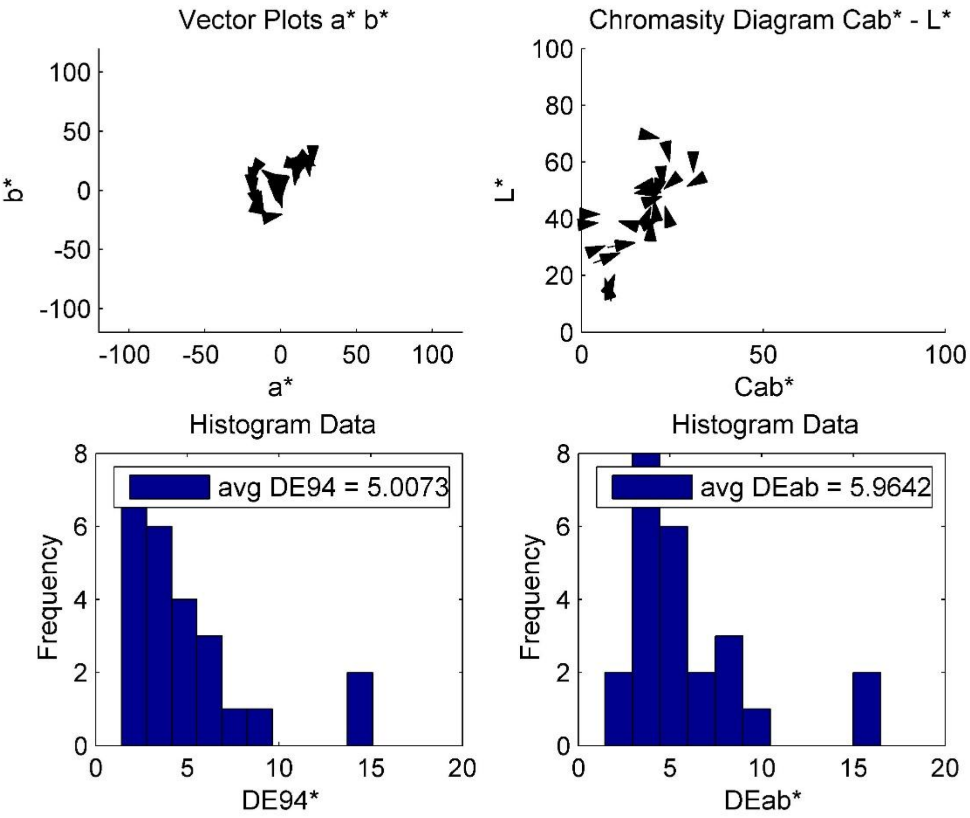

Figure 8-9 CIELAB Metrics Quad 3 RGB vs. Unmixed RGB

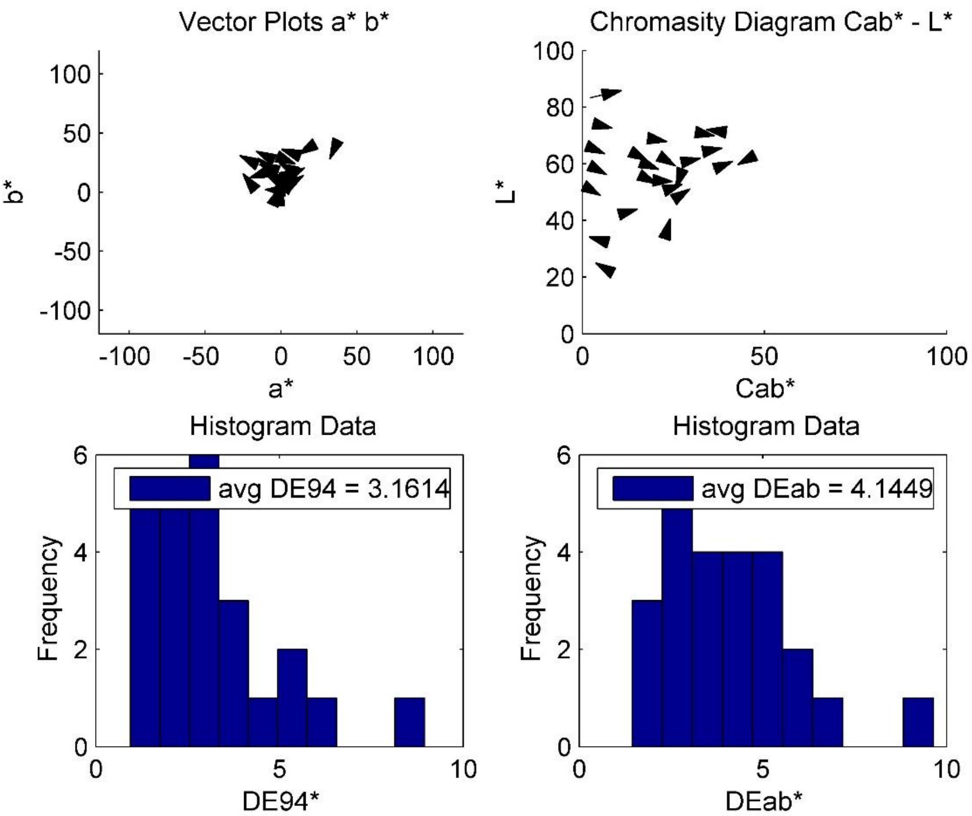

Figure 8-10 CIELAB Metrics Quad 4 RGB vs. Unmixed RGB

Figure 8-11 RGB (Left Column) and TBP1 (Right Column) Images Macbeth SG Quad1-4 Respectively

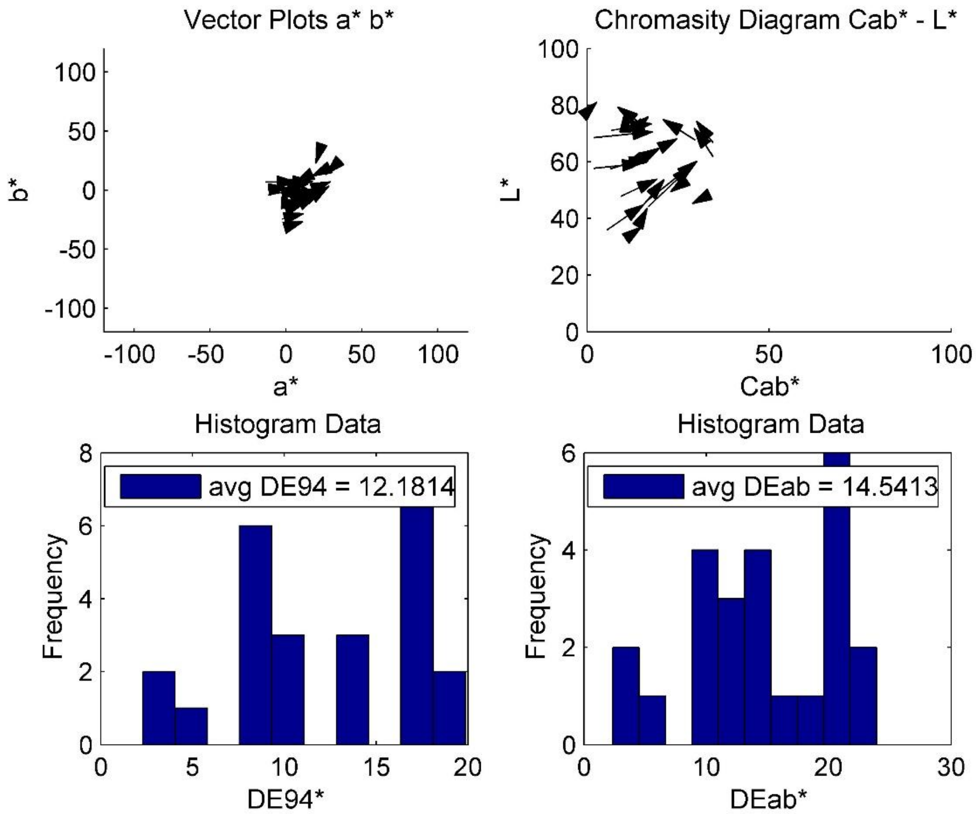

Figure 8-12 CIELAB Metrics Quad 1 RGB vs. TBP1

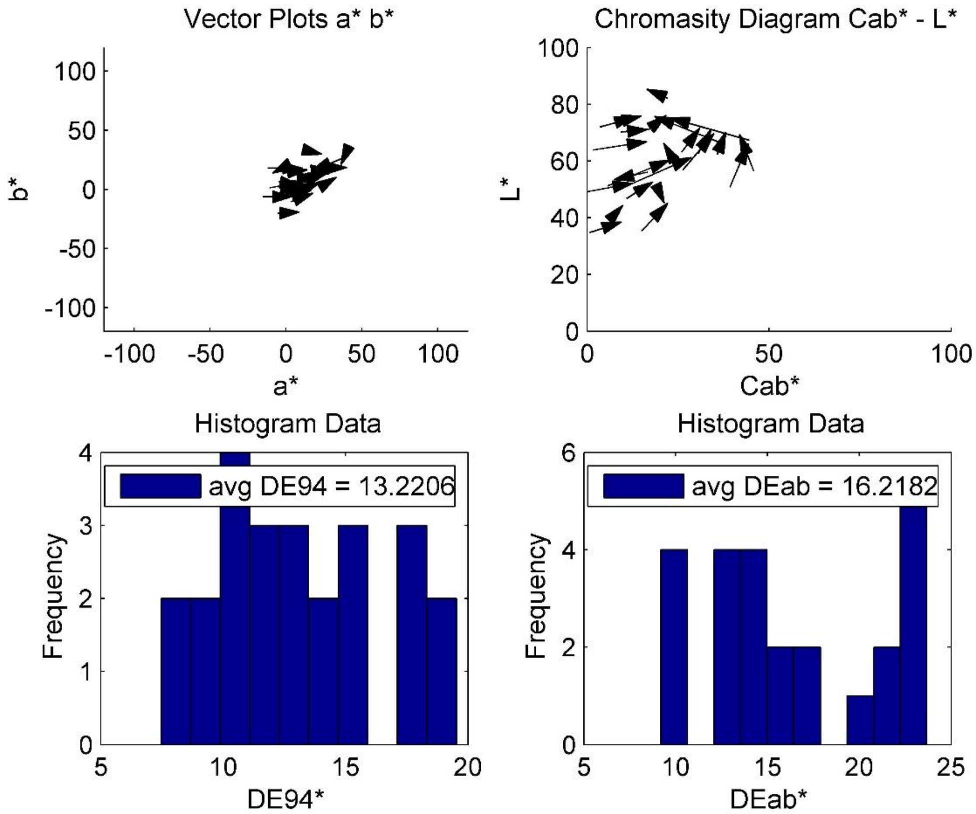

Figure 8-13 CIELAB Metrics Quad 2 RGB vs. TBP1

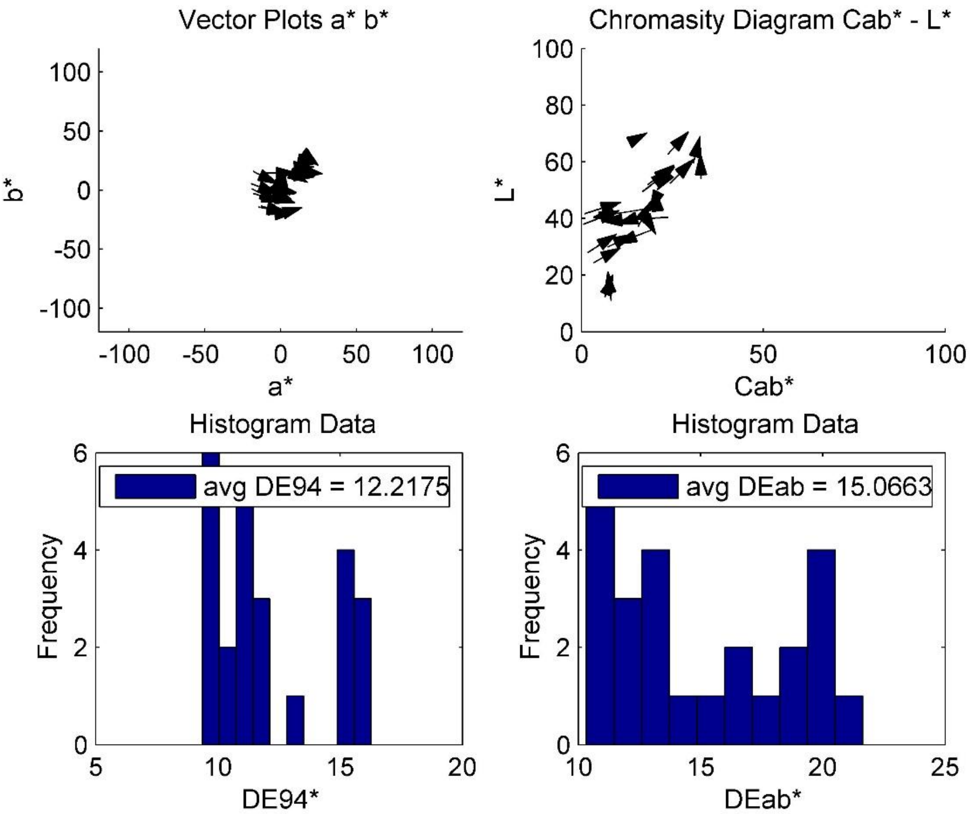

Figure 8-14 CIELAB Metrics Quad 3 RGB vs. TBP1

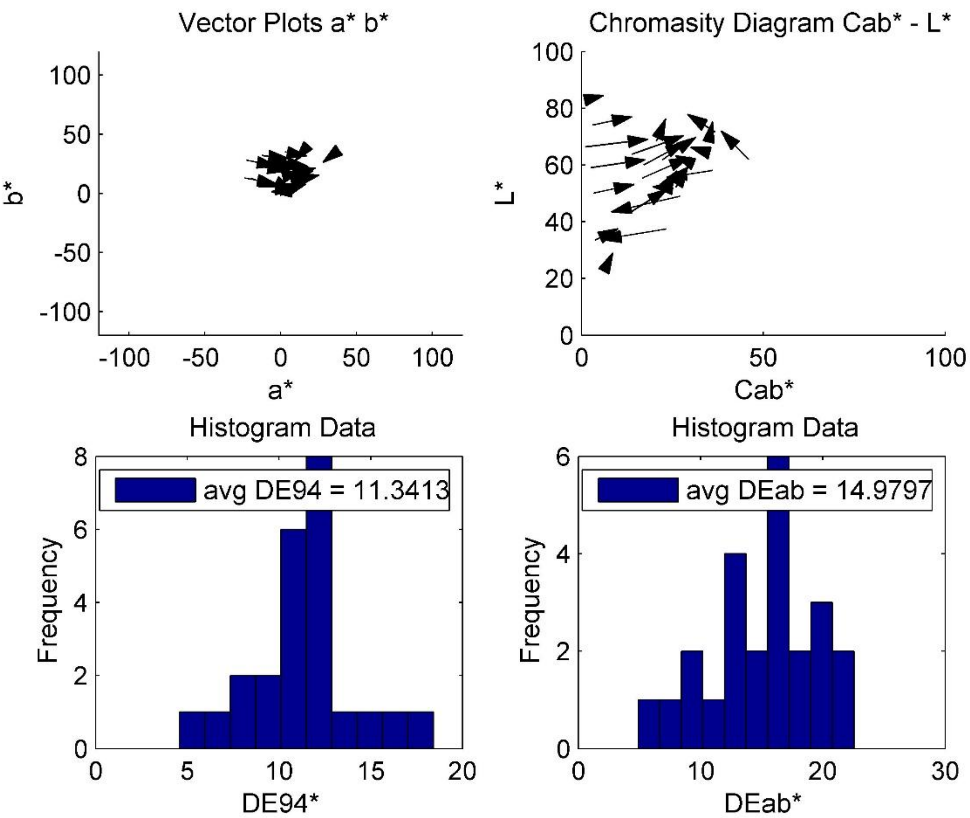

Figure 8-15 CIELAB Metrics Quad 4 RGB vs. TBP1

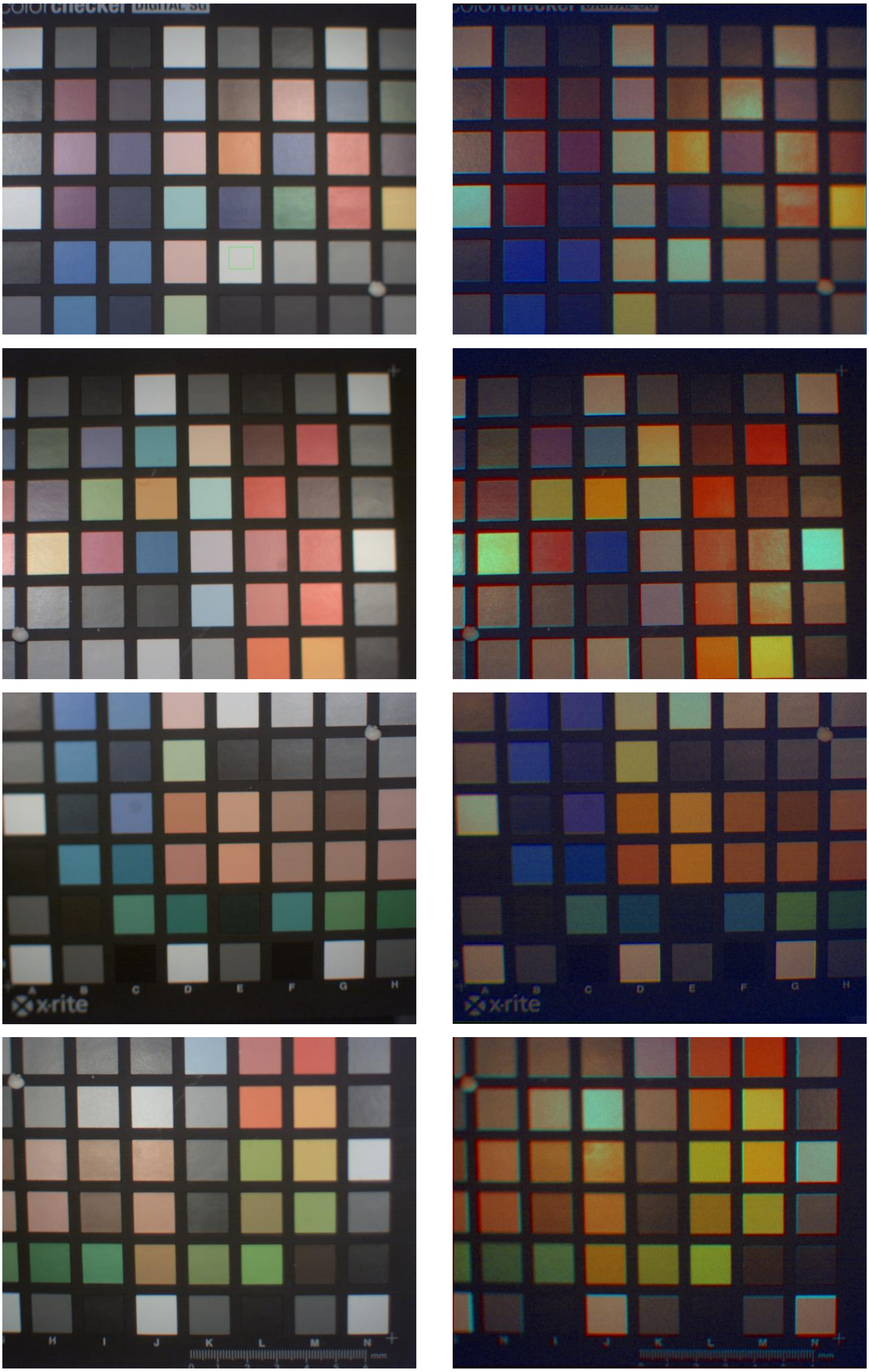

Figure 8-16 RGB (Left Column) and TBP1_Unmixed (Right Column) Images Macbeth SG Quad1-4 Respectively

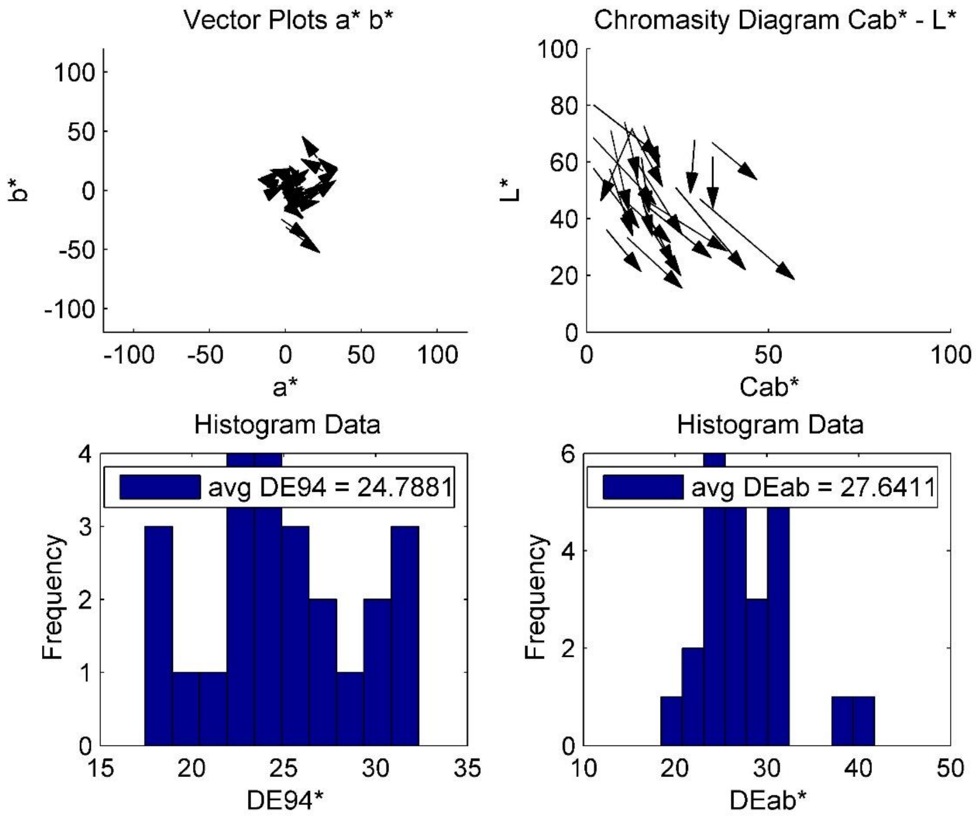

Figure 8-17 CIELAB Metrics Quad 1 RGB vs. TBP1_Unmixed

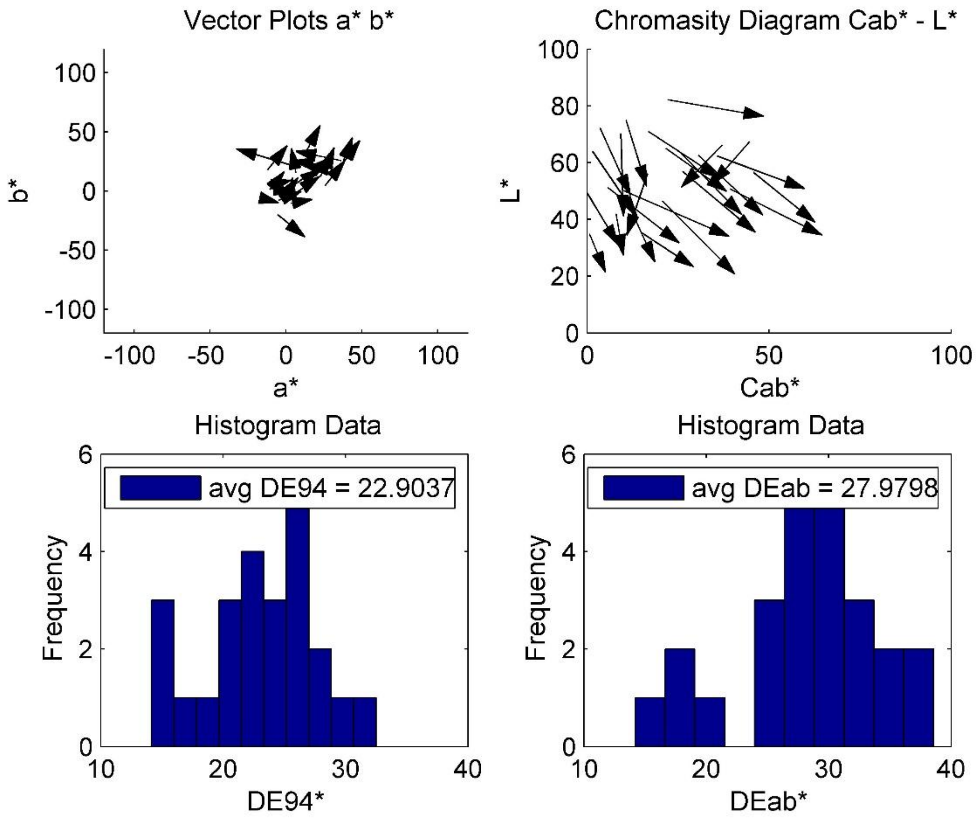

Figure 8-18 CIELAB Metrics Quad 2 RGB vs. TBP1_Unmixed

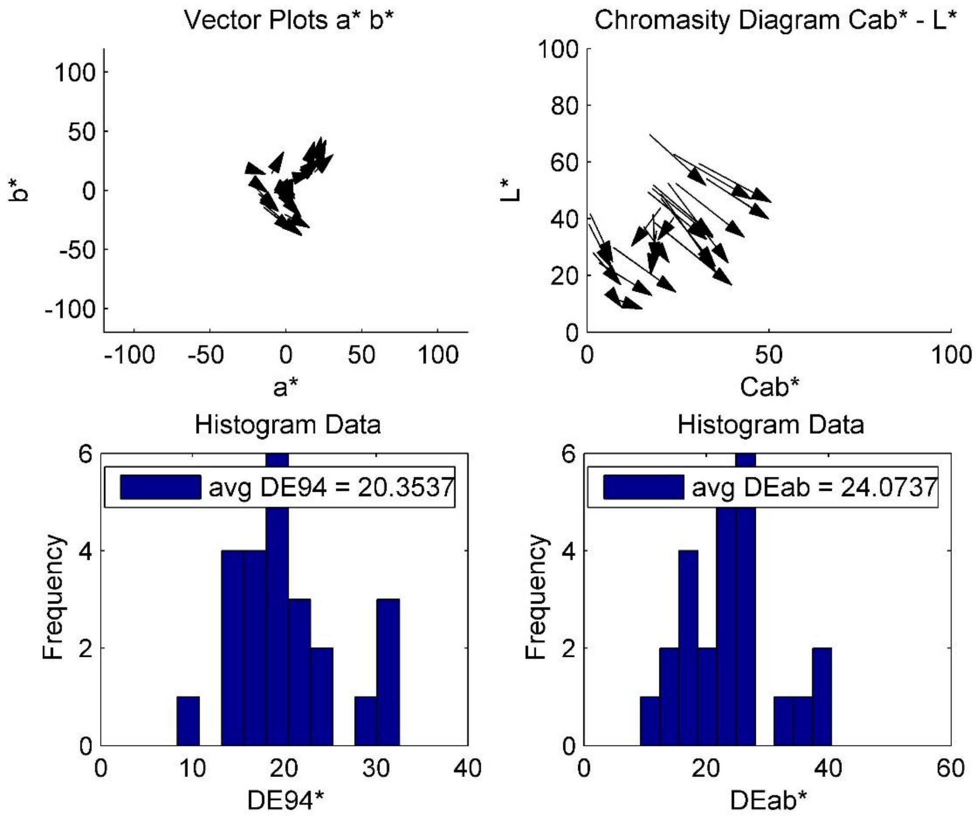

Figure 8-19 CIELAB Metrics Quad 3 RGB vs. TBP1_Unmixed

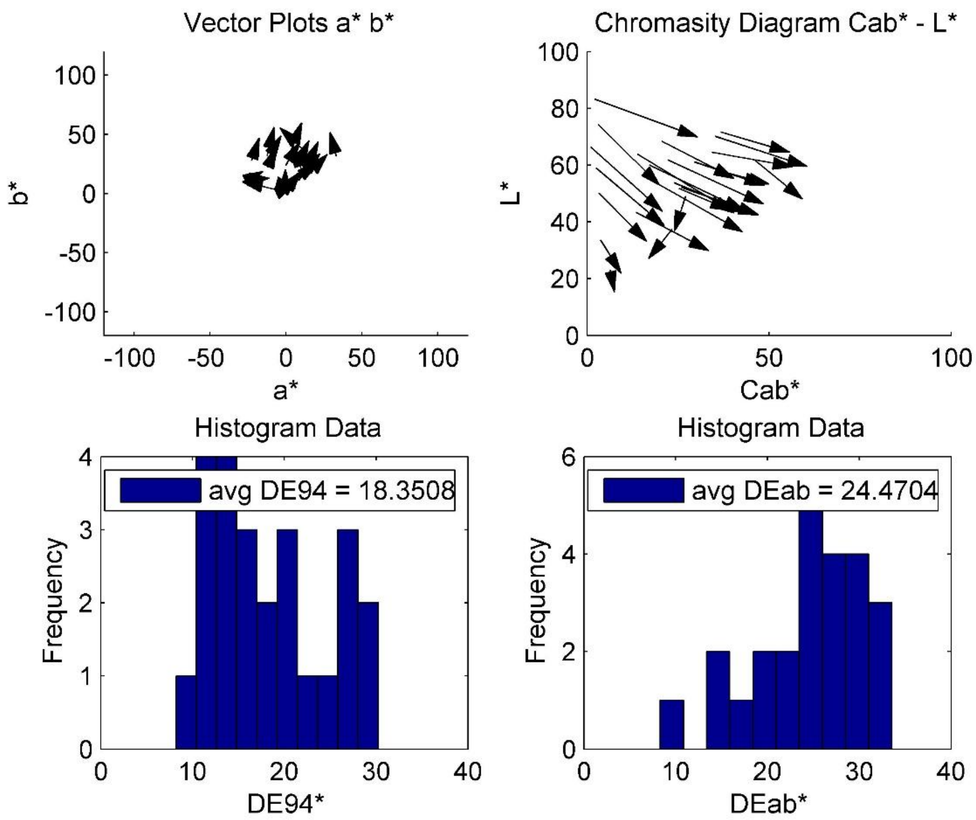

Figure 8-20 CIELAB Metrics Quad 4 RGB vs. TBP1_Unmixed

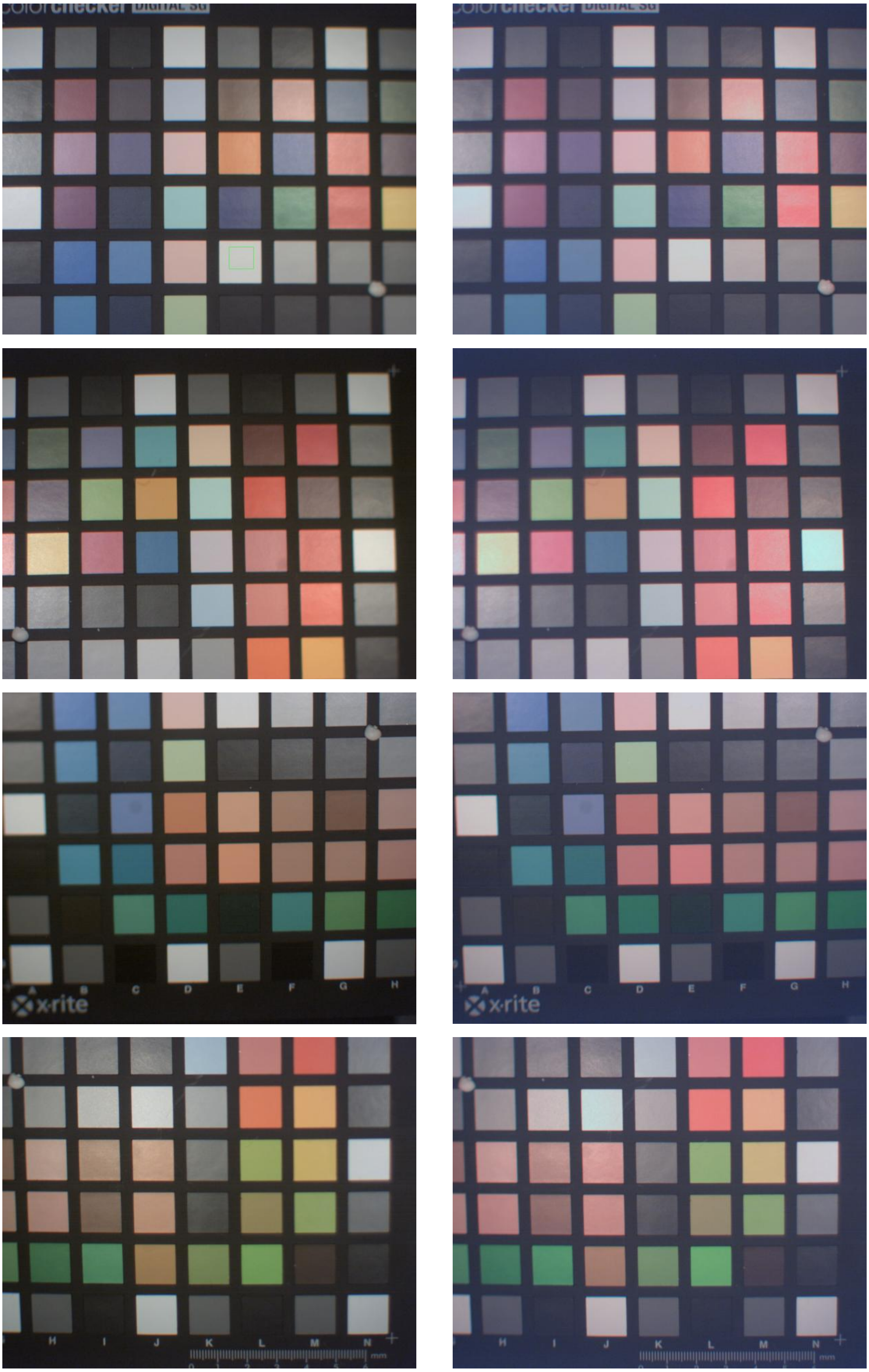

Figure 8-21 RGB (Left Column) and TBP2 (Right Column) Images Macbeth SG Quad1-4 Respectively

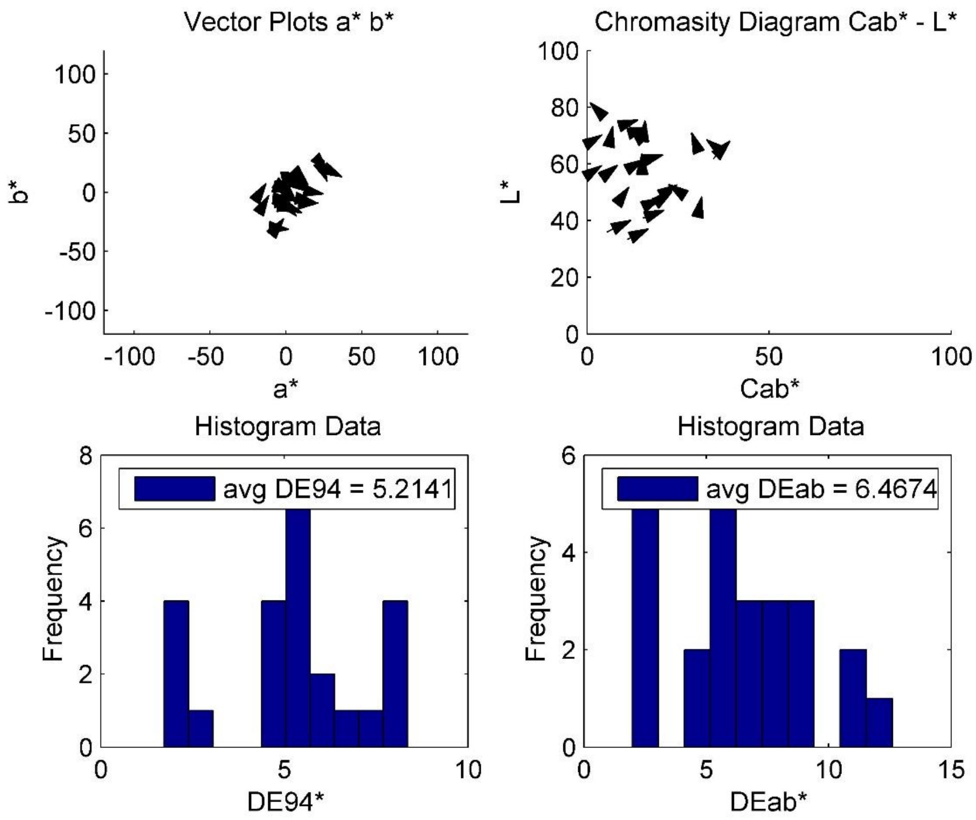

Figure 8-22 CIELAB Metrics Quad 1 RGB vs. TBP2

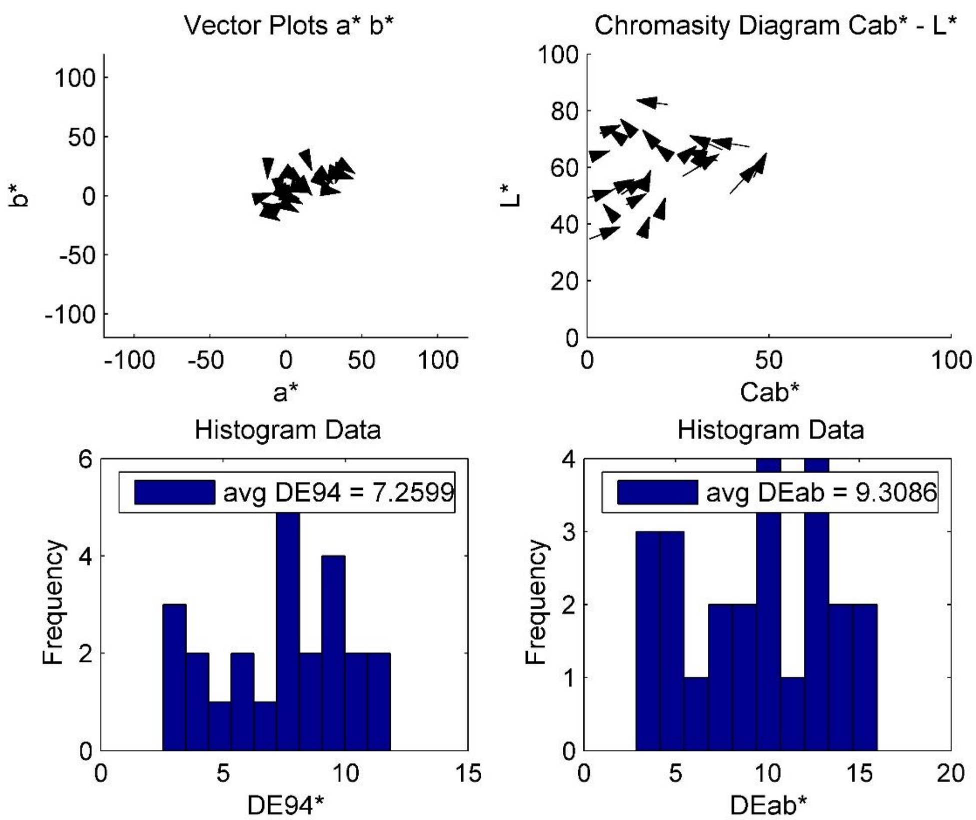

Figure 8-23 CIELAB Metrics Quad 2 RGB vs. TBP2

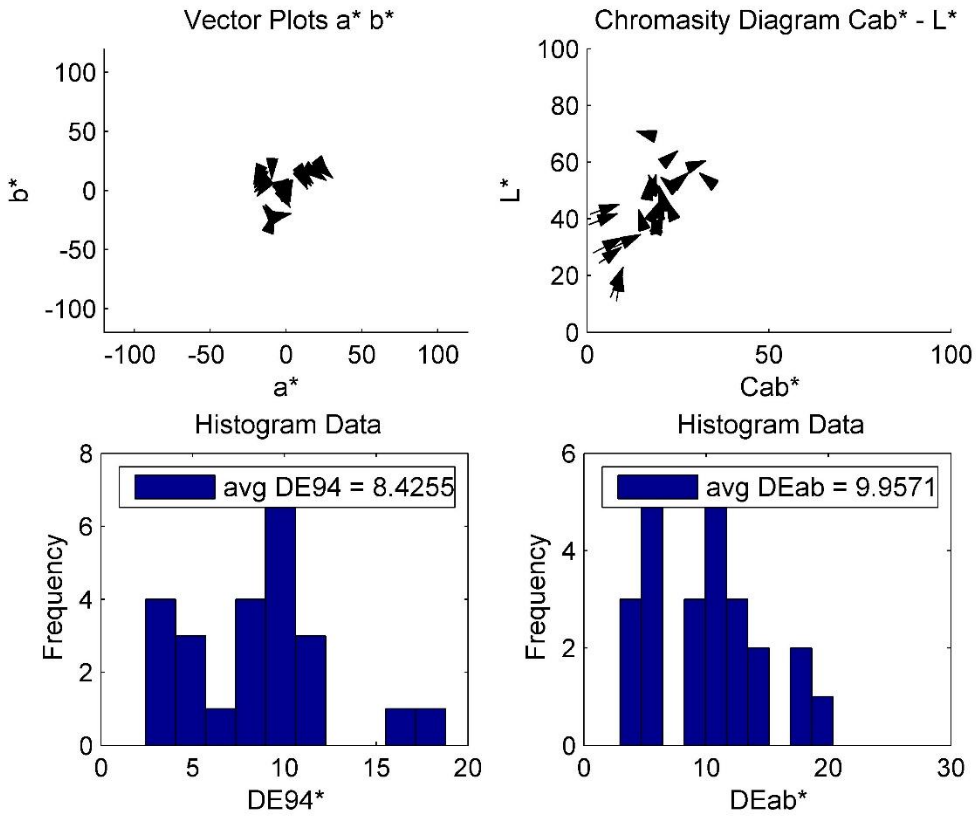

Figure 8-24 CIELAB Metrics Quad 3 RGB vs. TBP2

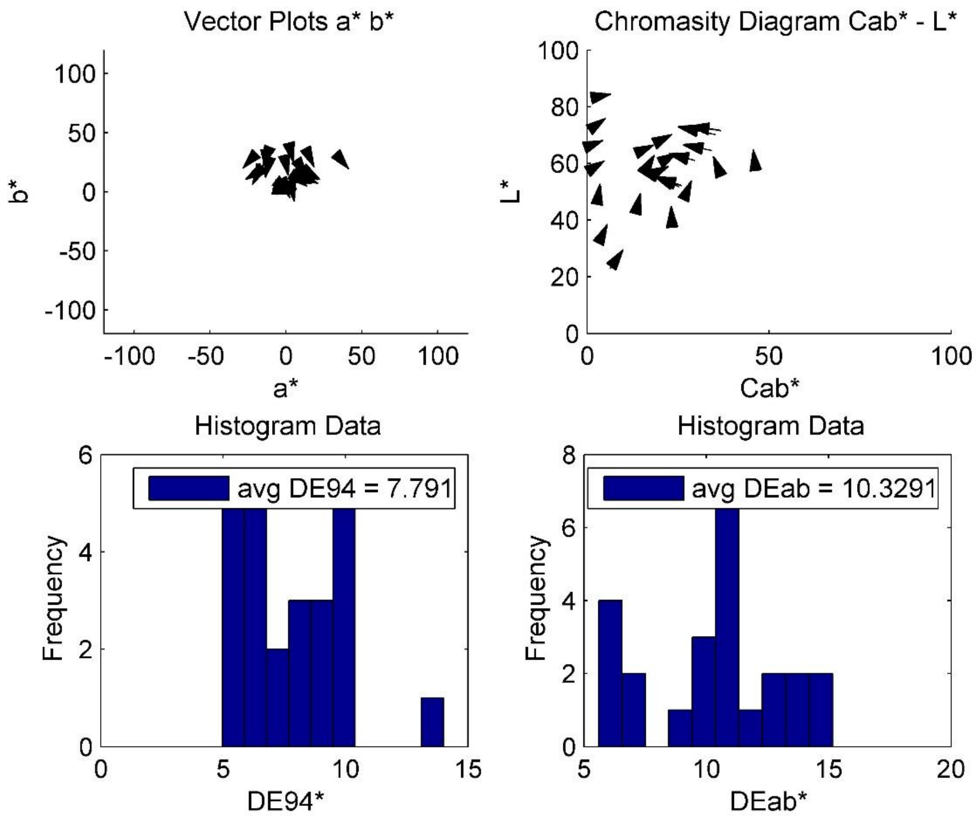

Figure 8-25 CIELAB Metrics Quad 4 RGB vs. TBP2

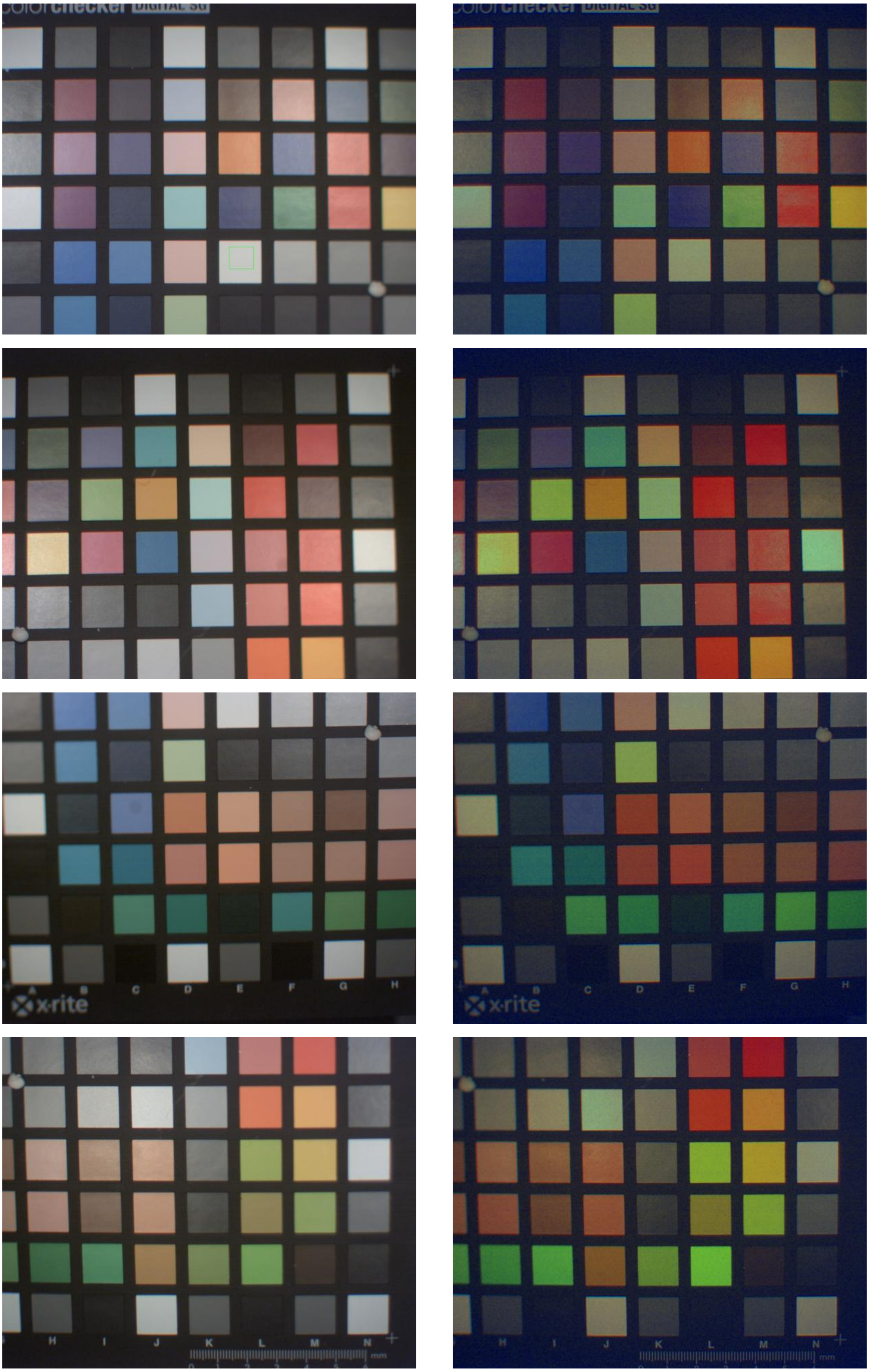

Figure 8-26 RGB (Left Column) and TBP2_Unmixed (Right Column) Images Macbeth SG Quad1-4 Respectively

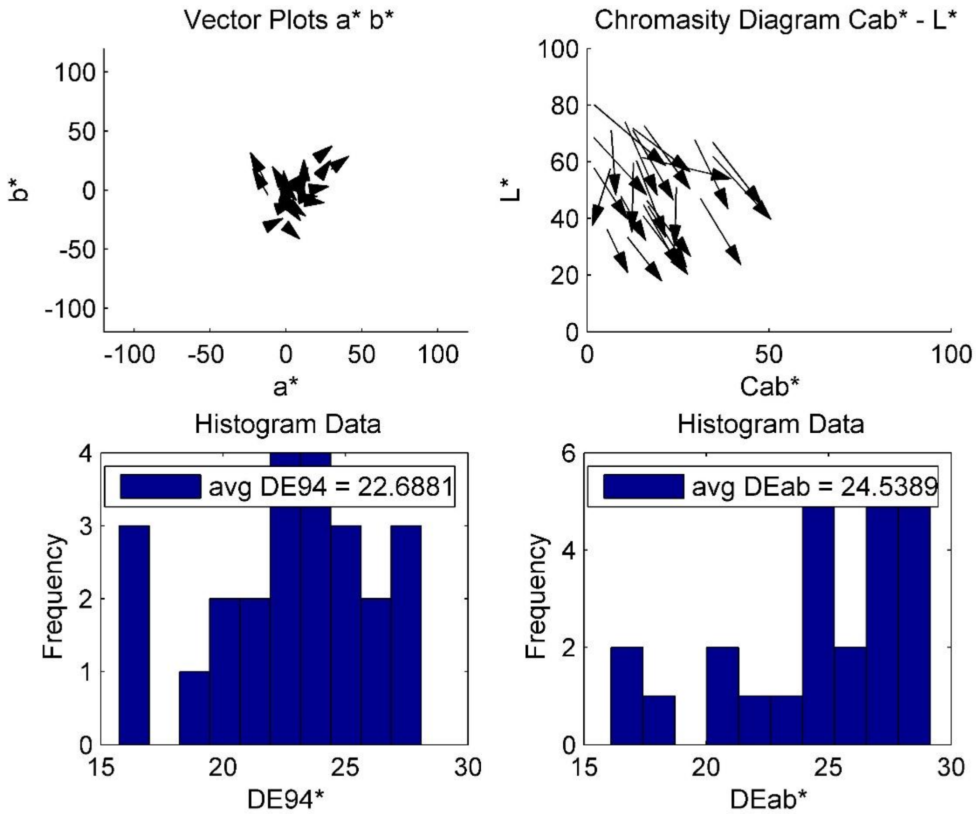

Figure 8-27 CIELAB Metrics Quad 1 RGB vs. TBP2_Unmixed

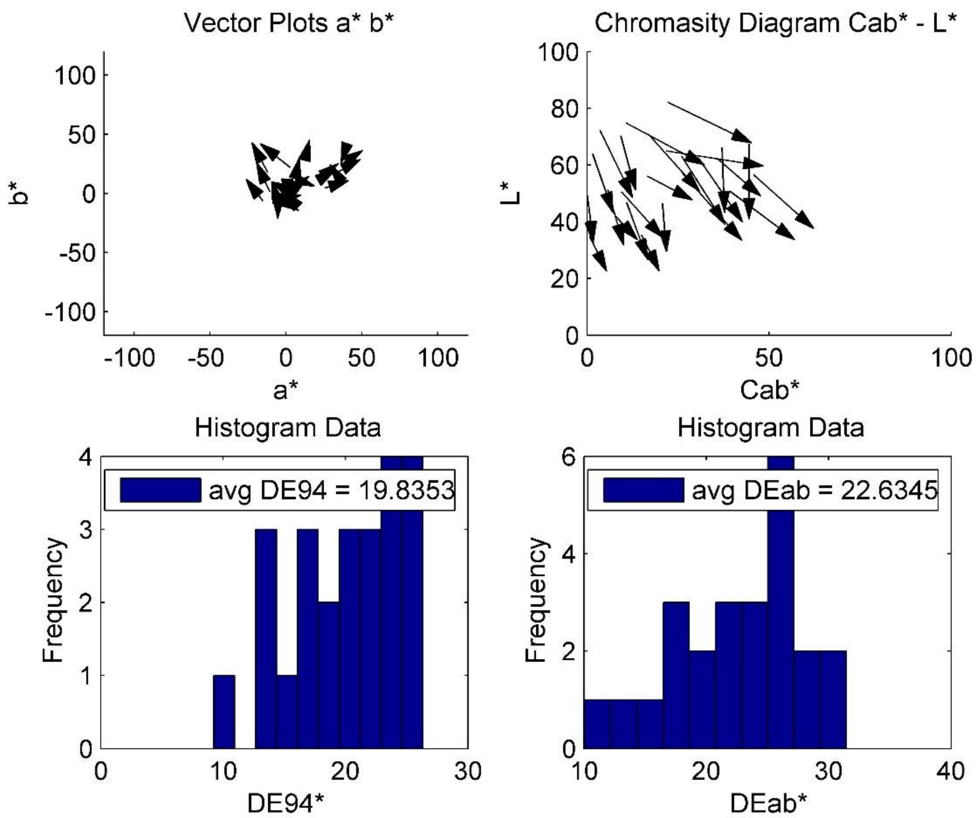

Figure 8-28 CIELAB Metrics Quad 2 RGB vs. TBP2_Unmixed

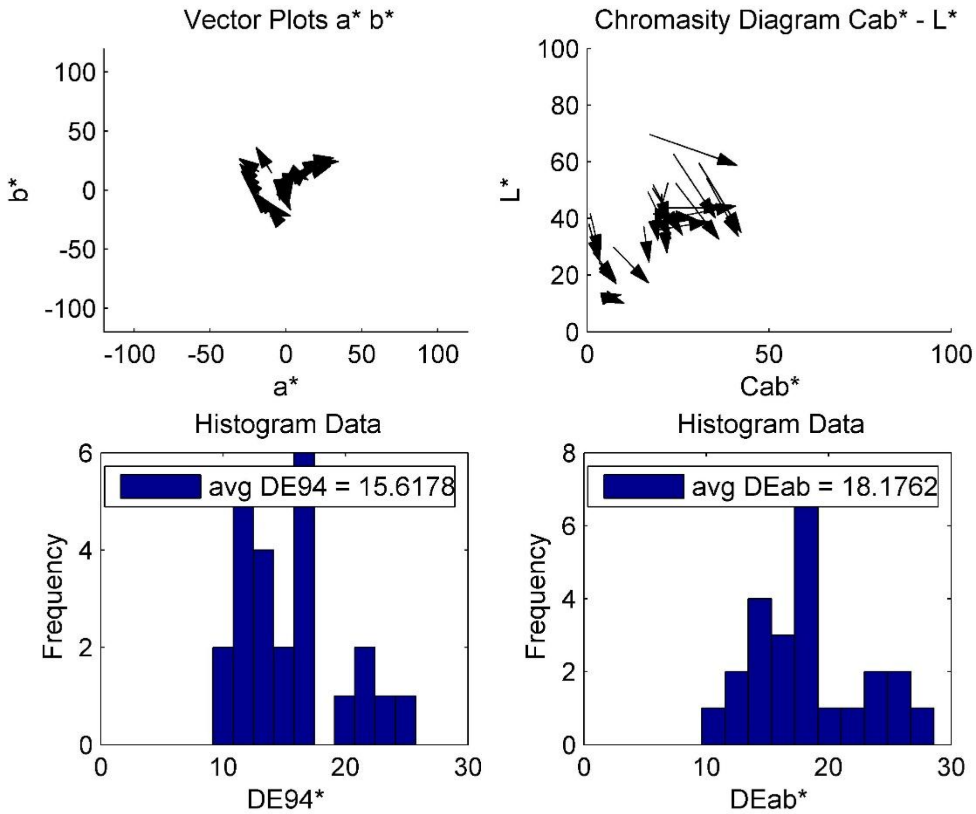

Figure 8-29 CIELAB Metrics Quad 3 RGB vs. TBP2_Unmixed

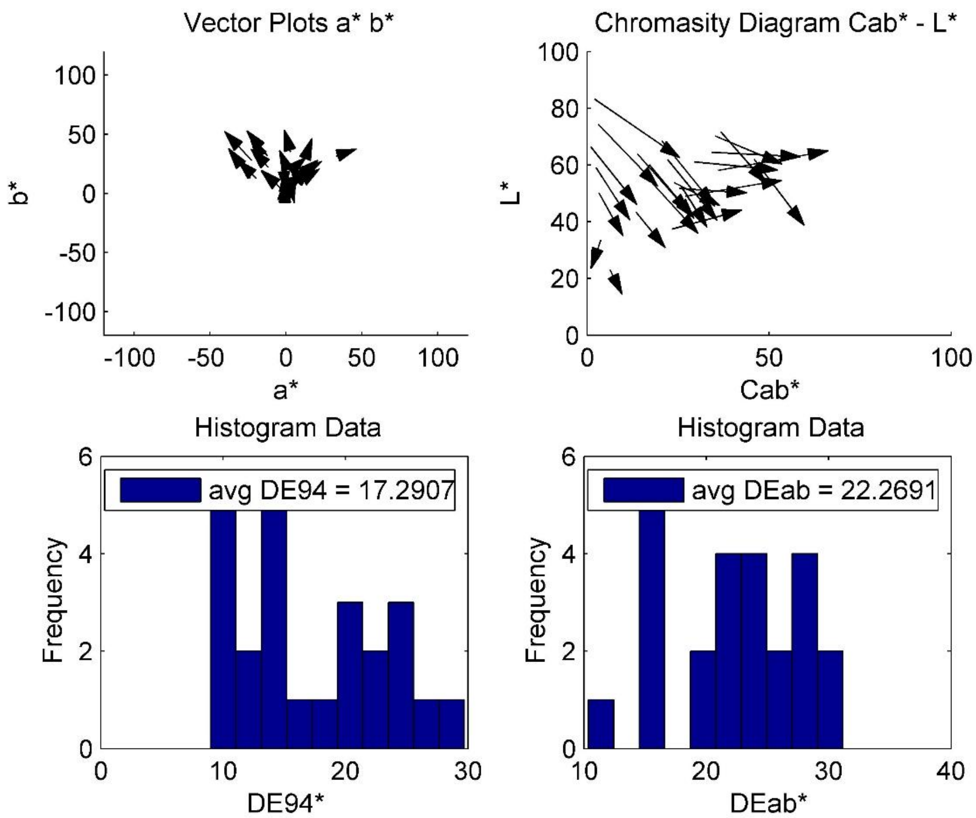

Figure 8-30 CIELAB Metrics Quad 4 RGB vs. TBP2_Unmixed

By carefully observing the above images and graphs of the patches of Macbeth Color Checker, it is easy to infer that the best results that match the RGB values of the object are the RGB_Unmixed results (Figure 8-7 - Figure 8-10) . This can be also noticed perceptually in Figure 8-6.

As aforementioned, the data from the Triple Band Pass Filters are compared as well. Beginning from TBPF1 (Figure 8-12 - Figure 8-15) it can be noticed that the average of the CIELAB DEab* is approximately 15, which means high color difference. Perceptually, the differences can be noticed in Figure 8-11. The same applies for TBPF2 (Figure 8-22 - Figure 8-25) whose DEab* is approximately 8. Although the error is high, comparing with the corresponding data from TBPF1 both numerically and perceptually (Figure 8-21), it can be seen that the color patches from TBPF2 match better in hue and chromasity to RGB than the TBPF1 color patches.

Finally, the Unmixing algorithm is performed and both TBPFs were unmixed. This meant that any cross-talking between the bands was removed and all six channels represented “pure” spectral information. That said the color difference between the unmixed and the RGB values should be noticeable. From Figure 8-17 - Figure 8-20 for TBPF1 and Figure 8-27 - Figure 8-30 for TBPF2 it can be seen that the difference was quite high. The lengths of the arrows in both Unmixed Bands were quite big which meant that there was high color difference between the RGB and Unmixed Band values. Moreover, statistically the color difference value DEab* averaging to 23 for TBPF2 and 27 for TBPF1, which also validated the high perceptual difference. Again, the TBPF2 perform better in comparison to TBPF1. That happens because the bands of the TBPF2 were evenly distributed among the EM-Spectrum and its peak transmittances were close to the RGB ones in comparison with the TBPF1. Finally, the perceptual difference between the Unmixed and the RGB Images is quite high as it can be noticed in Figure 8-16 and Figure 8-26. These results were expected since as aforementioned the values of the bands were unmixed thus represent “clean” spectral data. All these results can be seen in detail for all the cases in and can be seen in detail in Table 8-2.

Table 8-2 Color Reproduction Quantitative Results Comparison

DEab	Max	Min	Average
RGB_Unmixed	14,85	1,05	4,46
TBPF1	24,25	1,79	15,09
TBPF1_Unmixed	41,75	12,69	27,04
TBPF2	17,23	2,01	7,96
TBPF2_Unmixed	30,79	11,41	22,96

8.6 Spectral and Color Imaging Post Processing

Spectral and Color Imaging data may be needed for storage or post processing. For example, one of the main advantages in Color Reproduction is that given a spectral cube, the color of the sample can be reproduced under any illuminant or conditions.

For this reason, the system designed provides the user with the ability to store and use a complete spectral cube for any requirement. So, for both Spectral and Color Imaging the following options were enabled.

During Spectral imaging, it was mentioned that only one spectral band was reproduced at any given moment for real-time purposes. On demand, the spectrum of a single pixel could be evaluated and the SPD of the specific point recovered. Moreover, the complete spectral cube could be saved for the visible region of the spectrum.

During Color Imaging, the output of each camera could be saved independently. The images could be both the unmixed and mixed ones. The RGB_Unmixed value could be saved as well. Finally, the complete spectral cube could be evaluated in order to use it for color reproduction under various illumination conditions and not only the one at hand during the experiment.

8.7 Modulation Transfer Function

The Modulation Transfer Function (MTF) is an important parameter to evaluate the optical capabilities (resolution and contrast) of an optical system.

Resolution is an imaging system's ability to distinguish object detail. It is often expressed in terms of line-pairs per millimeter (where a line-pair is a sequence of one black line and one white line). This measure of line- pairs per millimeter (lp/mm) is also known as frequency. The inverse of the frequency yields the spacing in millimeters between two resolved lines. Bar targets with a series of equally spaced, alternating white and black bars are ideal for testing system performance.

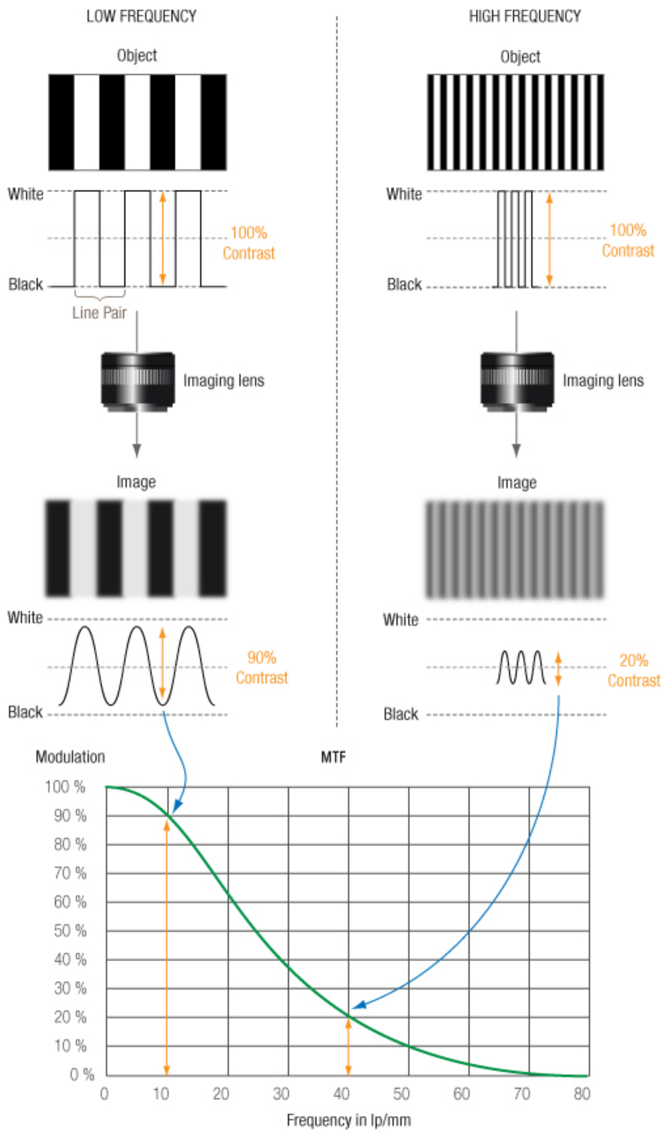

Figure 8-31 Perfect Line Edges before and after passing through a low-frequency pattern (left), high-frequency pattern (right), their corresponding MTF value (bottom).

Consider normalizing the intensity of a bar target by assigning a maximum value to the white bars and zero value to the black bars. Plotting these values results in a square wave, from which the notion of contrast can be more easily seen in Figure 8-32 . Mathematically, **contrast** is calculated with equation which is known as Michelson contrast equation:

$$Contrast\backslash Modulation \;= \frac{I_{max} - I_{min}}{I_{max} + I_{min}}$$

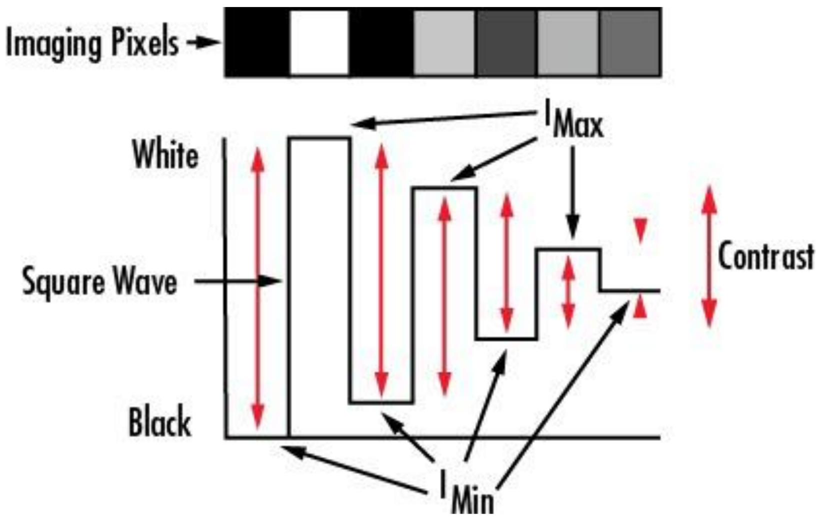

Figure 8-32 Contrast expressed as a square wave at different levels of resolution

In order to measure our systems' MTF the Variable Frequency Target (2.2.5 - VFT) was used. The CMOS sensor used for our system has a pixel size of 19.36μm which implies 0.01936 mm per pixel. Inverting this number (1/0.01936) gives the Nyquist frequency of 51.65 line pairs per millimeter. That means that the approximate MTF value of our system using the VFT would be 51 lp/mm.

From the MTF curve (Figure 8-33) we can estimate the resolution to be about 47 lines/mm (MTF value = 0.5) but the curve gives a more precise description of the optical system than this number. That resulted in a convergence between the theoretical and the experimental value as the measured MTF value is approximately the expected MTF resulting from the systems pixel size.

The small difference introduced was mainly due to focusing since for each block of line pairs/mm of the target different focus was needed for optimum results.

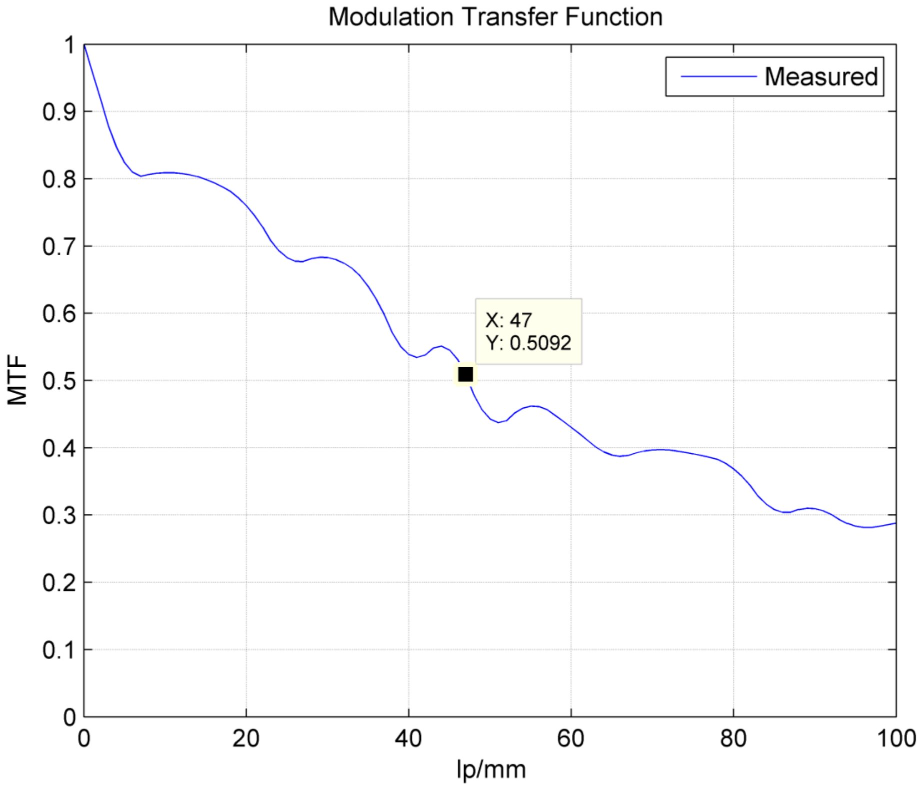

Figure 8-33 System's Modulation Transfer Function

Since our multispectral system is used to estimate spectra, the need to validate that the MTF of the system remained unaffected was at hand. The VFT target was captured and estimated and the MTF of the predicted bands was calculated as well.

In Figure 8-34 the MTF of the estimated band 560nm is presented versus the measured MTF of the system. Again for this process TBPF1 and TBPF2 were used and 15 spectral bands were estimated. The predicted MTF value was 45 lp/mm, which is approximately the same as the measured one. Moreover, the RMSE was 0.0219 which indicates low error factor.

The above result provides a validation of the fact that the performance of the camera was not affected by the spectral estimation process and that the images produced would have the same resolution and contrast as the corresponding measured ones.

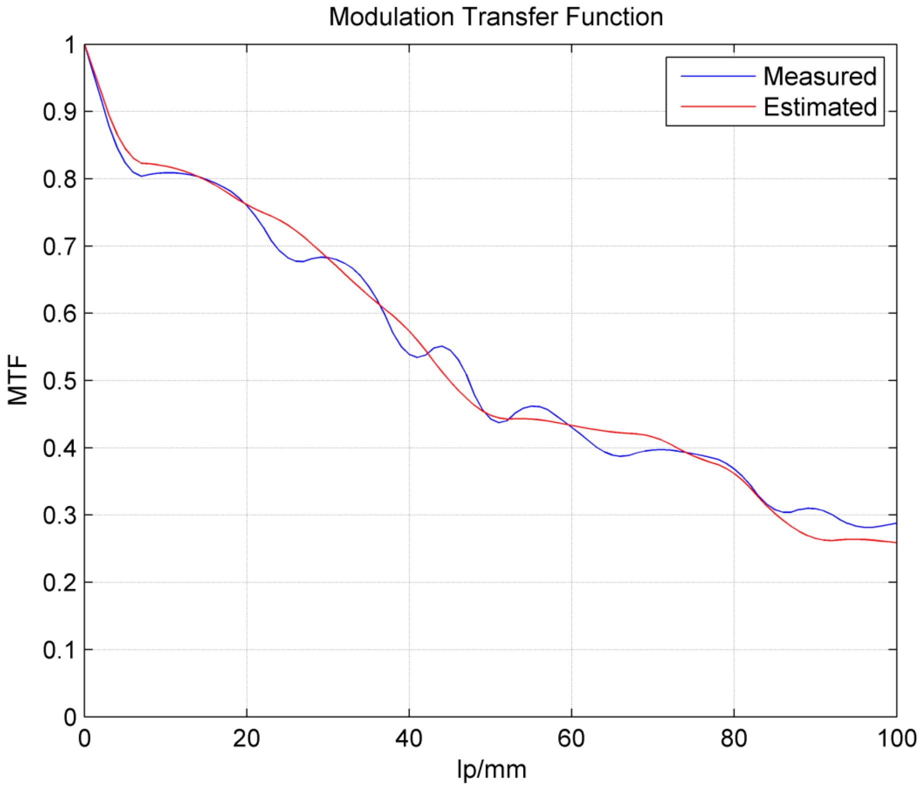

Figure 8-34 MTF of Estimated Band 560nm vs. Measured MTF

8.8 Color Gamut

A very important parameter of a Color Imaging system is the color gamut. Depending on the device itself as well as the type of the device (input, output) the Color Gamut and the method to evaluate can vary significantly. Amongst many methods that have been proposed to calculate the Color Gamut of Digital Cameras or Scanners [70][71][72], for our study we chose the "input device plus transform gamut". Under this concept, the camera was characterized by the way it responded to a set of reference set of colors such as Macbeth Color Checker CC. The three primary RGB colors were used in order to determine the highest colorfulness the stimulus can attain without saturation the camera response.

Our system comprises of two RGB cameras coupled with two Triple Band Pass Filters. In order to perform a thorough analysis of our system the Color Gamut was estimated for every possible case of tristimulus produced. In other words, Color Gamut was estimated for each TBPF, Mixed and Unmixed, as well for the Six Unmixed Spectral Bands system. All of these results are then compared to the RGB Color Gamut of the same camera coupled only with an IR-cut filter.

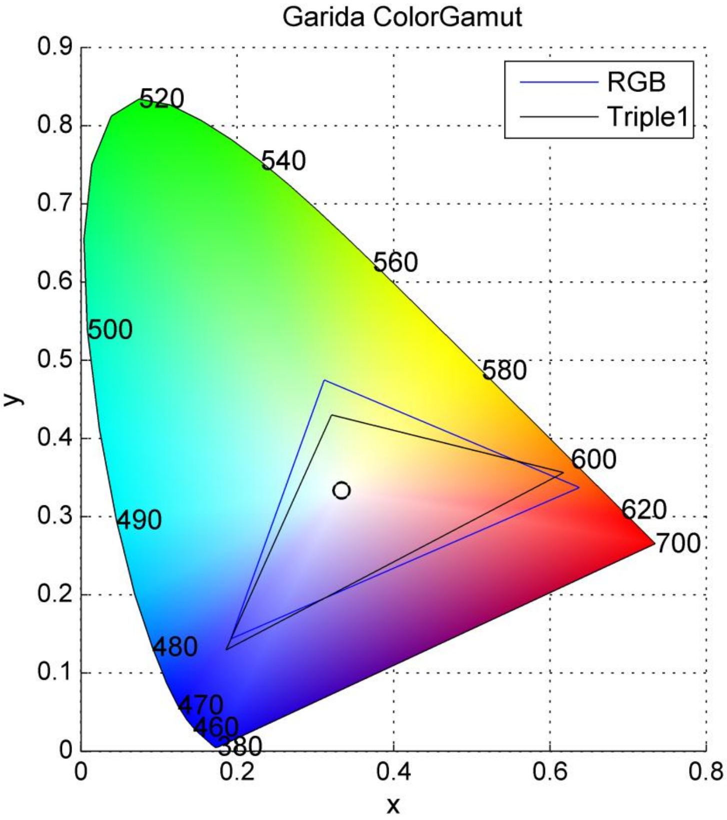

Figure 8-35 Color Gamut TBPF1 Mixed

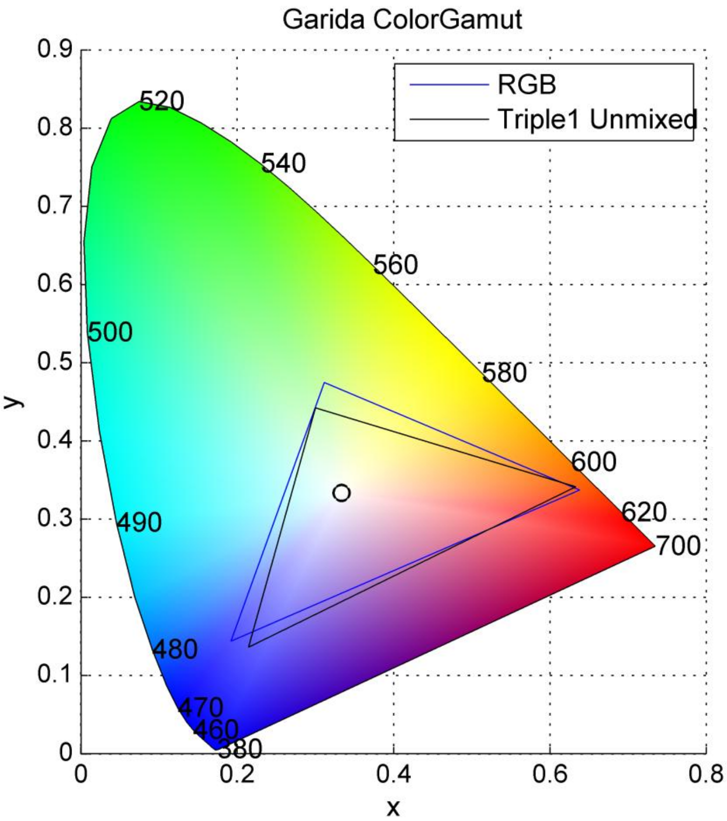

Figure 8-36 Color Gamut TBPF1 Unmixed

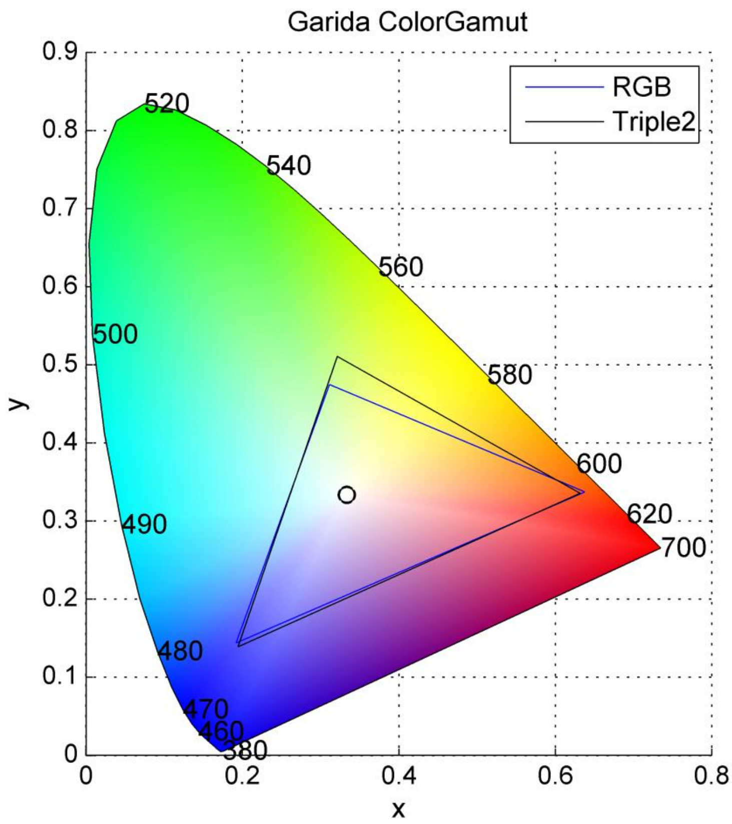

Figure 8-37 Color Gamut TBPF2 Mixed

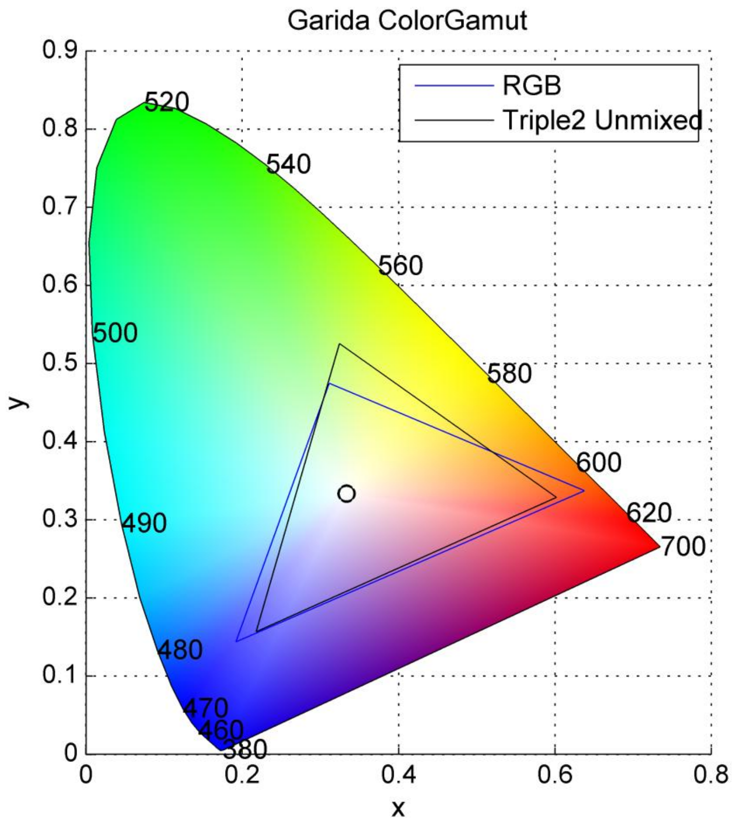

Figure 8-38 Color Gamut TBPF2 Unmixed

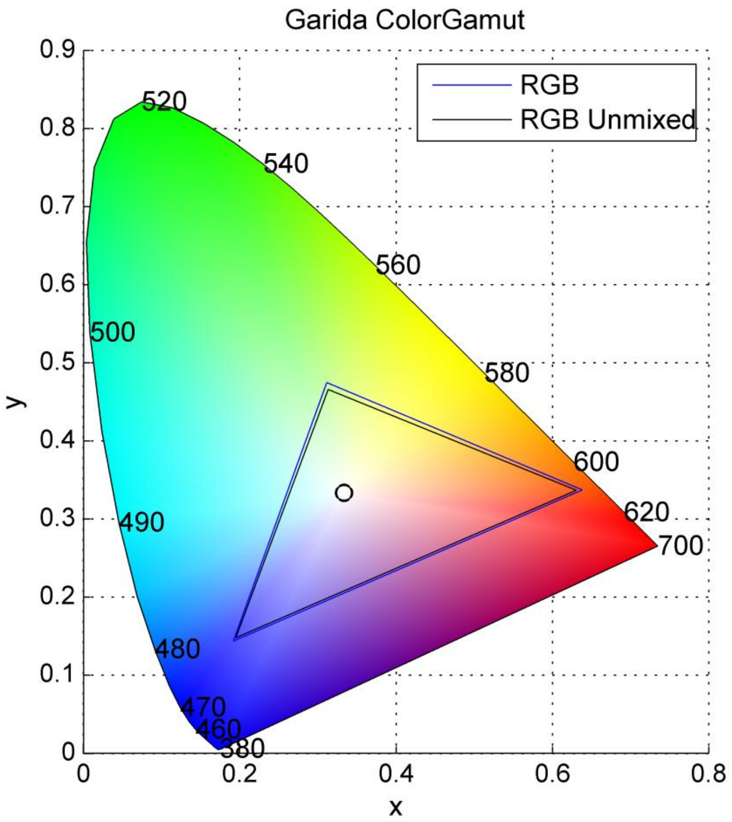

Figure 8-39 Color Gamut Garida Imaging System (Six Unmixed Spectral Narrow Bands)

From Figure 8-35 to Figure 8-39 the color gamut of all possible color inputs can be seen. It is noticeable that TBPF1, either mixed or unmixed, has significant difference with the regular RGB. On the other hand TBPF2 Mixed seemed to expand the Color Gamut which effectively meant that the colors obtained would be more saturated and perceptually different than those of the conventional RGB. TBPF2 expanded the gamut towards the Green area but seemed to lose chromasity over blue and red.

Lastly, the Color Gamut of the Six Unmixed Bands was evaluated. As it seems in Figure 8-39 the Color Gamut of our Six Unmixed Band Camera System and the conventionally RGB camera were approximately the same which indicated low chromasity difference and high fidelity color reproduction.

8.9 Metamerism

Color imaging systems suffer from the phenomenon of metamerism. Spectral Imaging systems provide a solution to this problem since the sample, scene or object, becomes independent of any illuminant (or other) conditions. Since all Hyper or Multispectral systems are independent of metamerism our system is also tested in order to be proven as such.

In order for a system to be proven metamerism independent, a test target is needed that contains a number of metamer sets [73]. Two surfaces that look the same under a certain illumination conditions but have different spectral distribution are called metamers. A new kind of test target was created at Munsell Color Science Laboratory [74], called METACOW, which contains the 24 color patches of Gretag Macbeth ColorChecker® with the metameric match of each one. It is represented by 24 cows where half the cow, from the middle and back, corresponds to the ColorChecker's color and spectral values and the rest of the cow represents the metameric match of this patch. The spectral values of each patch can be seen in Figure 8-40. This test target allowed investigating the effect of metamerism of our system. The RGB values of the METACOW target as measured in the Munsell lab, can be seen in Figure 8-41. As aforementioned, our system can reproduce color with two different methods. The first method estimates the spectrum of the target for the visible part of the spectrum and uses it to reproduce color under any illuminant conditions. The second method uses six weighted bands in order to reproduce color in real time. In Figure 8-42 the result of real time six weighted band color reproduction can be seen. It is important to note that the RGB image provided from Munsell and the one reproduced are acquired with different devices under different illumination conditions. From the results provided it is noticeable that the two parts of the cow are quite different. The half part that corresponds to Macbeth ColorChecker is reproduced and the color resembles the ones from Macbeth while the front half of the cow differs significantly. The color of the metameric match part is reproduced having a very different color perception than the rest of the cow since the Spectral Power Distribution of that part of the cow differs from the default values of Macbeth.

This result indicates that the color reproduction process of our Real Time multispectral system is independent from the phenomenon of metamerism. The result was quite expected since the system acquires six narrow spectral bands that have undergone an unmixing process which makes them contain pure spectral information without any cross-talking.

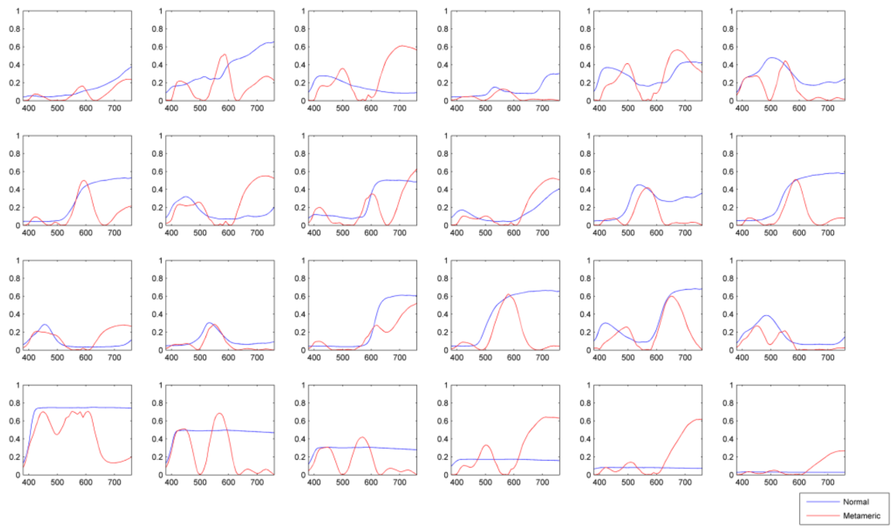

Figure 8-40 Spectral Reflectance of Macbeth Normal and Metameric Patches

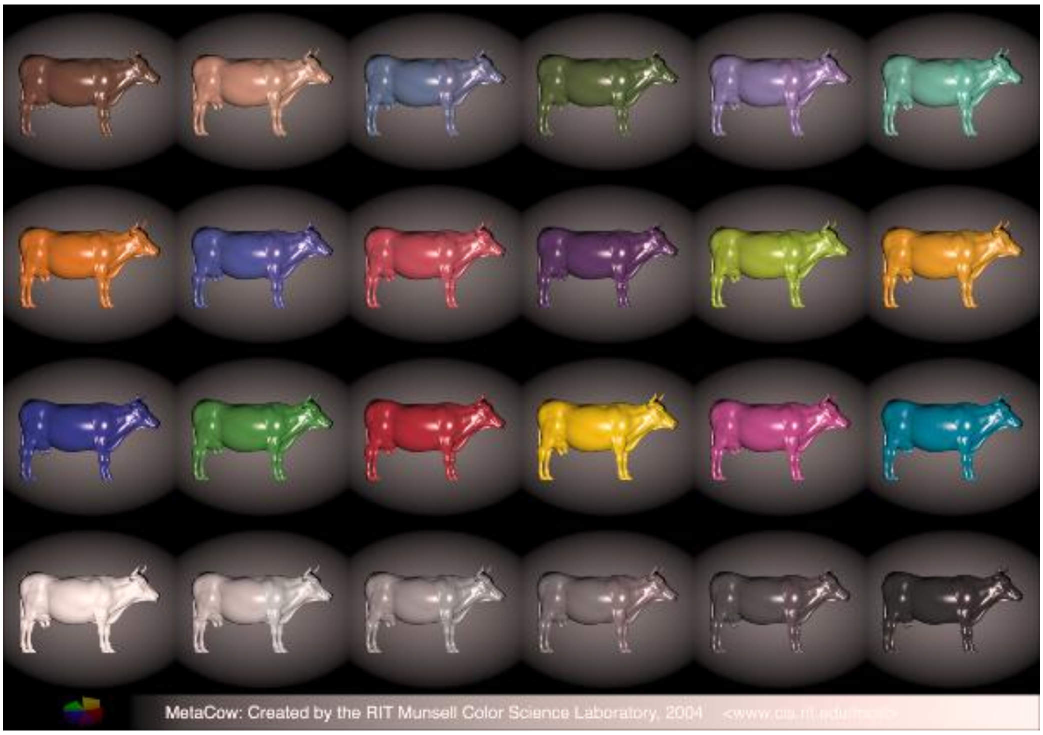

Figure 8-41 METACOW test target

Figure 8-42 METACOW Six Weighted Bands Color Reproduction

8.10 Real-Time Spectral Mapping

Finally, real-time spectral mapping processes where incorporated to our system creating the first Real-Time Spectral Mapper (RTSM)[69],[75]. The RTSM was used for performing real-time feature extraction from immunostained invasive histology breast cancer samples. The purpose of the analysis was to validate its accuracy when a natural target is analyzed. The invasive ductal breast carcinoma biopsy samples were immunostained for estrogen receptors (ERs) [utilizing the Quanto UltraVision HRP Immunodetection Kit (Thermo Scie., USA) and a primary antihuman Rabbit Monoclonal antibody (SP1 RM-9101, Neomarkers, USA, with DAB as chromogen)], and counterstained with Hematoxylin. Spectral mapping was performed with both the scanning HSI system and the RTSM, both adapted to a microscope (Olympus BX51). Figure 8-43 illustrates the spectral maps obtained with the RTSM (c), (d). In these color- coded images, pseudocolors represent different spectral classes and depict different immunostain uptake levels from the cell nuclei, which is of great diagnostic importance. Figure 8-43 (b) illustrates an image depicting quantitatively the differences between the experimental spectral cube collected with the HSI system and the spectral cube generated by the RTSM. Both cubes were obtained from the histology sample of Figure 8-43 (a). The comparison (in radians) was performed on a pixel-by-pixel level, using (again) the SAM algorithm for comparing spectra corresponding to the same spatial coordinates. The maximum spectral difference that was measured accross the image was 0.5 radians, indicating an exceptional similarity between the measured and the estimated spectral cube.

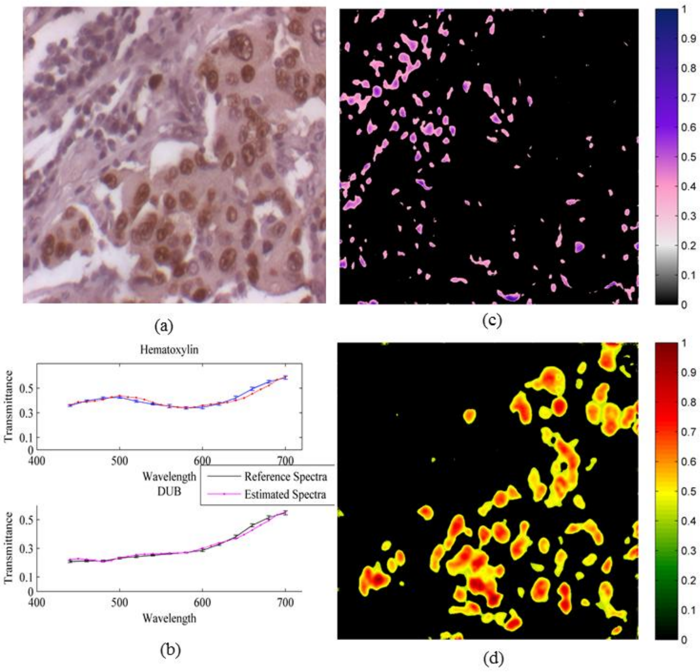

Figure 8-43 (a) Biopsy Image of Immunostained Biopsy (b) Measured and Estimated Spectrum (c) Spectral Map for Hematoxilin immunostain (d) Spectral Map for DAB Immunostain

9 Conclusions

Throughout this Master thesis, spectral color reproduction was studied using six narrow spectral bands for the visible regions of the EM-Spectrum. Spectral estimation was extended to the Near Infrared region of the EM-Spectrum and the use of six additional spectral bands within the NIR provided high accuracy results.

Spectral and Color Imaging Systems were used to validate the outcome of the aforementioned process. Results showed that six spectral bands can provide high accuracy spectral estimation within the visible region and that the spectral cube which resulted from this process could be used for color reproduction under any illumination condition and provide high fidelity color.

The use of two high-resolution RGB cameras was proposed, coupled with two Triple Band Pass Filters along with light dispersing elements, creating a novel multispectral system. Spectral estimation was performed with this system and the results validated our previous work, that six narrow spectral bands can be used for high accuracy spectral estimation. The fact that high fidelity color can be reproduced as before from the resulting spectral cube was validated alongside it.

A Spectral Unmixing algorithm as well as a Camera Sensitivity measurement were proposed in association with the aforementioned system to eliminate any cross-talking between the three spectral bands of each Triple Band Pass Filter for each of two RGB cameras. The resulting Unmixed Bands were used to perform weighted color reproduction. The results indicated that for the scene's given illumination, color reproduction can be performed without using a complete spectral cube and result in high fidelity color.

We report the first real time spectral mapper (RTSM) combining snapshot spectral imaging with the Wiener spectral estimation algorithm. The described RTSM system offers accurate spectral mapping as compared to scanning spectral imager, being, however, three orders of magnitude faster than conventional technologies. The technology is intended to enable spectral imaging and mapping in a series of biomedical in vivo and in vitro applications involving dynamic bio-optical phenomena and not stationary imaging conditions.

10 Discussion

A novel spectral and color imaging system was developed that could reproduce spectral reflectance for a specific wavelength and perform color imaging in real time as well as reproduce real-time color for the scene's given illuminant. The real-time spectral imaging system is described and validated for both spectral and color estimation. The color gamut, the MTF and the Metameric sensitivity of the system were also calculated resulting that the proposed system can estimate spectral correctly without modifying the MTF function of the system, reproduce High Fidelity color without modifying the Color Gamut of a corresponding RGB system or be prone to metameric effects.

This study was also the foundation of the first Real Time Spectral Mapper (RTSM) which allowed the simultaneous acquisition of spectrum and spectral mapping. RTSM will have a tremendous impact on Biomedical Sciences and it can be used in many fields of medicine such as endoscopy, microscopy, pathologoanatomy and so forth.

The aim of this study was to create novel spectral imaging systems that offer tremendous capabilities in both spatial and spectral resolution with instantaneous acquisition of spectral images. This will allow the observation of dynamically evolving phenomena and could revolutionize many clinical test by shortening the examination time and providing a non-invasive non-destructive analysis.

11 Future Work

This device could be extended to perform real-time spectral imaging to both the IR and UV regions of the spectrum in real-time. The study of spectral estimation for the NIR concluded that three narrow spectral bands could be used for accurate spectral estimation. For that purpose a three broad band camera with sensitivity to the NIR coupled with interference filter could be used in conjunction with the system, so to enhance its spectral resolution. Moreover, an extended analysis for spectral estimation within the UV region of the spectrum can be also performed. Again, the optimum number of bands that allow high accuracy spectral estimation must be set. After validating the number of bands, a new optical-mechanical design of the system will be in order, so to incorporate optical-dispersing elements that will allow the simultaneous capturing of any scene from three or more cameras.

12 References

[1] *H. Kang, Computational Color Technology, Illustrate. Society of Photo Optical, 2006, p. 511.*

[2] *S. Süsstrunk, R. Buckley, and S. Swen, "Standard RGB Color Spaces," pp. 1–8.*

[3] *Jon Y. Hardeberg, "Colorimetric and Multispectral Approaches"*

[4] *R. S. Berns, "The Science of Digitizing Paintings for Color-Accurate Image Archives: A Review" Imaging Sci. Technol., vol. 45, no. 4, 2001.*

[5] *M. R. Pointer, R. W. G. Hunt, Measuring Colour .*

[6] *I. Nimeroff and J. a. Yurow, "Degree of Metamerism," J. Opt. Soc. Am., vol. 55, no. 2, p. 185, Feb. 1965.*

[7] *R. L. Alfvin and M. D. Fairchild, "Observer Variability in Metameric Color Matches using Color Reproduction Media," pp. 174–188, 1996.*

[8] *Guowei Hong, M. Ronnier Luo and Peter A. Rhodes, "A Study of Digital Camera Colorimetric Characterization Based on Polynomial Modeling", Colour & Imaging Institute, University of Derby, Derby DE22 3HL, United Kingdom," Imaging.*

[9] *Y. S. Chung, J. H. Xin, and K. M. Sin, "Improvement of inter-instrumental agreement for reflectance spectrophotometers Coloration Technology," Color. Technol., 2004.*

[10] *M. D. Fairchild, M. R. Rosen, and G. M. Johnson, "Spectral and Metameric Color Imaging."*

[11] *B. Hill, "Color Capture Color Management and the problem of metamerism: does multispectral imaging offer the solution," vol. 3963, no. January, pp. 2–14, 2000.*

[12] *J. Y. Hardeberg, "Multispectral Color Imaging," no. February 1999, pp. 1–8, 2001.*

[13] *M. Yamaguchi, H. Haneishi, and N. Ohyama, "Beyond Red – Green – Blue (RGB): Spectrum-Based Color," vol. 52, no. 1, 2008.*

[14] *M. Yamaguchi, T. Teraji, K. Ohsawa, T. Uchiyama, and H. Motomura, "Color image reproduction based on the multispectral and multiprimary imaging: Experimental evaluation," vol. 4663, pp. 15–26, 2002.*

[15] *R. S. Berns, F. H. Imai, P. D. Burns, and D. Tzeng, "Multi-spectral-based color reproduction research at the Munsell Color Science Laboratory."*

[16] *R. S. Berns, "Challenges for Color Science in Multimedia Imaging."*

[17] *P. D. Burns, R. S. Berns, and N. York, "Analysis Multispectral Image Capture," pp. 19–22, 1996.*

[18] *B. Hill, "Optimization of total multispectral imaging systems: best spectral match versus least observer metamerism," pp. 2–3.*

[19] *D. L. Lau and R. Yang, "Real-time multispectral color video synthesis using an array of commodity cameras," Real-Time Imaging, vol. 11, no. 2, pp. 109–116, Apr. 2005.*

[20] *H. H. Szu, M. Vetterli, W. J. Campbell, J. R. Buss, N. Gat, and O. Systems, "Imaging Spectroscopy Using Tunable Filters : A Review," vol. 4056, pp. 50–64, 2000.*

[21] *K. Ohsawa, Takeyuki Ajito, and Y. Komiya, "Six Band HDTV Camera System for Spectrum-Based Color Reproduction.pdf."*

[22] *R. Shrestha and J. Y. Hardeberg, "Multispectral Image Capture using two RGB cameras," pp. 1801–1805, 2010.*

[23] *G. Themelis, J. S. Yoo, and V. Ntziachristos, "Multispectral imaging using multiple-bandpass filters," vol. 33, no. 9, pp. 1023–1025, 2008.*

[24] *R. Shrestha, J. Y. Hardeberg, and A. Mansouri, "One-Shot Multispectral Color Imaging with a Stereo Camera," Electron. Imaging, pp. 787609–787609–11, Jan. 2011.*

[25] *R. Shrestha, A. Mansouri, and J. Hardeberg, "Multispectral imaging using a stereo camera: concept, design and assessment," EURASIP J. Adv. Signal Process., vol. 2011, no. 1, p. 57, 2011.*

[26] *Costas Balas, George Epitropou, Christos Pappas "Multi/Hyper Spectral Imaging"*

[27] *D. Tzeng, R. S. Berns, and N. York, "Spectral-Based Six-Color Separation Minimizing Metamerism," pp. 342–347, 2000.*

[28] *J. Gerhardt and J. Y. Hardeberg, "Spectral color reproduction minimizing spectral and perceptual color differences," Color Res. Appl., vol. 33, no. 6, pp. 494–504, Dec. 2008.*

[29] *R. S. Berns, "Color-Accurate Image Archives Using Spectral Imaging," pp. 105–119.*

[30] *F. H. Imai, R. S. Berns, M. Color, C. F. Carlson, I. Science, and N. York, "High-Resolution Multi-Spectral Image Archives: A Hybrid Approach," pp. 224–227, 1998.*

[31] *H. Haneishi, T. Hasegawa, A. Hosoi, Y. Yokoyama, N. Tsumura, and Y. Miyake, "System Design for Accurately Estimating the Spectral Reflectance of Art Paintings," Appl. Opt., vol. 39, no. 35, pp. 6621–6632, Dec. 2000.*

[32] *Shiobara, T., Zhou, S., Haneishi, H., Tsumura, N., & Miyake, Y. (1996),"Improved color reproduction of electronic endoscopes", Journal of Imaging science and Technology, 40(6), 494-501.*

[33] *Parra-Blanco A, Jiménez A, Rembacken B, González N, Nicolás-Pérez D, Gimeno-García AZ, Carrillo-Palau M, Matsuda T, Quintero E.," Validation of Fujinon intelligent chromoendoscopy with high definition endoscopes in colonoscopy." , World J Gastroenterol. 2009; 15:5266–5273.*

[34] *M. Yamaguchi, "Medical Application of a Color Reproduction System with a Multispectral Camera ", pp. 33–38, 2001.*

[35] *M. Yamaguchi, M. Mitsui, Y. Murakami, H. Fukuda, and N. Ohyama, "Multispectral color imaging for dermatology: application in inflammatory and immunologic diseases."*

[36] *P. Stigell, K. Miyata, and M. Hauta-Kasari, "Wiener estimation method in estimating of spectral reflectance from RGB images," Pattern Recognition and Image Analysis, vol. 17, no. 2, pp. 233-242, Jun. 2007.*

[37] H.-L. Shen, P.-Q. Cai, S.-J. Shao, and J. H. Xin, "Reflectance reconstruction for multispectral imaging by adaptive Wiener estimation." Optics express, vol. 15, no. 23, pp. 15545-54, Dec. 2007.

[38] Y. Murakami, M. Yamaguchi, and N. Ohyama, "Piecewise Wiener estimation for reconstruction of spectral reflectance image by multipoint spectral measurements.," Applied optics, vol. 48, no. 11, pp. 2188-202, May 2009.

[39] P. Urban, M. R. Rosen, and R. S. Berns, "Spectral image reconstruction using an edgepreserving spatio-spectral Wiener estimation," America, vol. 26, no. 8, pp. 1865-1875, 2009.

[40] N. Shimano, "Recovery of spectral reflectances of objects being imaged without prior knowledge.," IEEE transactions on image processing : a publication of the IEEE Signal Processing Society, vol. 15, no. 7, pp. 1848-56, Jul. 2006.

[41] H. -L. Shen, H.-J. Wan, and Z.-C. Zhang, "Estimating reflectance from multispectral camera responses based on partial least-squares regression," Journal of Electronic Imaging, vol. 19, no. 2, p. 020501, 2010.

[42] Alamin Mansouri, Tadeusz Sliwa, Jon Y. Hardeberg, Yvon Voisin, "Representation and Estimation Of Spectral Reflectances Using Projection on PCA and Wavelet Bases" (2008)

[43] Alamin Mansouri, Tadeusz Sliwa, Jon Y. Hardeberg, Yvon Voisin, "An Adaptive-PCA Algorithm for Reflectance Estimation from Color Images" (2008)

[44] O.-seol Kwon, C.-hee Lee, H.-keun Lee, and Y.-ho Ha, "Improved Spectral-Reflectance (SR) Estimation Using Set of Principle Components Separately Organized for Each SR Population with Similar SRs," Electrical Engineering, pp. 562-565, 2003.

[45] T. Harifi, S. H. A. M. Ã, and F. A. Gahian, "Recovery of Reflectance Spectra from Colorimetric Data Using Principal Component Analysis Embedded Regression Technique," Optical Review, vol. 15, no. 6, pp. 302-308, 2008.

[46] S. H.Amirshahi and S. A. Amirhahi, "Adaptive Non-Negative Bases for Reconstruction of Spectral Data from Colorimetric Information," Optical Review, vol. 17, no. 6, pp. 562-569, 2010.

[47] V. Babaei, S. H. Amirshahi, and F. Agahian, "Using weighted pseudo-inverse method for reconstruction of reflectance spectra and analyzing the dataset in terms of normality," Color Research & Application, vol. 36, no. 4, pp. 295-305, Aug. 2011.

[48] Y. Zhao and R. S. Berns, "Image-based spectral reflectance reconstruction using the matrix R method," Color Research & Application, vol. 32, no. 5, pp. 343-351, Oct. 2007.

[49] D. Connuh, Y. Jon, S. Westland "Comparison of linear spectral reconstruction methods for multispectral imaging," Media, pp. 1497-1500, 2004.

[50] H.-liang Shen, J. H. Xin, and S.-jie Shao, "Improved reflectance reconstruction for multispectral imaging by combining different techniques," Science, vol. 15, no. 9, pp. 5531-5536, 2007.

[51] Francisco H. Imai, Roy S. Berns and Di-Y Tzeng, "A Comparative Analysis of Spectral Reflectance Estimated in Various Spaces Using a Trichromatic Camera System"

[52] Eva M. Valero, Juan L. Nieves, Sérgio M. C. Nascimento, Kinjiro Amano, David H. Foster , "Recovering spectral data from natural scenes with an RGB digital camera and colored filters"

[53] Francisco H. Imai, Roy S. Berns, "Spectral Estimation Using Trichromatic Digital Cameras"

[54] M. a López-Alvarez, J. Hernández-Andrés, and J. Romero, "Developing an optimum computer-designed multispectral system comprising a monochrome CCD camera and a liquid-crystal tunable filter." Applied optics, vol. 47, no. 24, pp. 4381-90, Aug. 2008.

[55] M. a López-Alvarez, J. Hernández-Andrés, E. M. Valero, and J. Romero, "Selecting algorithms, sensors, and linear bases for optimum spectral recovery of skylight." Journal of the Optical Society of America. A, Optics, image science, and vision, vol. 24, no. 4, pp. 942-56, May 2007.

[56] D. Connah, S. Westland, and M. G. A. Thomson, "Recovering spectral information using digital camera systems Coloration Technology," Coloration Technology, vol. 117, pp. 309-312, 2001.

[57] Francisco H. Imai , Mitchell R. Rosen , Roy S. Berns, "Comparison of Spectrally Narrow-Band Capture Versus Wide-Band with a Priori Sample Analysis for Spectral Reflectance Estimation "(2000)

[58] J. Y. Hardeberg, F. Schmitt, H. Brettel, J.-pierre Crettez, and H. Maitre, "Multispectral Image Acquisition and Simulation of Illuminant Changes," 1999.

[59] C. Plata, J. L. Nieves, E. M. Valero, and J. Romero, "Trichromatic red-green-blue camera used for the recovery of albedo and reflectance of rough-textured surfaces under different illumination conditions.," Applied optics, vol. 48, no. 19, pp. 3643-53, Jul. 2009.

[60] C. Chi, H. Yoo, and M. Ben-Ezra, "Multi-Spectral Imaging by Optimized Wide Band Illumination," International Journal of Computer Vision, vol. 86, no. 2-3, pp. 140-151, Nov. 2008.

[61] J.-il Park, M.-hyun Lee, M. D. Grossberg, and S. K. Nayar, "Multispectral Imaging Using Multiplexed Illumination," Work.

[62] J. L. Nieves, E. M. Valero, J. Hernández-Andrés, and J. Romero, "Recovering fluorescent spectra with an RGB digital camera and color filters using different matrix factorizations.," Applied optics, vol. 46, no. 19, pp. 4144-54, Jul. 2007.

[63] Bore-Kuen Lee, Feng-Chi Shen and Chun-Yen Chen, "Defense Technical Information Center Compilation Part Notice Spectral Estimation and Color Appearance Prediction of Fluorescent Materials," Imaging, 2000.

[64] J. A. Toque, Y. Sakatoku, and A. Ide-ektessabi, "PIGMENT IDENTIFICATION BY ANALYTICAL IMAGING USING MULTISPECTRAL IMAGES," Advanced Imaging, pp. 2861-2864, 2009.

[65] P. Chen, Y. Xiao, and T. Xie, "Spectrum Endoscope System," Image (Rochester, N.Y.), no. 1, pp. 0-3, 2009.

[66] D.Anglos, C.Balas, C.Fotakis, "Laser spectroscopic and optical imaging techniques in chemical and structural diagnosis of painted artworks" ,Am.Lab.(October)(1999)60–67.

[67] C.Balas, "An imaging method and apparatus for the non-destructive analysis of paintings and monuments", International PatentApp. PCT/GR00/00039.

[68] C.Balas, "A novel optical imaging method for the early detection, quantitative grading and mapping of cancerous and precancerous lesions of cervix", IEEE Trans. Biomed. Eng. 48(2001)96–104.

[69] G. Epitropou, V. Kavvadias, D. Iliou, E. Stathopoulos, and C. Balas, "A real-time spectral mapper as an emerging diagnostic technology in biomedical sciences.," Conf. Proc. IEEE Eng. Med. Biol. Soc., vol. 2013, pp. 1422–5, Jul. 2013.

[70] B. Pope, F. Hsu, and F. Sigg, "A New Approach to Analyzing Color Gamut Color Gamut Quantified," 2004.

[71] R. Balasubramanian, E. Dalal, X. Corporation, and W. Ny, "A method for quantifying the color gamut of an output device," pp. 2–8.

[72] F. Martı, M. J. Luque, P. Capilla, and J. Pujol, "Concerning the Calculation of the Color Gamut in a Digital Camera," vol. 31, no. 5, 2006.

[73] G. Finlayson and P. Morovic, "Metamer sets," J. Opt. Soc. Am. A 22, 810-819 (2005).

[74] M. D. Fairchild and G. M. Johnson, "METACOW : A Public-Domain , High- Extended-Dynamic-Range , Spectral Test Target for Imaging System Analysis and Simulation."

[75] Balas C. , Epitropou G., Kavvadias V. , Iliou D., Patsea E., Stathopoulos S., "A novel Real-Time Spectral Mapping Camera - Improves objectivity, accuracy and processing time of routine histological examination", (2014) 11th Annual National Greek Conference of pathologo-anatomy